AERODYNAMICS
OF TWO-DIMENSIONAL
SAIL WINGS

A thesis

submitted in partial fulfilment

of the requirements for the Degree

of

Master of Science in Physics

at the

University of Waikato

by

MICHAEL STEPHEN BUNDOCK.

University of Waikato

1980

ABSTRACT

The purpose of this work is to obtain the exact solution for the profile and characteristics of a two-dimensional sail, immersed in an inviscid incompressible fluid. An experimental investigation was also performed and results are compared with theoretical predictions.

The sail was assumed to be an infinitely flexible, non-porous membrane of zero thickness, fixed at the leading and trailing edges, and stretched under a constant tension T in the sail surface. An aerofoil model was considered where the airflow remains smoothly attached over the entire profile.

All known previous studies have also used the inviscid fluid approximation, but made the further assumptions of small angle of attack and negligible profile slopes. These assumptions enable the use of thin aerofoil theory predictions for pressure distribution and linearisation of the sail equation.

In contrast this investigation obtains the exact solution. An iterative numerical method is devised whereby an initial estimate is made for the profile using thin aerofoil theory. The pressure distribution is then determined using Theodorsen's method and the profile recalculated using the full sail equation, so that tension and pressure forces are balanced. The cycle of redetermining the pressure distribution and profile is repeated until a convergent solution is obtained.

Results are shown for the profile, lift coefficient and centre of pressure, for various angles of attack and states of tension. For sails with non-negligible camber, values of lift coefficient and centre of pressure are found to differ significantly from those predicted by the linear approximations. Previous researchers have established the existence of a critical tension state where the tension force is unable to contain the pressure forces acting on the sail, and predicted that the value of this state (K_{Tc}) was independent of angle of attack. However this study indicates that K_{Tc} increases with increasing angle of attack. Centre of pressure calculations, for various angles of attack and states of tension, indicate that two-dimensional sails may possess either static longitudinal stability or instability, depending on the tension state. Experimental results for the profile, K_{Tc}, lift coefficient and centre of pressure are compared with theory, and areas of agreement and disagreement discussed. Experimental values for the drag coefficient and the lift to drag ratio were obtained and are discussed in detail.

ACKNOWLEDGEMENTS

I wish to express my gratitude to Dr A.D. Sneyd for the many hours spent in discussion and review of this manuscript. Professor R.J. Hosking is thanked for his helpful comments and discussion of the theory. I am indebted to the staff at the University of Auckland Department of Mechanical Engineering, for making available the wind tunnel facilities, and especially to D.H. Freeston, C.W. Claxton and R.D. Earl for their help and discussion of the experimental investigation. Typing of the thesis was ably carried out by Mrs S. McColl and Mrs J. Tait. Finally I wish to thank my wife Lesley, for her never ending patience, help and encouragement during the writing of this thesis.

C O N T E N T S

LIST OF FIGURES

LIST OF PLATES

LIST OF FREQUENTLY USED SYMBOLS

Symbol	Meaning
a	quarter chord
$a\,e^{c_0}$	radius of circle in ξ_1-plane
b	average radius of approximate circle in ξ -plane
c	aerofoil chord
$C(x) = y(x)/c$	aerofoil camber function
C	boundary of circle in ξ_1-plane
$C_L = L/\frac{1}{2}\rho c u_0^2$	lift coefficient
$\bar{C}_L = C_L/\alpha$	normalised lift coefficient
$C_D = D/\frac{1}{2}\rho c u_0^2$	drag coefficient
$c_0 = \ln\left(\frac{b}{a}\right)$	constant
D	drag force acting on sail
$f(\xi_1)$	complex potential in ξ_1-plane
$F(\varphi)$	an analytic function on C
$G(x,t)$	Green's function
$g(t)$	point load at $x = t$
$h = y(c/2)$	camber of profile at half chord point.
$K_T = \dfrac{T}{\frac{1}{2}\rho c u_0^2}$	tension number
K_{Tc}	critical tension number
L	lift developed by sail wing
M	moment about the origin in z-plane
$P(x)$	pressure difference through sail at x
r	radius

LIST OF FREQUENTLY USED SYMBOLS

Symbol	Meaning
$Re = u_0 L/\nu$	Reynolds number
s	arc length along sail
S	sail surface, or total membrane length between leading and trailing edges
T	tension in sail surface (chord wise)
$\underset{\sim}{u}_0$	fluid velocity at ∞
$u(z)$	fluid speed at z
x_P	position of centre of pressure (fraction of chord)
$y(x)$	camber of sail profile at x
α	angle of attack
β	angle between tangent to sail surface and chord line
$\gamma = \varphi + \varepsilon(\varphi)$	angle that differs slightly from φ
δ	boundary layer thickness
$\varepsilon(\varphi)$	function used in second conformal transformation
κ	circulation about circle
ν	kinematic viscosity
ξ	plane defining transformed profile
ξ_1	plane defining true circle
ρ	air density
σ	sail element
φ	angle in ξ-plane
$\psi(\varphi)$	error function in ξ-plane

CHAPTER 1 INTRODUCTION

Despite the many achievements in the field of theoretical aerodynamics during the last century little attention has been focused on the characteristics of flexible aerofoils. Such aerofoils are commonly used as lifting devices, the most classical example being yacht sails, while more modern developments include the parawing and hang glider. The most notable property of sail wings is their development of a characteristic convex profile. Observation of yacht sails indicates that the camber is a complex function of angle of attack, tension and wind speed. This prompts the questions:

(i) What is the profile for a given set of conditions?

(ii) What are the forces acting on the sail and where do they act?

(iii) What happens to (i) and (ii) if the conditions change?

For a flexible membrane, not only is the pressure distribution dependent on the profile, but conversely the profile is dependent on the pressure distribution. This interrelationship between profile and pressure distribution imposes an extra constraint in the mathematical formulation of the aerodynamic problem for flexible membranes. The result is a non-linear integral equation, often referred to as the *'sail equation'*, which relates pressure and tension forces.

During the last two decades there has been a rapid development of hang gliders, utilizing wings of single and double skinned fabric

membranes. These craft are now obtaining a quite respectable soaring performance although their glide slope is somewhat steeper than that for conventional gliders. The hang glider has developed from a study of parawings carried out by the United States Air Force in the late 1950's and the early 1960's. The purpose was to investigate parawings as a device for slowing and controlling spacecraft descent following re-entry (Rogallo et al. (1960)). However, little theoretical work has been carried out on hang gliders and most performance improvements have been obtained by a process of trial and error.

In 1961 Thwaites presented a significant paper on the aero-dynamics of flexible membrane wings. He followed the linearized aerodynamic theory for two-dimensional rigid aerofoils in inviscid flow (thin aerofoil theory) and then derived the additional constraint relating pressure and tension forces. The resultant integral equation (sail equation) was linearized and evaluated numerically using a trigonometric substitution.

Concurrently, research sponsored by the United States Air Force was directed toward the design of flexible rotors. Theoretical studies included the development of a theory of two-dimensional flexible inelastic aerofoil sections in incompressible irrotational flow. Again thin aerofoil theory was used to calculate the sail camber. However the profile slopes were expressed in a Fourier series expansion, so that the linearized sail equation became an infinite series of simultaneous equations. Numerical results were obtained by evaluating the first

eighteen harmonics using computer matrix methods. Some wind tunnel tests were also carried out to determine the validity of the theoretical predictions. In 1963 Nielsen presented a paper describing this work and comparing the results with those obtained by Thwaites (1961).

Sneyd et al. (1979) also used thin aerofoil theory but approximated the profile slopes by a polynomial. Thus the linearized sail equation reduces to a set of linear simultaneous equations for the polynomial coefficients which may be evaluated analytically.

All three methods give essentially the same results, predicting purely convex profiles only if the tension is greater than the aerodynamic forces. If the tension is insufficient, these theories predict more complex profiles, although their stability in physical reality is doubtful. Their predictions for lift and centre of pressure are also in close agreement.

The present study is considered to be the next step toward the real situation. Previous studies assumed the slopes and angle of attack to be small so that: i) classical thin aerofoil theory could be used to determine the pressure distribution, and ii) the sail equation could be linearized.

This study retains the complete formulation and attacks the problem of finding the exact solution in a direct numerical way. An iterative method for calculating the profile is developed. Beginning with an initial guess at the sail shape, the airflow around the profile

is calculated using Theodorsen's method (Theodorsen (1931) , Theodorsen and Garrick (1933) and Thwaites (1960)), and the resultant pressure distribution determined from Bernoulli's theorem. The sail profile is then redetermined using the full sail equation. An iterative method using a Green's function is described. The airflow around this new estimate of the sail shape is determined and the process repeated until convergence.

Theodorsen's method for calculating the velocity distribution has been used extensively for the analysis of rigid profiles in irrotational flow (Thwaites (1960), Pope (1951)). It involves the use of two conformal mappings to transform the profile into a shape about which the flow is readily determined. The convergence and accuracy of Theodorsen's method has been discussed by Garrick (1952), Ostrowski (1952) and more recently Stern (1973).

Chapter 2 gives a detailed account of the theory required for the exact solution and outlines its computer implementation. Solid aerofoils and sails of large tension are examined in chapter 3. Results are compared with those of thin aerofoil theory and experimental investigations, primarily as a check on Theodorsen's method of determining the pressure distribution. A comprehensive wind tunnel investigation of two-dimensional sails (with constant tension) was performed, and details of the method are discussed in chapter 4.

Chapter 5 displays results of typical profiles, the lift, and centre of pressure for two-dimensional sails. Comparisons are made

between results obtained from the exact solution, thin aerofoil theory and the wind tunnel tests. No theoretical results for drag are shown as the assumption of irrotational, incompressible flow results in the prediction of zero drag. This result was long known as D'Alembert's paradox. For an aerofoil the zero drag results simply from the circumstance that the high speed, and hence low pressure, in the flow around the leading edge generates a thrust that just balances a rearward force produced by the rear portion of the profile. Thus only experimental results are shown for drag and lift to drag ratio.

CHAPTER 2 THEORY

2.1 OUTLINE OF METHOD

Our object is to determine an exact solution for the shape and properties of a two-dimensional sail moving in an inviscid, incompressible fluid. The shape taken up by the sail is a function of the pressure distribution, which is itself dependent on the profile. This interplay between pressure distribution and profile results in an equilibrium sail shape where the pressure forces are exactly balanced by the tension forces. In this chapter we describe the theory of an iterative process to determine the profile: viz.,

(i) estimate profile using thin airfoil theory;

(ii) determine pressure distribution for profile;

(iii) redetermine profile;

(iv) go to (ii).

Determination of the pressure distribution involves the use of conformal mapping techniques to transform the profile into a circle about which the flow is easily calculated. Conformal transformations with application to inviscid, incompressible flows are well described by Milne-Thomson (1968), Woods (1961) and Batchelor (1967), for example. The method we use to calculate the pressure distribution is due to Theodorsen (1932) and although originally intended for graphical analysis is amenable to numerical analysis on a digital computer.

Theodorsen's method maps the profile into a circle by two successive conformal transformations. Inviscid, incompressible flow around the outside of a circle constitutes a two-dimensional external Dirichlet problem (Marsden (1973)), with well known solution. The circulation around the circle is adjusted so that Joukowski's hypothesis is satisfied on the profile. Once the flow about the circle is thereby determined, we use the appropriate transformation to map the velocity field back to points on the sail profile. From this velocity distribution, we calculate the dynamic pressure forces acting across the sail. A full account of Theodorsen's method, with variations, is given by Pope (1951).

Re-calculation of the sail profile is achieved by finding the exact solution to the non-linear equation relating pressure and tension forces. An iterative method using a Green's function shall be described.

2.2 *DEFINITION OF SAIL*

Consider a two-dimensional flexible sail stretched under constant tension T between the fixed points $x = 0$, $y = 0$ and $x = c$, $y = 0$ (c.f. Fig. 1). The sail is flown at an angle of attack α relative to the incident airstream. We denote the fluid velocity at infinity by $\underline{u}_0$, and the camber taken up by the sail by $y(x)$.

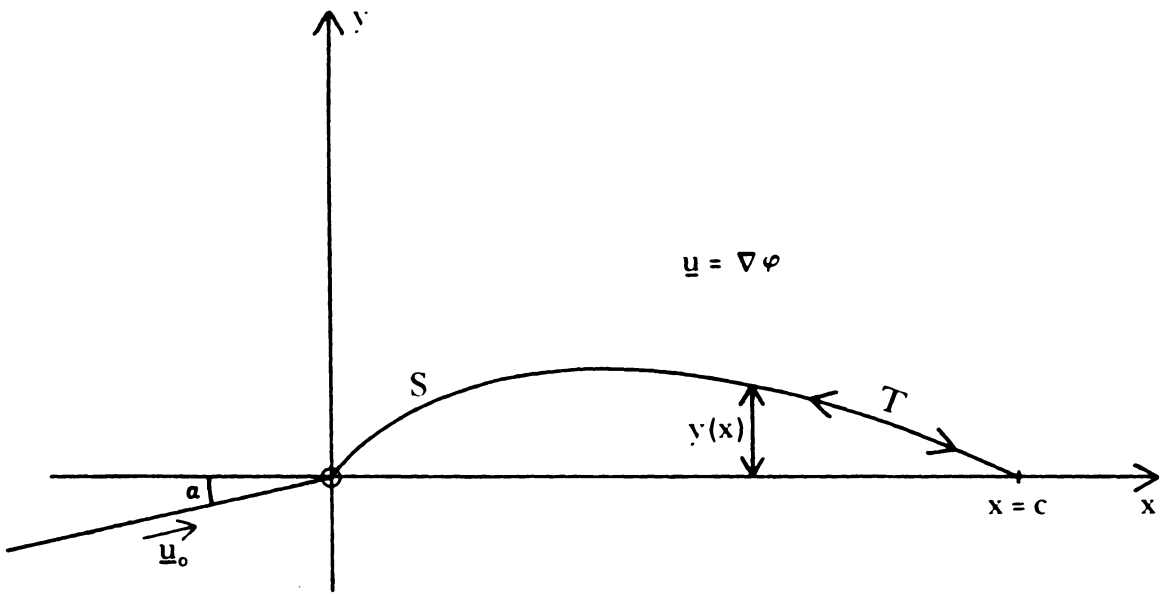

Fig. 2.1 Variables defining two-dimensional sail in inviscid flow.

The mathematical problem is to solve for the velocity potential φ which satisfies the Laplace equation

$$\nabla^2\varphi = 0,$$

subject to the conditions

$$\nabla\varphi \cdot \hat{\underset{\sim}{n}} = 0 \quad \text{on} \quad S, \quad (\hat{\underset{\sim}{n}} \text{ denotes the unit normal})$$

$$\nabla\varphi \to \underset{\sim}{u}_0 = u_0\cos\alpha\,\underset{\sim}{i} + u_0\sin\alpha\,\underset{\sim}{j} \quad \text{at} \quad \infty,$$

$$\nabla\varphi \quad \text{is finite at} \quad x = c;$$

and hence obtain the pressure difference across the sail

$$P = \tfrac{1}{2}\rho\,(\nabla\varphi)^2_{\text{TOP}} - \tfrac{1}{2}\rho\,(\nabla\varphi)^2_{\text{BOTTOM}}$$

$$= \kappa T,$$

where

$$\kappa = \frac{y''(x)}{(1 + y'(x)^2)^{3/2}} \qquad \text{is the curvature.}$$

Introducing dimensionless variables

$$y' = y/c, \quad x' = x/c, \quad \varphi' = \varphi/(u_0 c),$$

$$\kappa' = c\kappa, \quad P' = P/(\tfrac{1}{2}\rho u_0^2),$$

the above problem becomes:

$$\nabla'^2\varphi' = 0 \tag{1a}$$

$$\nabla'\varphi' \cdot \hat{\underset{\sim}{n}} = 0 \quad \text{on} \quad S \tag{1b}$$

$$\nabla'\varphi' \to \cos\alpha\, \underset{\sim}{i} + \sin\alpha\, \underset{\sim}{j} \quad \text{at} \quad \infty \tag{1c}$$

$\nabla'\varphi'$ finite at trailing edge

and
$$P' = \frac{T}{\tfrac{1}{2}\rho u_0^2 c}\,\kappa'$$

$$= K_T\,\kappa'. \tag{1d}$$

We see that only two parameters are required to characterise the sail; viz.,

(i) α the angle of attack,

(ii) the dimensionless variable $K_T = \frac{T}{\tfrac{1}{2}\rho c\, u_0^2}$. We call K_T the *tension number* and it influences the camber taken up by the sail. For large K_T the tension is large compared to the dynamic pressure, and hence the sail has little camber; as the tension number decreases, the sail takes up more camber. The sail length S is variable, even though the chord c and tension T are constant. The tension along the sail is independent of x, since the pressure forces are

perpendicular to the surface.

We proceed (in the following sections) to solve the dimensionless problem expressed by equations (1), but drop the dashes. It will however be more convenient to choose axes such that the leading and trailing edges are at $x = \mp 2a$, where a is a constant (c.f. Fig. 2).

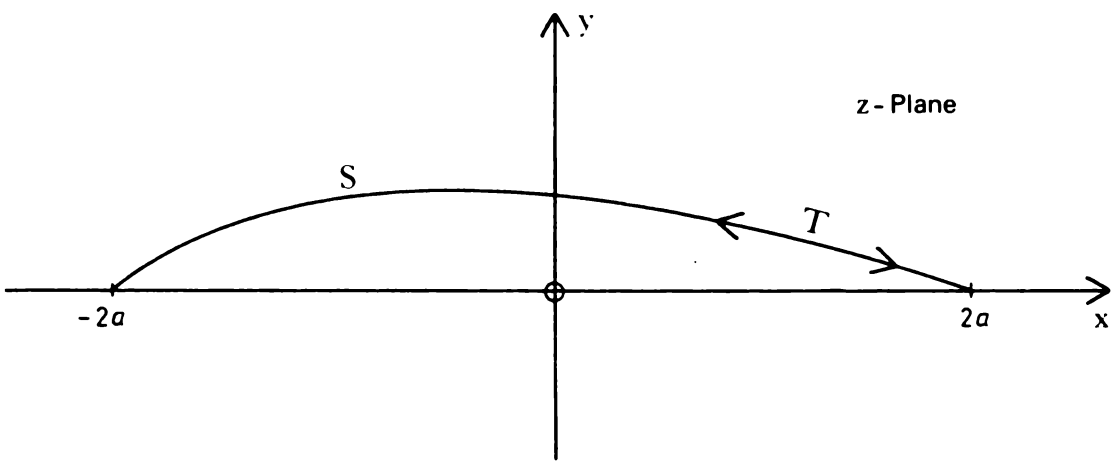

Fig. 2.2 Sail definition in complex z-plane.

We shall define the sail shape by the complex variable

$$z(x) = x + i\, y(x). \tag{2}$$

2.3 *THE JOUKOWSKI TRANSFORM*

The Joukowski transform is defined as

$$z = \xi + \frac{a^2}{\xi}, \tag{3}$$

with inverse transform

$$\xi = \frac{z + \sqrt{z^2 - 4a^2}}{2} \quad . \tag{4}$$

Equation (4) transforms the sail profile defined in the z-plane into a closed curve in the ξ-plane. (The sign of the square root is chosen so that $\xi \to z$ at infinity.)

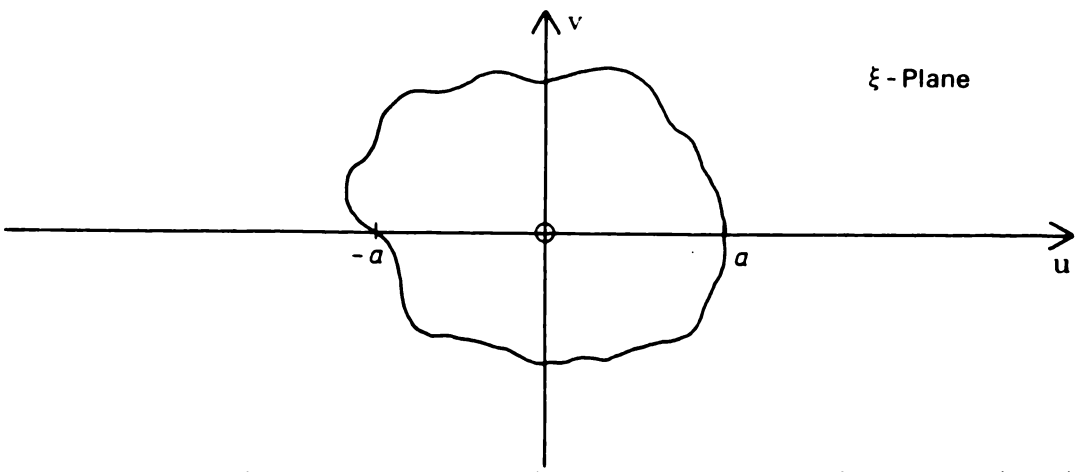

Fig. 2.3 Joukowski transform of profile resulting in approximate circle in ξ-plane.

The curve in the ξ-plane may be described by the complex function

$$\xi = u + i\,v \quad . \tag{5}$$

If the profile in the z-plane is a circular arc, then the transformed curve will be a circle. However, in general the transformed curve is only approximately circular, and is not centred on the origin.

At this point it is necessary to derive two results which will be used later. Consider the case where the z-plane profile is a circular arc (c.f. Fig. 4(a)).

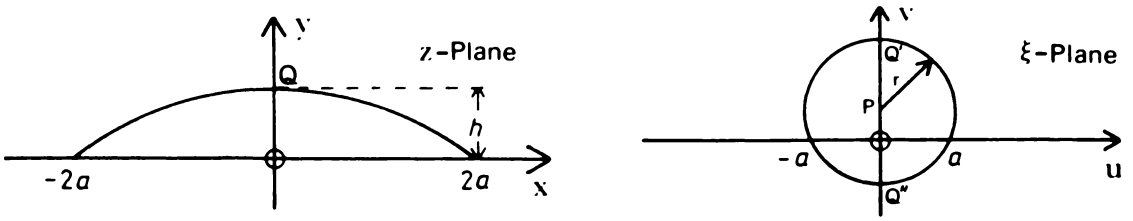

Fig. 2.4 Joukowski transform of circular arc profile.

Note that point Q transforms into the two points, Q' and Q'': thus

$$z = ih \qquad \text{(at } Q\text{)}$$

so that
$$\xi_{Q'} = \frac{z + \sqrt{z^2 - 4a^2}}{2}$$

$$= \frac{i}{2}\left(h + \sqrt{h^2 + 4a^2}\right)$$

and
$$\xi_{Q''} = \frac{i}{2}\left(h - \sqrt{h^2 + 4a^2}\right) .$$

Hence the centre of the circle in the ξ-plane has ordinate

$$\xi_P = \tfrac{1}{2}(\xi_{Q'} + \xi_{Q''})$$

$$= i\,\frac{h}{2}$$

- i.e. the centre is at

$$\xi = (0, \tfrac{h}{2}), \tag{6}$$

and the radius is

$$r = \tfrac{1}{2}\sqrt{h^2 + 4a^2} \tag{7}$$

2.4 *TRANSFORMATION OF APPROXIMATE CIRCLE INTO EXACT CIRCLE*

We require a second conformal transformation to map the approximate circle in the ξ-plane into a true circle. Consider a general sail profile, so that application of the Joukowski transform yields a non-circular closed curve which is not centred on the origin (c.f. Fig. 5).

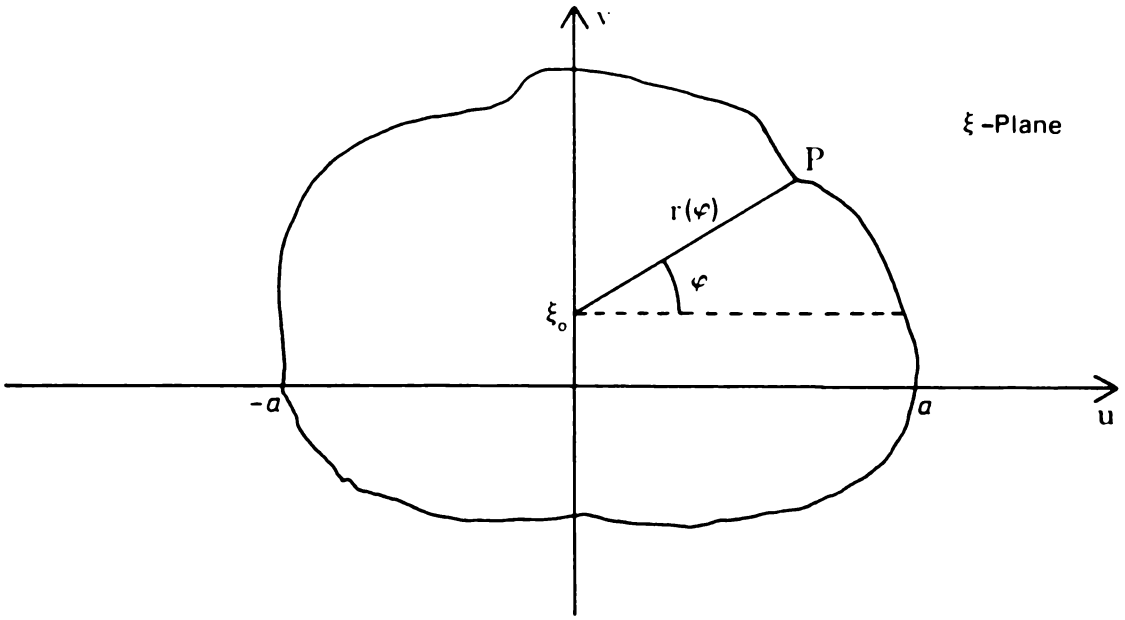

Fig. 2.5 Definition of variables in ξ-plane.

Let the "radius" of this closed curve be given by the function

$$r(\varphi) = b\, e^{\psi(\varphi)} \tag{8}$$

where b is a constant. Letting ξ_0 denote the centre of the approximate circle, the equation of the curve is

$$\xi = \xi_0 + b\, e^{\psi(\varphi) + i\varphi}. \tag{9}$$

In the standard Theodorsen method (Pope (1951)), ξ_0 is assumed to be at the origin. In the present modification the functions $r(\varphi)$ and $\psi(\varphi)$ have a smaller variation and we anticipate the convergence of the method is enhanced.

Let the constant b take the value of the average radius of the approximate circle - i.e.

$$b = \frac{1}{2\pi}\int_0^{2\pi} r(\varphi)\,d\varphi\ . \tag{10}$$

Consequently, the value of the function $\psi(\varphi)$ is equally distributed about the origin - i.e. from (8)

$$\int_0^{2\pi} \psi(\varphi)\, d\varphi = 0,$$

so that

$$\psi(\varphi) = \ln\left[\frac{r(\varphi)}{b}\right] \quad . \tag{11}$$

It follows from the Riemann Mapping Theorem (Marsden (1973)) that the ξ - plane can be mapped conformally into the ξ_1 - plane, such that:

(i) the curve is a circle about the origin in the ξ_1 -plane

(ii) $\dfrac{\xi_1}{\xi - \xi_0} \to 1$ at infinity.

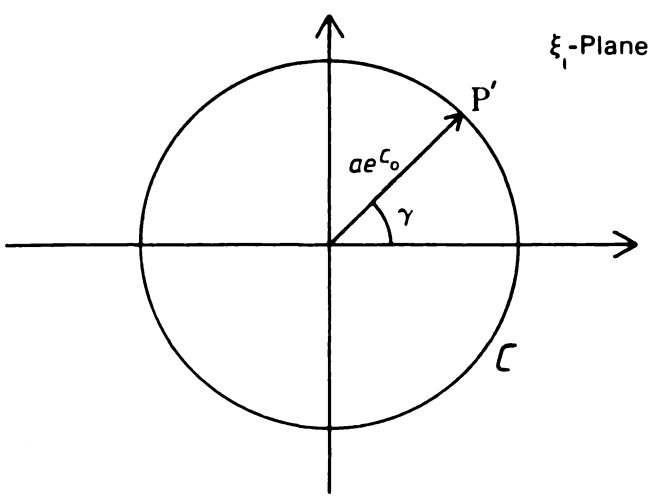

Fig. 2.6 Circle in ξ_1-plane of radius $a\, e^{c_0}$.

The equation of the circle C is given by

$$\xi_1 = a\, e^{c_0} + c\gamma, \tag{12}$$

where γ is an angle that differs slightly from φ - say by an amount $\varepsilon(\varphi)$, so that

$$\gamma = \varphi + \varepsilon(\varphi) \tag{13}$$

where $\varepsilon(\varphi)$ is a small unknown function. The constant c_0 may be evaluated as

$$c_0 = \frac{1}{2\pi}\int_0^{2\pi} \psi(\varphi)\,d\varphi + \ln\left(\frac{b}{a}\right)$$

$$= \ln\left(\frac{b}{a}\right) \quad . \tag{14}$$

Consider the analytic function

$$\ln\left[\frac{a\, e^{c_0(\xi - \xi_0)}}{b\, \xi_1}\right] \quad ,$$

which on C may be written as

$$F(\varphi) = \ln\left[\frac{e^{\psi(\varphi) + i\varphi}}{e^{i\gamma}}\right]$$

$$= \psi(\varphi) - i\,\varepsilon(\varphi) \quad . \tag{15}$$

The real and imaginary parts, $\psi(\varphi)$ and $-\varepsilon(\varphi)$, of the analytic function $F(\varphi)$ are harmonic conjugate functions. Writing

$\varepsilon(\varphi) = \bar{\varepsilon}(\gamma)$, where γ is given by (13), it follows that

$\psi(\gamma - \bar{\varepsilon}(\gamma))$ and $-\bar{\varepsilon}(\gamma)$ are conjugate harmonic functions on the circle. To determine the function $\bar{\varepsilon}(\gamma)$ we assume initially $\bar{\varepsilon}_0(\gamma) = 0$, and iterate using the scheme

$$\bar{\varepsilon}_n(\gamma) = -\ \text{CONJUGATE}\ \ \psi(\gamma - \bar{\varepsilon}_{n-1}(\gamma)). \tag{16}$$

Having determined $\bar{\varepsilon}(\gamma)$, we have

$$\varepsilon(\varphi) = \bar{\varepsilon}(\varphi + \varepsilon(\varphi)), \tag{17}$$

e.g. by initially guessing $\varepsilon_0(\varphi) = 0$, and then solving iteratively using the scheme

$$\varepsilon_n(\varphi) = \bar{\varepsilon}(\varphi + \varepsilon_{n-1}(\varphi)) \ . \tag{18}$$

To use equation (16) we must find the conjugate harmonic function of $\psi(\gamma - \bar{\varepsilon}_{n-1}(\gamma))$. The method used to do this is due to Watson (1945) - see also Thwaites (1960), Stern (1973) and Appendix 1. If the function ψ is tabulated at $2N$ points around the circle C, then the conjugate function $-\bar{\varepsilon}$ is given by

$$\bar{\varepsilon}_m = \frac{-1}{N} \sum_{\substack{p=1 \\ (p \text{ odd})}}^{N-1} \cot\left(\frac{p\pi}{2N}\right) [\psi_{m+p} - \psi_{m-p}] \tag{19}$$

where $\bar{\varepsilon}_m = \bar{\varepsilon}(\varphi_m)$,

$\psi_n = \psi(\varphi_n)$,

and $\varphi_p = \frac{p\pi}{N}$.

2.5 *CALCULATION OF FLUID VELOCITY AND PRESSURE DISTRIBUTION ON THE SAIL SURFACE*

So far we have transformed our sail profile into a circle in the ξ_1 - plane. Our problem now is to solve for the flow around the circle, and transform the results back into the z - plane.

The solution for two-dimensional flow of an inviscid, incompressible fluid past a cylinder is a classical problem, treated in most hydrodynamic texts (e.g. Milne - Thomson (1968) and Batchelor (1967)). Recalling that α is the angle of attack in radians, then for

$$|\xi_1| \geq a\, e^{c_0}$$

we have the complex potential in the ξ_1 - plane given by

$$f(\xi_1) = u_0\, \xi_1\, e^{-i\alpha} + \frac{u_0\, a^2 e^{2c_0}\, e^{i\alpha}}{\xi_1} + i\kappa \quad \ln(\xi_1), \qquad (20)$$

where the last term represents the circulation.

On C, $\xi_1 = a\, e^{c_0 + i\gamma}$, hence the complex potential is given by

$$f(\xi_1) = 2\, u_0\, a e^{c_0} \cos(\gamma-\alpha) - \kappa\left[(\gamma-\alpha) - i\, \ln(a e^{c_0})\right] \qquad (21)$$

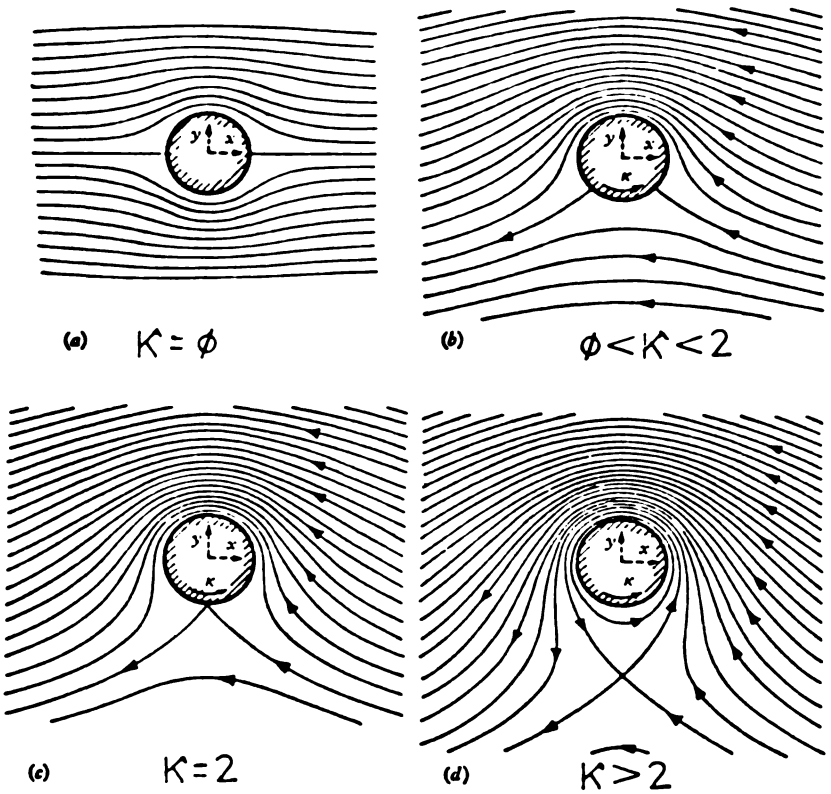

Fig. 2.7 Adjusting the circulation κ to shift the stagnation points. (Batchelor (1967))

The circulation $2\pi\kappa$ about the cylinder is at present undetermined; by adjusting the magnitude of κ, we move the stagnation points around the surface of the cylinder, and hence along the surface of the z-plane sail profile. By Joukowski's hypothesis we require that the rear stagnation point on the profile coincides with the trailing edge. This hypothesis may be justified by observation of real viscous flows over lifting surfaces; it is seen that a vortex is shed from the airfoil, leaving precisely the circulation required to shift the rear stagnation point to the trailing edge. The flow around the sharp trailing edge would otherwise cause a singularity in the velocity distribution; shifting the stagnation point to the edge effectively cancels the singularity leaving a finite velocity.

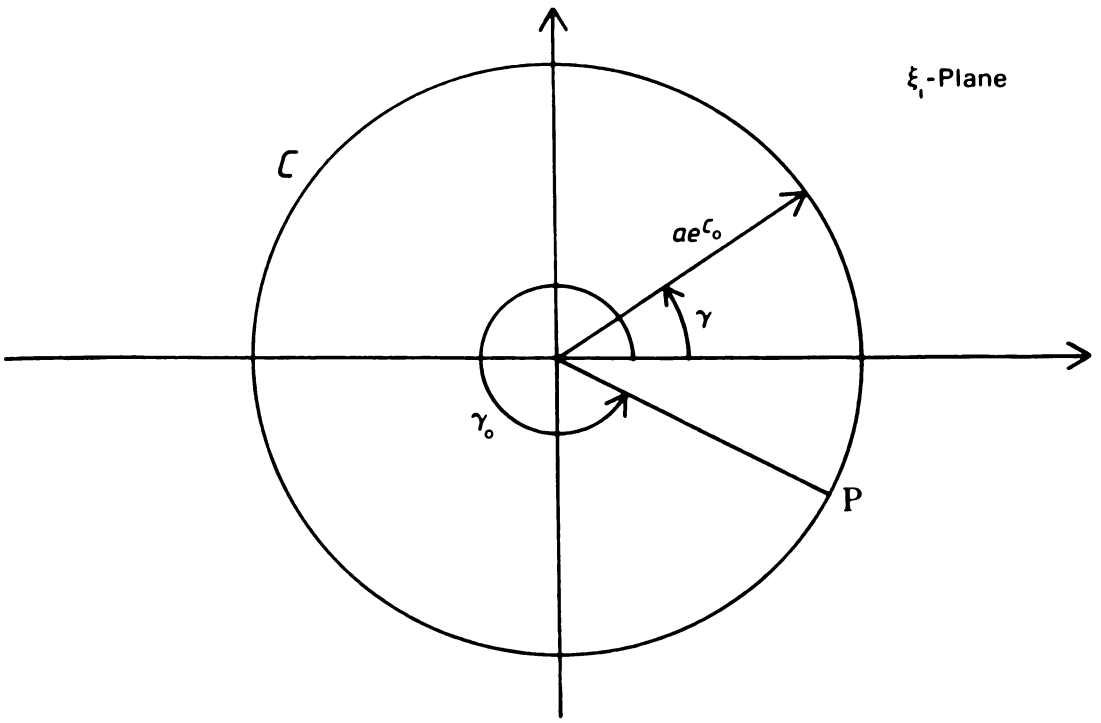

Fig. 2.8 Definition of variables in ξ_1-plane.
P corresponds to trailing edge of sail profile.

The fluid speed over the surface of the sail is

$$u(z) = \left| \frac{d\, f(\xi_1)_C}{dz} \right|$$

$$= \left| \frac{d\, f(\xi_1)_C}{d\, \xi_1} \right| \left| \frac{d\, \xi_1}{d\xi} \right| \left| \frac{d\xi}{dz} \right| . \qquad (22)$$

The first factor may be evaluated as

$$\left| \frac{d\, f(\xi_1)_C}{d\xi_1} \right| = \left| \frac{d\, f(\xi_1)_C}{d\gamma} \right| \left| \frac{d\gamma}{d\xi_1} \right| ,$$

where

$$\left| \frac{d\, f(\xi_1)_C}{d\gamma} \right| = | - 2u_0\, ae^{c_0} \sin(\gamma-\alpha) - \kappa | ,$$

and

$$\left| \frac{d\gamma}{d\xi_1} \right| = \left| \frac{-i}{ae^{c_0} + i\gamma} \right| ;$$

hence

$$\left| \frac{d\, f(\xi_1)_C}{d\xi_1} \right| = \left| \frac{2i\, u_0\, ae^{c_0} \sin(\gamma-\alpha) + i\kappa}{ae^{c_0} + i\gamma} \right|$$

which defines the fluid speed on the boundary C in the ξ_1 plane. If the trailing edge of the sail profile transforms to point $P(\gamma=\gamma_0)$ on the curve C, then the rear stagnation point in the plane must also be at P - thus at γ_0 we have

$$\left| \frac{d\, f(\xi_1)_C}{d\xi_1} \right|_{(\gamma\, =\, \gamma_0)} = 0,$$

so that

$$\kappa = -2\, u_0\, ae^{c_0} \sin(\gamma_0 - \alpha).$$

Hence the first factor of (22) becomes

$$\left| \frac{d\, f(\xi_1)_C}{d\xi_1} \right| = \left| 2i\, u_0\, e^{-i\gamma} [\sin(\gamma-\alpha) - \sin(\gamma_0-\alpha)] \right| . \tag{23}$$

The second factor $\left| \frac{d\,\xi_1}{d\xi} \right|$ is now evaluated. Recalling from equations (12) and (13) that

$$\xi_1 = ae^{c_0} + i(\varphi + \varepsilon(\varphi)) \quad ,$$

and differentiating, we obtain

$$\frac{d\,\xi_1}{d\varphi} = ai(1 + \varepsilon'(\varphi))e^{c_0} + i(\varphi + \varepsilon(\varphi))$$

where $\varepsilon'(\varphi) = \frac{d}{d\varphi}\varepsilon(\varphi)$.

Similarly, from equation (9) we have

$$\frac{d\xi}{d\varphi} = (\psi'(\varphi) + i)be^{\psi(\varphi) + i\varphi}$$

where $$\psi'(\varphi) = \frac{d}{d\varphi}\psi(\varphi),$$

and hence

$$\left| \frac{d\,\xi_1}{d\xi} \right| = \left| \frac{i\,a(1 + \varepsilon'(\varphi))e^{c_0 + i(\varphi + \varepsilon(\varphi))}}{(\psi'(\varphi) + i)(\xi - \xi_0)} \right| . \quad (24)$$

The third factor is straightforward to evaluate from the Joukowski transform. Differentiating equation (3) and rearranging yields

$$\left| \frac{d\xi}{dz} \right| = \left| \frac{\xi^2}{\xi^2 - a^2} \right| . \quad (25)$$

Finally, multiplying the three factors together gives

$$u(z) = \left| \frac{2\,u_0\,\xi^2\,ae^{c_0}(1 + \varepsilon'(\varphi))}{(\xi - \xi_0)(\xi^2 - a^2)(i + \psi'(\varphi))} [\sin(\gamma - \alpha) - \sin(\gamma_0 - \alpha)] \right| \quad (26)$$

where $\gamma = \varphi + \varepsilon(\varphi)$.

It should be noted that the R.H.S. of (26) is a function of φ only. The point (x,y) in the z plane to which the speed $u(z)$ corresponds is given by

$$z = \xi(\varphi) + \frac{a^2}{\xi(\varphi)} ,$$

where $\xi(\varphi)$ is on the boundary of the approximate circle.

The pressure difference across the sail follows from Bernoulli's equation

$$p + \tfrac{1}{2}\rho u^2 = \text{constant:}$$

thus pressure difference

$$P(z) = \tfrac{1}{2}\rho \left(u(z)^2_{\text{BOTTOM}} - u(z)^2_{\text{TOP}}\right), \tag{27}$$

and we have a method for finding the pressure distribution of a sail of arbitrary profile.

We now proceed to evaluate the limiting velocity at the trailing edge. Recall that at the trailing edge we have the stagnation point coinciding with a singularity in the velocity distribution. The result that the velocity at this point is well defined and finite may be used as a check on the accuracy of the numerical method.

We consider $u(z)$ as z approaches the trailing edge:

$$\lim_{z\to \text{T.E.}} u(z) = \lim_{\xi\to a} \left| \frac{2u_0\ \xi^2\ ae^{\mathcal{C}_0}(1+\varepsilon'(\varphi))}{(\xi-\xi_0)(\xi^2-a^2)(i+\psi'(\varphi))} [\sin(\gamma-\alpha)-\sin(\gamma_0-\alpha)] \right|$$

Using L'Hopital's rule we evaluate

$$\lim_{\varphi\to\varphi_0} \left[\frac{\sin(\varphi + \varepsilon(\varphi) - \alpha) - \sin(\varphi_0 - \varepsilon(\varphi_0) - \alpha)}{\xi - a} \right]$$

$$= \lim_{\varphi\to\varphi_0} \left[\frac{\frac{d}{d\varphi}\{\sin(\varphi + \varepsilon(\varphi) - \alpha) - \sin(\varphi_0 - \varepsilon(\varphi_0) - \alpha)\}}{\frac{d}{d\varphi}(\xi - a)} \right]$$

$$= \frac{(1+\varepsilon'(\varphi_0))\ \cos(\varphi_0 + \varepsilon(\varphi_0) - \alpha)}{(a-\xi_0)(i + \psi'(\varphi_0))} \quad .$$

Thus the velocity at the trailing edge is given by

$$u_{T.E.} = u_0\ a^2\ e^{c_0} \left| \frac{(1+\varepsilon'(\varphi_0))^2\ \cos(\varphi_0 + \varepsilon(\varphi_0) - \alpha)}{(i + \psi'(\varphi_0))^2\ (a-\xi_0)^2} \right| . \qquad (28)$$

FLOWCHART FOR DETERMINING EXACT PRESSURE DISTRIBUTION

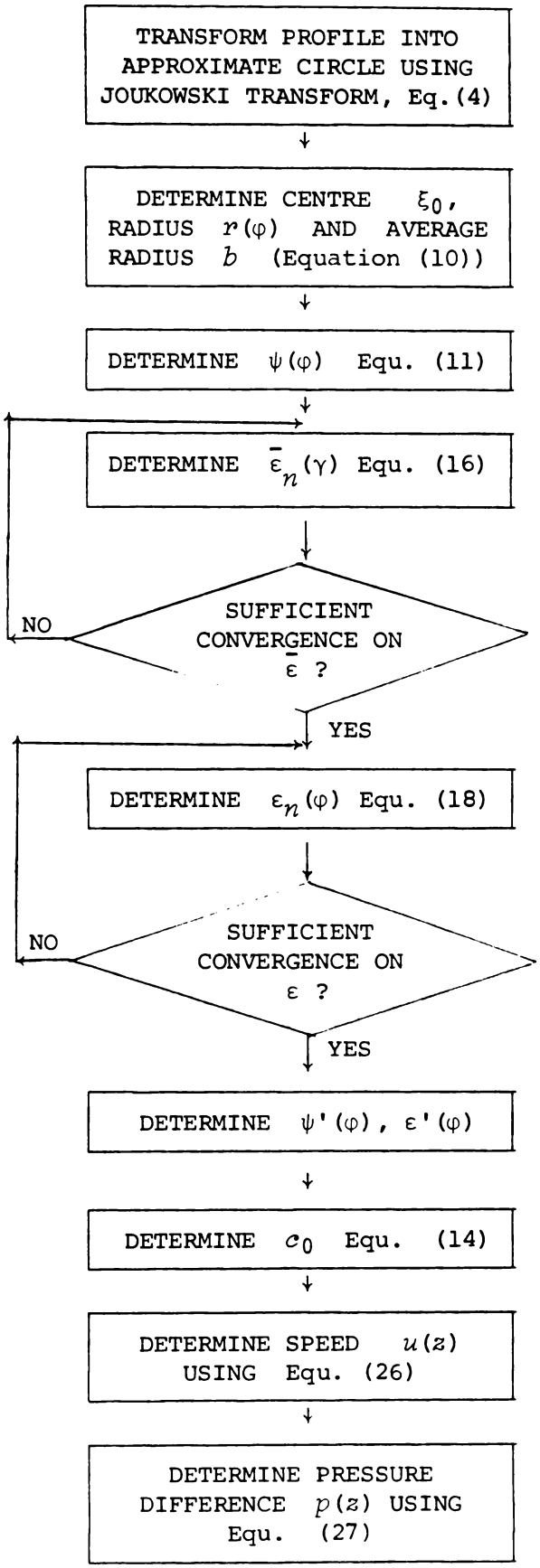

Flowchart 1

2.6 *DETERMINATION OF SAIL PROFILE FOR A GIVEN PRESSURE DISTRIBUTION*

We consider our theoretical sail to be a very thin flexible membrane, so that the unique shape it takes up is such that pressure and tension forces are balanced.

Consider the sail cross-section shown in Fig. 9.

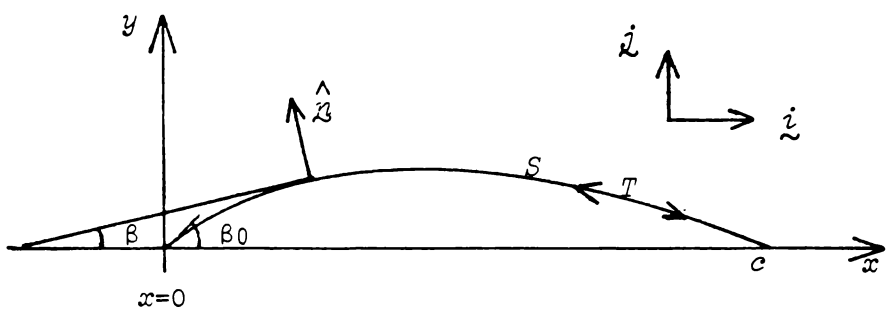

Fig. 2.9 Parameters defining sail profile.

Here β denotes the angle between the tangent to the sail and the x axis, s the arc length along the sail, $P(s)$ the pressure difference across the sail, T the (constant) tension and $\hat{n}$ the local unit normal where

$$\hat{n} = - \sin\beta\, i + \cos\beta\, j \ .$$

The pressure difference on the sail element $d\sigma$ produces a nett force $P(\sigma)\ \hat{n}\ d\sigma$, hence the total nett force on the sail (between $s = 0$ and $s = S$) is

$$\int_0^S P(\sigma)\hat{\underset{\sim}{n}}\, d\sigma.$$

For equilibrium, this pressure force must be balanced by the tension i.e.

$$T(\cos\beta\,\underset{\sim}{i} + \sin\beta\,\underset{\sim}{j}) - (\cos\beta_0\,\underset{\sim}{i} + \sin\beta_0\,\underset{\sim}{j})$$
$$+ \int_0^S P(\sigma)\hat{\underset{\sim}{n}}\, d\sigma = 0.$$

Differentiating with respect to s, and equating like components, gives

$$\frac{d}{ds}(T\cos\beta) = P(s)\sin\beta \tag{29}$$

and

$$\frac{d}{ds}(T\sin\beta) = -P(s)\cos\beta\,. \tag{30}$$

Considering sail element ds (c.f. Fig. 10),

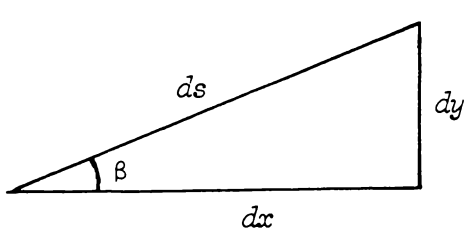

Fig. 2.10 Sail element ds

we have

$$\frac{d}{ds} = \cos\beta\,\frac{d}{dx} \tag{31}$$

and

$$y'(x) = \tan\beta \tag{32}$$

and hence from equation (32)

$$\sin\beta = \frac{y'(x)}{(1 + y'(x)^2)^{\frac{1}{2}}} \quad .$$

Substituting equations (31) and (33) into (30) we obtain

$$\frac{d}{dx}\left(\frac{T\, y'(x)}{(1 + y'(x)^2)^{\frac{1}{2}}} \right) = - P(x),$$

or

$$P(x) = \frac{-T\, y''(x)}{(1 + y'(x)^2)^{3/2}} \quad . \tag{34}$$

Thus the problem of determining the camber taken up by the sail for a given pressure distribution reduces to that of solving equation (34) subject to boundary conditions

$$\left.\begin{aligned} y(0) &= 0 \\ \text{and} \qquad y(c) &= 0. \end{aligned}\right\} \tag{35}$$

We may rewrite equation (34) in a more convenient form, viz.

$$-T\, y''(x) = g(x) \tag{36}$$

where $$g(x) = (1 + y'(x))^{3/2}\ P(x),$$

which is the differential equation for a string, under load $g(x)$. The solution of (36) may be found using a Green's function $G(x,t)$, representing the displacement of the string under a point load at $x = t$ (c.f. Fig. 11).

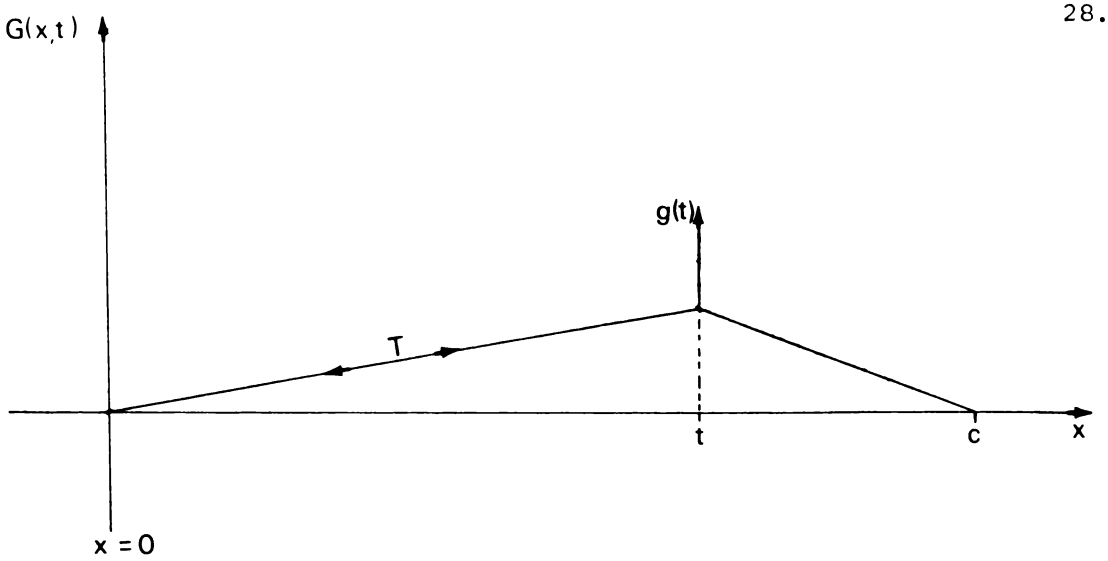

Fig. 2.11 Definition of Green's function $G(x,t)$, as the displacement of a string under a point load $g(t)$.

We have the form

$$G(x,t) = Ax \qquad (0 \leq x \leq t)$$

$$= B(c-x) \qquad (t \leq x \leq c) \quad ,$$

where $At = B(c-t)$

and for a unit force applied at $x = t$

$$T(A + B) = 1.$$

Solving for A and B we obtain

$$A = \frac{c - T}{cT}$$

and $$B = \frac{t}{cT} \quad ,$$

so that the Green's function is

$$\left.\begin{aligned} G(x,t) &= \frac{x(c-t)}{cT} \quad (0 \leq x \leq t) \\ &= \frac{t(c-x)}{cT} \quad (t \leq x \leq c). \end{aligned}\right\}, \tag{37}$$

and hence from equation (36)

$$y(x) = \int_0^c G(x,t)\ P(t)\,[1 + y'(t)^2]^{3/2}\ dt\,. \tag{38}$$

Equation (38) is an integral equation equivalent to equations (34) and (35), and may be solved iteratively using the scheme

$$y_n(x) = \int_0^c G(x,t)\ P(t)\,[1 + y'_{n-1}(t)^2]^{3/2}\ dt \tag{39}$$

where $y_n(x)$ is the nth approximation to $y(x)$.

It should be noted that this scheme for calculating the sail profile yields the exact solution. The previous thin airfoil theory studies of this problem (Thwaites (1961), Nielsen (1963)), have linearised (34), by making the assumption that the slopes, $y'(x)$, are negligible over the sail - i.e. consider the reduced equation

$$P(x) = -\,T\,y''(x),$$

which is often called the cable equation.

FLOWCHART TO DETERMINE PROFILE, GIVEN P(x)

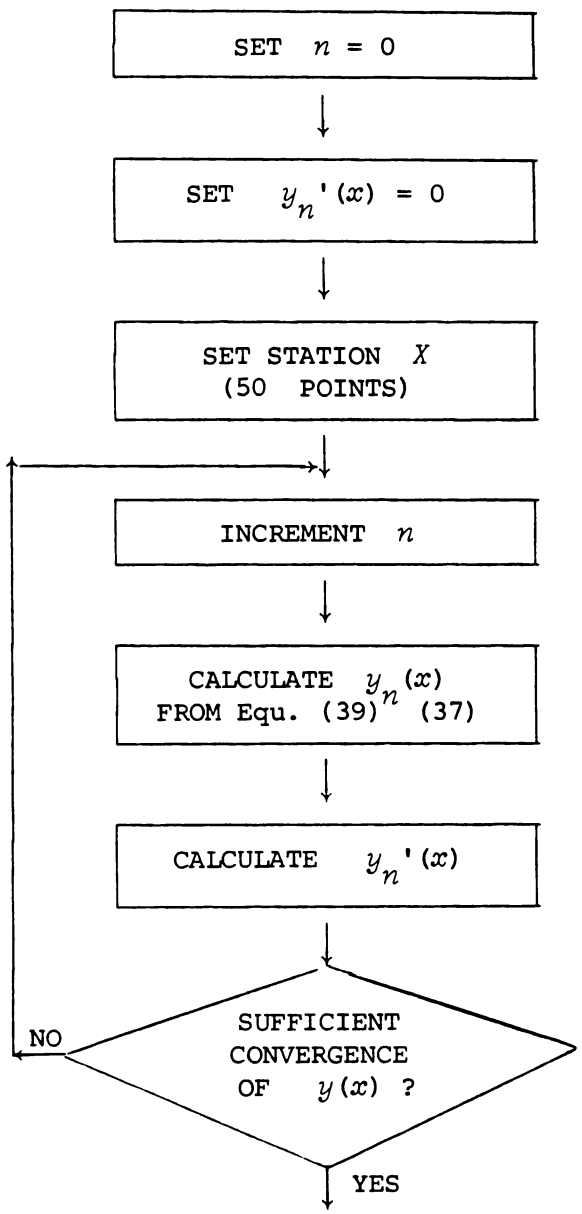

Flowchart 2

Consider the behaviour of a physical sail under a sudden change of conditions - say a rapid increase in air velocity (wind gust). There will be an initial change in the pressure distribution over the sail, thus altering the profile, e.g. increasing the camber. However the change in camber will cause the pressure distribution to change. This interplay between pressure distribution and camber will continue until the pressure forces are exactly balanced by the tension force. A computer program may be developed to operate in the same manner - viz., determine the pressure distribution for a given profile, re-estimate the profile and pressure distribution iteratively (with satisfactory convergence anticipated). The flowchart for such a scheme is shown on the following page.

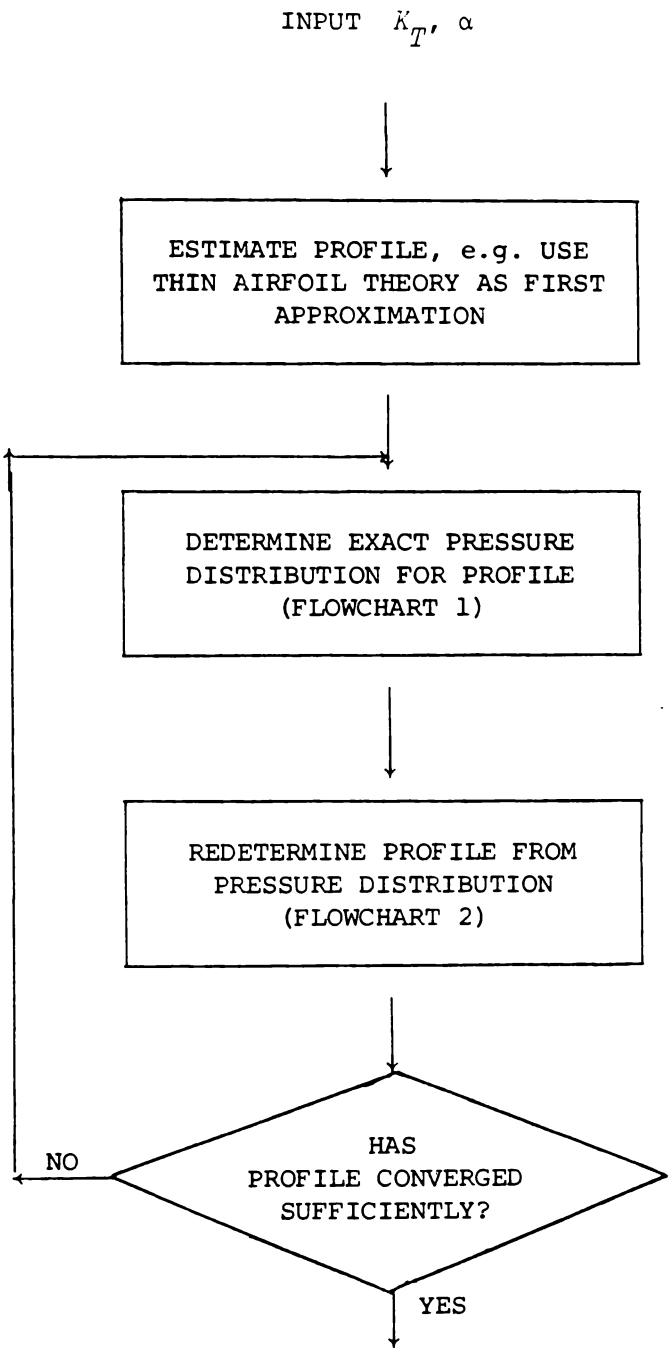
INPUT K_T, α
ESTIMATE PROFILE, e.g. USE THIN AIRFOIL THEORY AS FIRST APPROXIMATION
DETERMINE EXACT PRESSURE DISTRIBUTION FOR PROFILE (FLOWCHART 1)
REDETERMINE PROFILE FROM PRESSURE DISTRIBUTION (FLOWCHART 2)
HAS PROFILE CONVERGED SUFFICIENTLY?
NO
YES

Flowchart 3

2.7 *LIFT, CENTRE OF PRESSURE AND PROFILE CHARACTERISTICS*

The most important performance features of a wing are its lift, drag and stability. The assumption that the fluid has negligible viscosity (c.f. Chapter 1) precludes SAIL from calculating results for drag. The lift acting on the sail is readily calculated by integrating the appropriate component of the pressure difference across the sail. A small correction is then included for the leading edge force. Static longitudinal stability may be determined by studying the centre of pressure movement with variation of angle of attack and tension number.

The most important profile characteristics are the maximum camber and position of maximum camber. Other parameters that may be of interest are the ratio of sail to chord length, and the leading and trailing edge angles.

2.7.1 *LEADING EDGE FORCE*

The stagnation point, for an aerofoil flown at a positive angle of attack, is on the lower surface just behind the leading edge. Consequently back-flow occurs from the stagnation point around the leading edge to the upper surface.

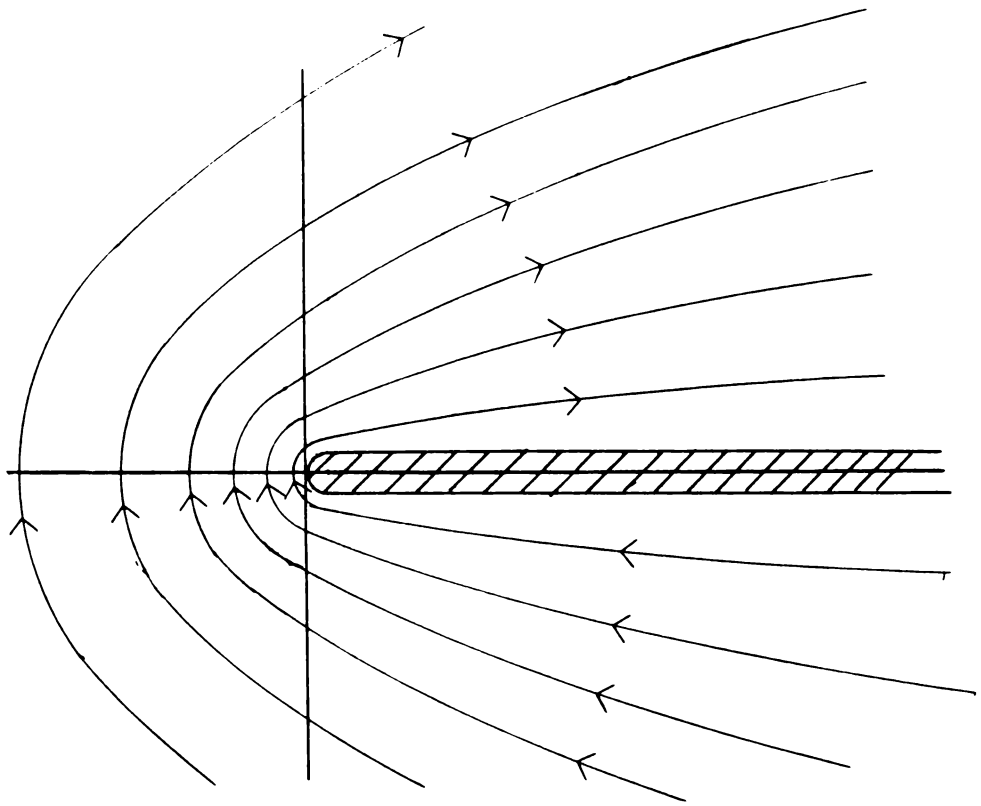

Fig. 2.12 Stream lines very close to leading edge of a flat plate.

The fluid speed around the leading edge increases as the leading edge radius is decreased, creating an area of reduced pressure. This effectively results in a suction force being applied to the profile through the leading edge.

We now set out to determine the leading edge force (denoted F_{LE}) acting on the sail. Consider the flat plate, at an angle of attack α to the incident airstream.

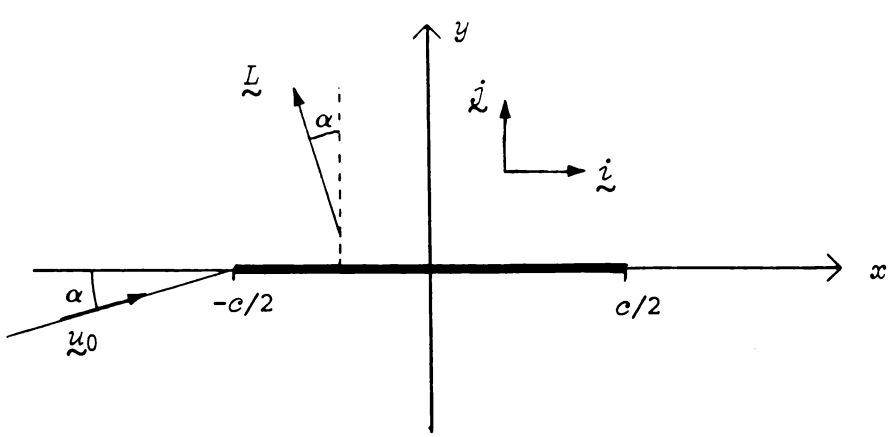

Fig. 2.13 Configuration of a flat plate to determine leading edge force.

Near the leading edge, it can be shown that the fluid speed on the plate surface is given by

$$q_s \approx u_0 \sqrt{\frac{c}{s}} \sin\alpha \qquad (40)$$

where s is the arc length along the surface behind the leading edge. The edge force is given by the x-component of the lift, namely

$$\underset{\sim}{F}_{LE} = -\pi \rho u_0^2 c \sin^2\alpha \, \underset{\sim}{i} \qquad (41)$$

For circular arc profiles equation (40) is modified slightly to allow for the leading edge angle, i.e.

$$q_s \approx u_0 \sqrt{\frac{c}{s}} \sin\alpha \cos\gamma_1$$

where γ_1 is the leading edge angle. In general for cambered profiles we can write

$$q_s \approx u_0 \sqrt{\frac{c}{s}} \sin\alpha \, \lambda \qquad (42)$$

where λ is a number of order 1.

Note that although there is a discontinuity in the pressure distribution at the leading edge (Fig. 2.15) it is acting at an infinitely small point, and hence gives a finite leading edge force.

2.7.2 *LIFT*

The lift is usually expressed as a non-dimensional lift coefficient, defined as

$$C_L = \frac{L}{\frac{1}{2}\rho c u_0^2} \,. \tag{43}$$

for two dimensional flow. The lift L is defined to be that force acting on the aerofoil orthogonal to the free stream velocity $\underset{\sim}{u}_0$.

Consider a sail as defined in Fig. 2.14 with a chord of 2 units (leading edge at $x = -1$, trailing edge at $x = +1$).

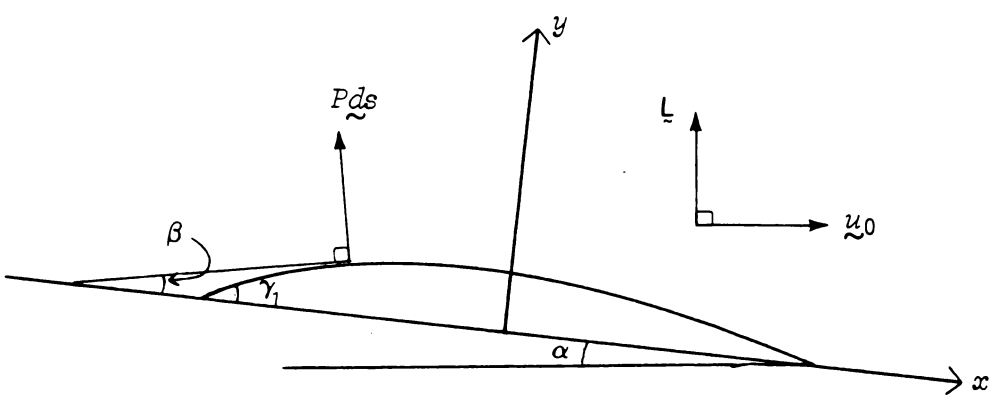

Fig. 2.14 Notation and forces acting on sail.
P is the pressure difference between the upper and lower surfaces at s.

Note that Pds acts in a direction normal to the sail surface. Thus the lift generated by the sail element ds is

$$dL^* = Pds \cos(\beta-\alpha) \tag{44}$$

Substitution of equations (31) and (32) into (41) and integration w.r.t. x yields

$$L^* = \int_{-1}^{+1} P(x)(\cos\alpha + y'(x)\sin\alpha)\,dx \tag{45}$$

where L^* is the lift due to the pressure difference only. Considering drag D on sail element ds we have

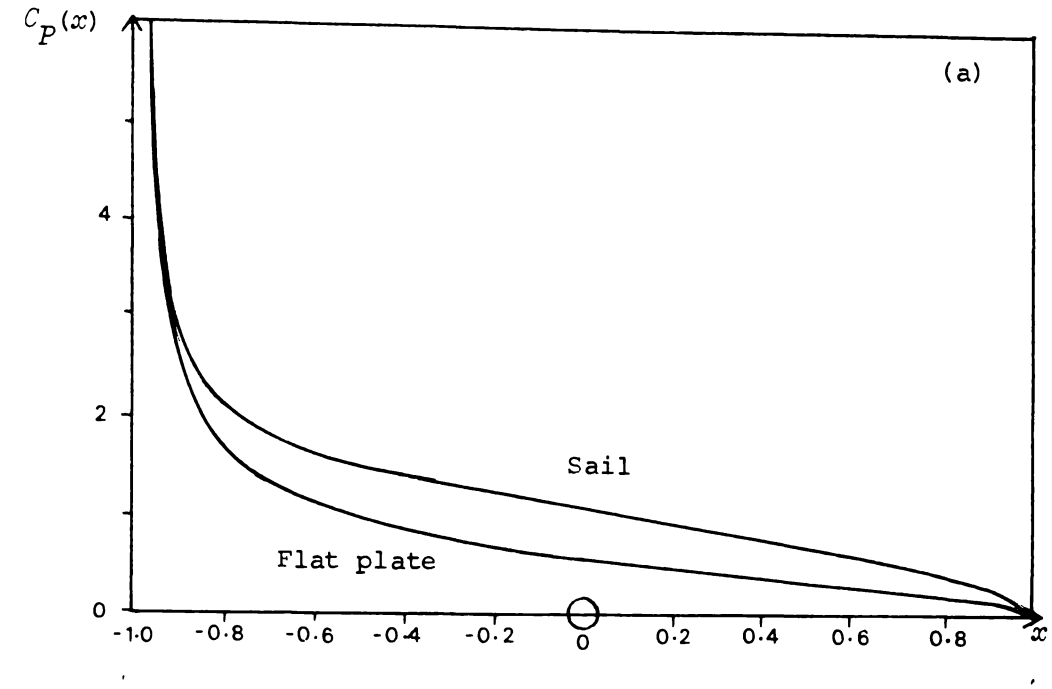

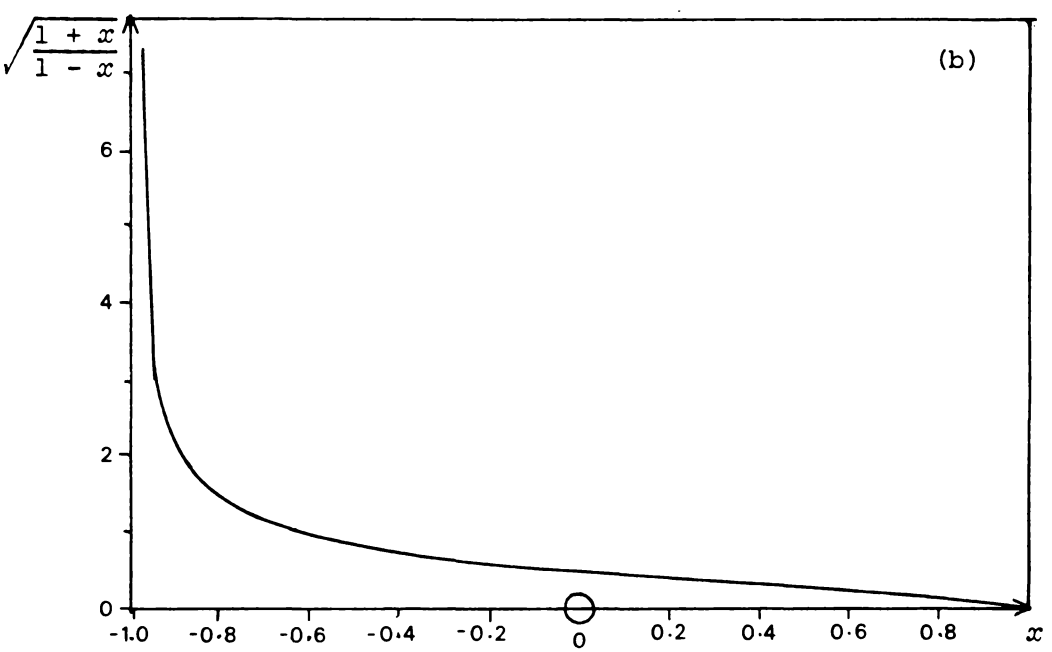

Fig. 2.15 (a) Typical pressure distributions for a sail and flat plate, showing the singularity at the leading edge. ($C_P(x) = P(x)/\frac{1}{2}\rho c u_0^2$)

(b) The function $\sqrt{\frac{1+x}{1-x}}$ having a similar form to the above pressure distributions.

$$dD = P\,ds\,\sin(\beta-\alpha)$$
$$= P\,\tan\beta\,\cos\alpha\,dx - P\,\sin\alpha\,dx\ .$$

Integration yields

$$D = \cos\alpha \int_{-1}^{1} P(x)y'(x)\,dx - \sin\alpha \int_{-1}^{1} P(x)\,dx.$$

However inviscid flow theory predicts zero drag so we have

$$\int_{-1}^{1} P(x)y'(x)\,dx = \tan\alpha \int_{-1}^{1} P(x)\,dx.$$

Substitution into (45) gives

$$L^* = \cos\alpha \int_{-1}^{1} P(x)\,dx + \tan\alpha\,\sin\alpha \int_{-1}^{1} P(x)\,dx$$

$$= \frac{1}{\cos\alpha} \int_{-1}^{1} P(x)\,dx. \qquad (46)$$

Thus the total lift is

$$\left.\begin{aligned} L &= L^* + F_{LE}\,\sin(\gamma_1-\alpha) \\ \text{where}\quad F_{LE} &= -\pi\rho\,u_0{}^2 c\,\sin^2\alpha\,\lambda^2 \\ \text{and}\quad \lambda &= \lim_{s\to 0} \frac{q_s}{u_0\,\sin\alpha}\,\sqrt{\frac{s}{c}}\ . \end{aligned}\right\} \qquad (47)$$

The integral in equation (46) must be evaluated numerically so the pressure distribution $P(x)$ must be well behaved. Observation of the form of $P(x)$ (Fig. 2.15) shows the existence of a singularity at the leading edge. The sail results shown are for a typical sail, and were calculated by the routine developed in this chapter. The flat plate results are from thin-aerofoil theory.

Numerical integration using the trapezoidal rule is accurate over most of the profile. However it breaks down in the vicinity of the singularity where another method is required.

Thin aerofoil theory predicts a pressure distribution of the form (c.f. Fig. 15(b))

$$P(x) \propto \sqrt{\frac{1 - x}{1 + x}} \tag{48}$$

for $-1 \leq x \leq 1$. From Fig. 15 we see that (48) is of the same form as our exact results. Hence near the leading edge we choose an approximation to the pressure distribution of the form

$$P(x) = \frac{a + bx}{\sqrt{1 + x}} \quad , \tag{49}$$

where a and b are constants and $-1 \leq x \leq x_0$. Figure 2.16 clearly shows that (49) is a valid approximation near the singularity.

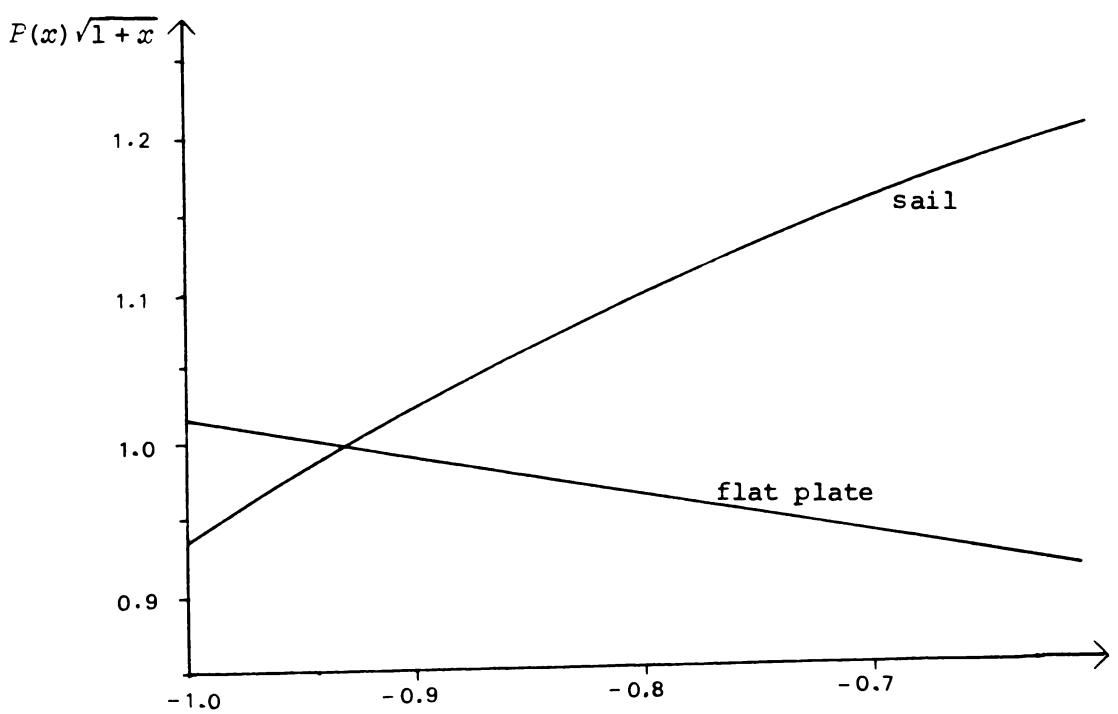

Fig. 2.16 The function $P(x)\sqrt{1+x}$ near the leading edge.

Thus over a small region near the leading edge ($-1 \leq x \leq x_0$) we will use the approximation

$$\underset{-1\leq x\leq x_0}{L^*} \approx \frac{1}{\cos\alpha} \int_{-1}^{x_0} \frac{a + bx}{\sqrt{1 + x}}\, dx. \tag{50}$$

The constants a and b may be obtained from Fig. 2.16 as

$$\left.\begin{aligned} b &= \frac{P(x_2)\sqrt{1 + x_2} - P(x_1)\sqrt{1 + x_1}}{x_2 - x_1} \\ \text{and} \qquad a &= P(x_2)\sqrt{1 + x_2} - b\, x_2 \quad , \end{aligned}\right\} \tag{51}$$

where x_1 and x_2 lie in the range $[-1, x_0]$ at which $P(x)$ is tabulated.

Evaluating equation (50) analytically using the substitution $\omega = 1 + x$, yields

$$\begin{aligned} \underset{-1\leq x\leq x_0}{L^*} &\approx \frac{1}{\cos\alpha} \left[\int_0^{1+x_0} \omega^{-\frac{1}{2}} (a-b)\, d\omega \right. \\ &\qquad \left. + \int_0^{1+x_0} b\, \omega^{\frac{1}{2}} d\omega \right] \\ &= \frac{2\sqrt{x_0 + 1}}{\cos\alpha} \left[(a-b) + \tfrac{1}{3} b (x_0+1) \right] . \end{aligned} \tag{52}$$

Thus when determining the total lift on the airfoil, we use equations (51) and (52) between the leading edge and x_0, numerical integration of (46) using the trapezoidal rule between the trailing edge and x_0 and evaluation of F_{LE} using (47).

A small study was undertaken to determine the value of x_0 which gave the most accurate results. It was found that for

$-0.92 \leq x_0 \leq -0.82$ almost no change in C_L could be detected, while outside these limits small variations of x_0 gave significant (> 1%) variation in C_L. Following this empirical study a value of -0.88 was chosen for x_0.

2.82 *CENTRE OF PRESSURE*

The centre of pressure (x_P) may be defined as the point of intersection between the profile chord and the line of action of the total force. It is usually given as a fraction of the chord, as measured from the leading edge. In finding the centre of pressure, we are finding the point on the chord about which the moments vanish.

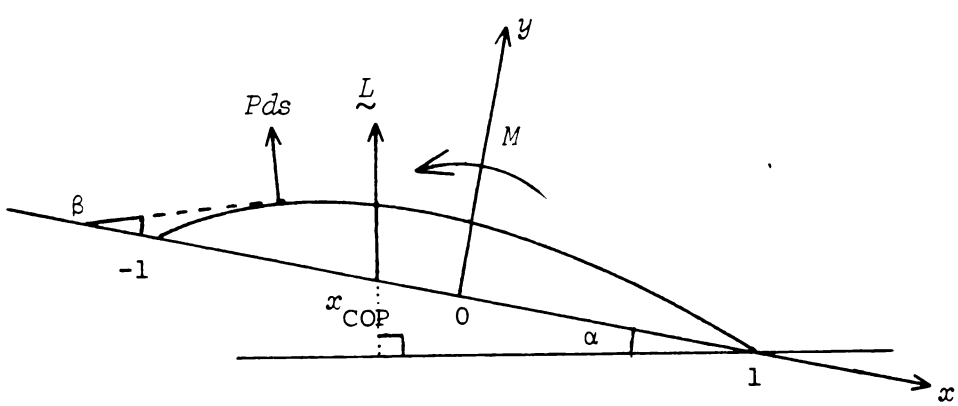

Fig. 2.17 Notation and forces acting on sail for centre of pressure.

We define as positive, a moment that tends to rotate the profile anticlockwise about the origin.

Consider a sail element ds . The moment about the origin will be given by (noting sign convention)

$$dM = xP(x)ds \cos\beta + yP(x)ds \sin\beta \qquad (53)$$

Substitution of (31) and (32) into (53) yields

$$dM = P(x)(x + y(x)y'(x))dx ,$$

so the total moment about the origin is

$$M = \int_{-1}^{1} P(x)(x + y(x)y'(x))dx \qquad (54)$$

Recalling that the lift acts in a direction normal to $\underset{\sim}{u}_0$, then the moment about the origin is

$$M = L \cos\alpha \, x_{COP} ,$$

where x_{COP} is defined in Fig. 2.17. Substitution into equation (54) gives the result we require, namely

$$x_{COP} = \frac{\int_{-1}^{1} P(x)(x + y(x)y'(x))dx}{L \cos\alpha} . \qquad (55)$$

Thus the centre of pressure x_P , as a fraction of the chord, will be given by

$$x_P = \frac{1 + x_{COP}}{2} .$$

Again we wish to evaluate the integral numerically, but at the leading edge the singularity in the pressure distribution requires an

approximation of the form

$$x\,P(x) \approx \frac{x(a + bx)}{\sqrt{1 + x}}$$

which is analogous to (50). Thus in the region $-1 \leq x \leq x_0$, the first term of (55) is approximated by

$$\int_{-1}^{x_0} xP(x)\,dx \approx \int_{-1}^{x_0} \frac{x(a + bx)}{\sqrt{1 + x}} \qquad (56)$$

where a and b are defined by (51).

Evaluation of (56) yields

$$\int_{-1}^{x_0} x\,P(x)\,dx \approx \frac{2}{15}\,(1 + x_0)^{\frac{1}{2}}[(5a - 4b)(x_0 - 2) + 3bx_0^2] \qquad (57)$$

The second term of (55) $(P(x)y(x)y'(x))$ is well behaved, as can be seen from Fig. 2.18.

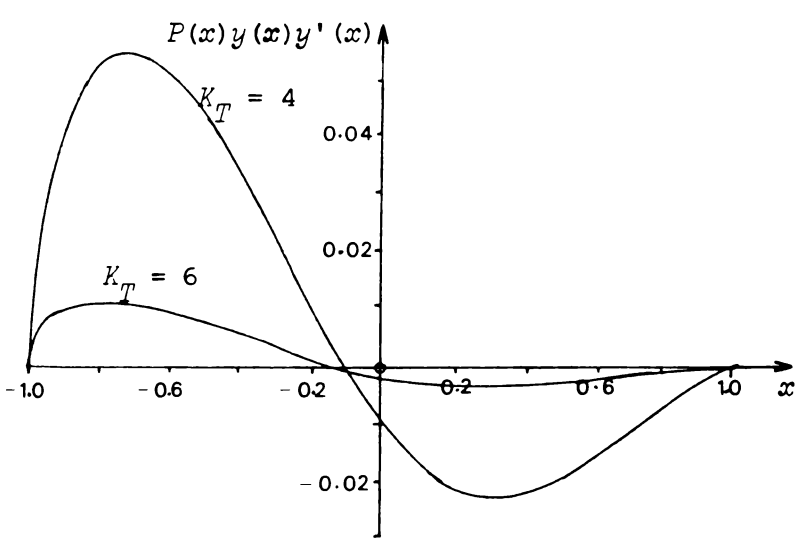

Fig. 2.18 The function $P(x)y(x)y'(x)$ is well behaved over the entire profile.

The singularity in $P(x)$ does not appear in the function. As a check, consider

$$\lim_{x \to -1} P(x)y(x)y'(x) \ .$$

We know that the slopes are finite at all points across the profile so let

$$\lim_{x \to -1} y'(x) = \gamma_1 .$$

Using Taylor's Theorem

$$y(x) \sim \gamma_1 (1 + x) \qquad \text{near } x = -1.$$

Hence

$$\lim_{x \to -1} P(x)y(x)y'(x) \sim \lim_{x \to -1} \frac{a + bx}{\sqrt{1 + x}} \ \gamma_1^2 (1 + x)$$

$$= \lim_{x \to -1} (a + bx) \ \gamma_1^2 \sqrt{1 + x}$$

$$= 0 \ .$$

Thus we can confidently use the trapezoidal rule over the entire profile for evaluating the second term of equation (55).

CHAPTER 3 PROGRAM TESTING

3.1 INTRODUCTION

A FORTRAN IV PLUS code was developed from the procedures discussed in chapter 2. The choice of language was influenced by several factors, including

(i) facilities for handling complex numbers;

and (ii) speed of execution.

On the machine used (PDP 11/70), standard FORTRAN IV runs approximately seven times as fast as the equivalent BASIC program. Use of a task-builder with routine optimiser further reduced execution times by a factor of two. Even with the resulting highly efficient object code, the calculation of a typical sail profile requires approximately one minute C.P.U. time. A complete listing of the code (named 'SAIL') is given in Appendix 2.

Most of the routines used were tested independently and then incorporated into the SAIL code. We may test much of the program by comparing the results obtained from SAIL (the exact solution to the problem) against results obtained from the linearised theories. Results for the pressure distribution, centre of pressure and lift coefficient of fixed profiles are compared here, while sails will be discussed in the remaining chapters. The test cases chosen are

(i) the flat plate;

(ii) the parabolic airfoil ($y = \alpha(1 - x^2)$);

(iii) the profile NACA a = 0.0 (Riegels 1961);

and (iv) the profile Göttingen 417a (Riegels 1961).

For this chapter we will again define the profiles such that the leading edge is at $x = -1$ and the trailing edge at $x = +1$, unless specifically stated otherwise.

3.2 *PRESSURE DISTRIBUTION*

Thin airfoil theory predicts that the flat plate pressure distribution is given by (Riegels (1961))

$$P(x) = 2\rho u_0^2 \cos\alpha \sin\alpha \sqrt{\frac{1 - x}{1 + x}} \quad ; \qquad (1)$$

and for a parabolic airfoil we have (Sneyd (1978))

$$P(x) = 2\rho u_0^2 \alpha \sqrt{\frac{1 - x}{1 + x}} (3 + 2x) \quad , \qquad (2)$$

where the angle of attack α is in radians. In Figs. 1 and 2 the excellent agreement between results obtained from the linearised theory and from SAIL is shown.

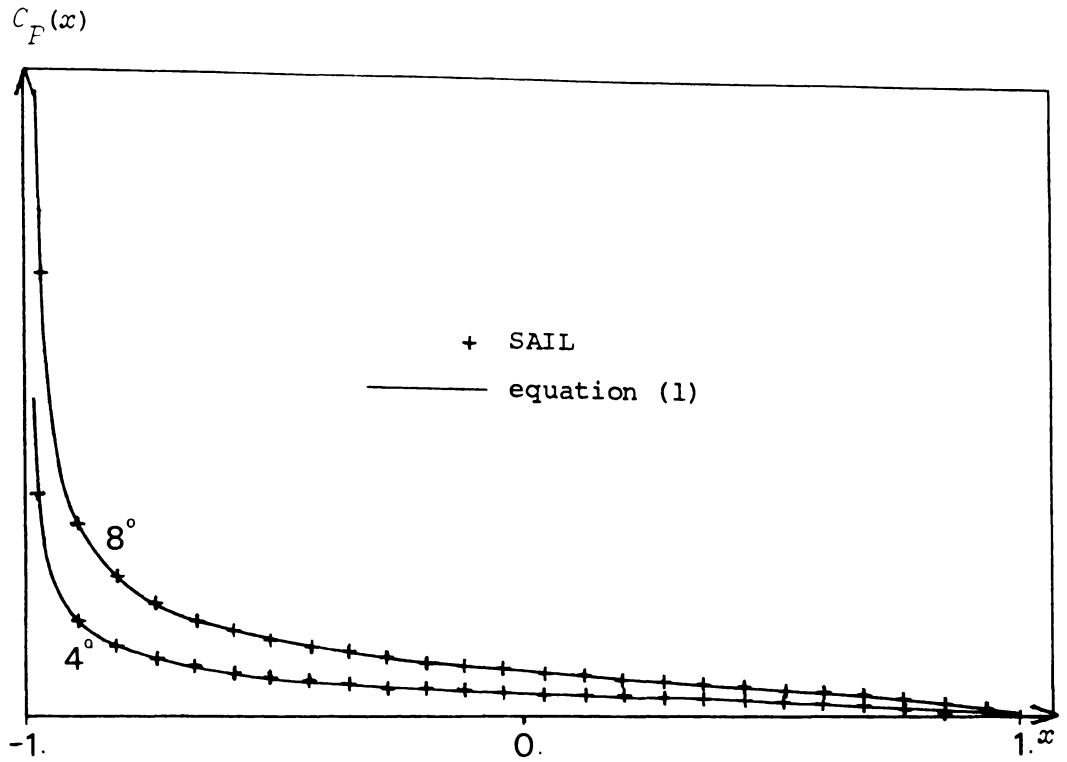

Fig. 3.1 Pressure distribution for the flat plate. $C_P(x)$ is the pressure coefficient.

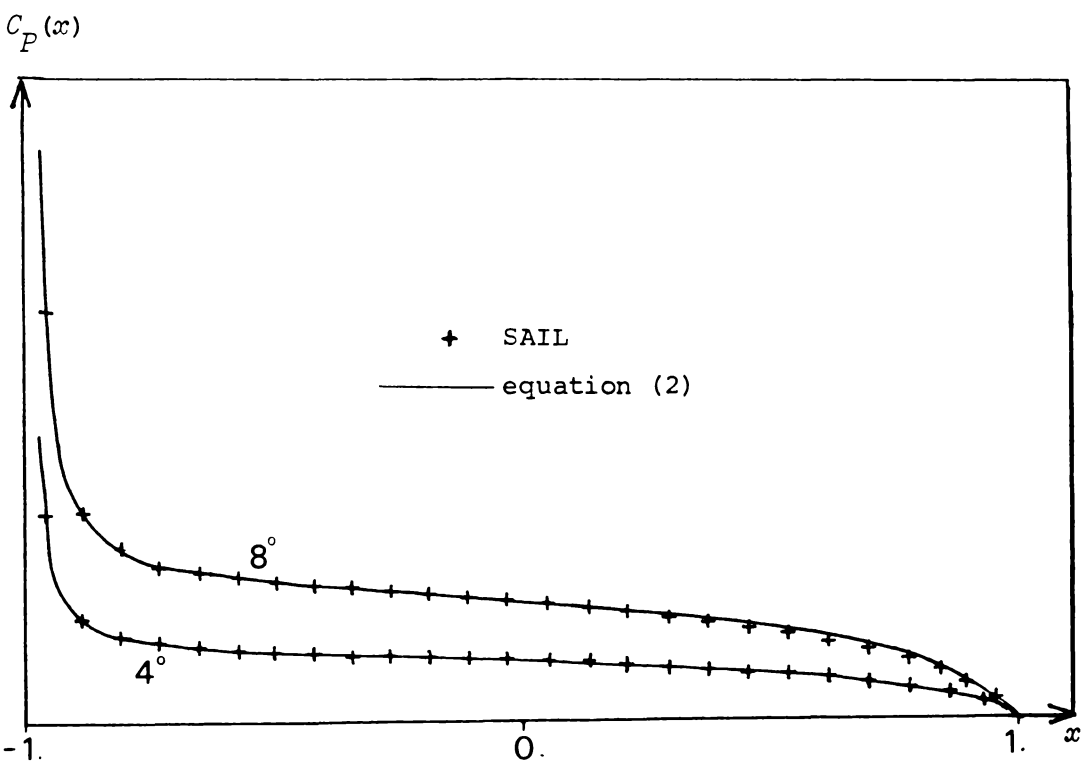

Fig. 3.2 Pressure distribution for the parabolic profile.

As another check on the calculation of the pressure distribution, we compare the velocity distribution

$$\left(\frac{u(x)_{\text{TOP}} - u(x)_{\text{BOTTOM}}}{u_0} \right)$$

for the profile NACA a = 0.0. This section is simply a camber line designed (from linearised theory) to give a particular velocity distribution. As can be seen from Fig. 4, agreement is again very good. The discrepancy at the leading edge is caused by the profile slope becoming infinite there, a characteristic of this series of profiles, which leads to the breakdown of linear theory.

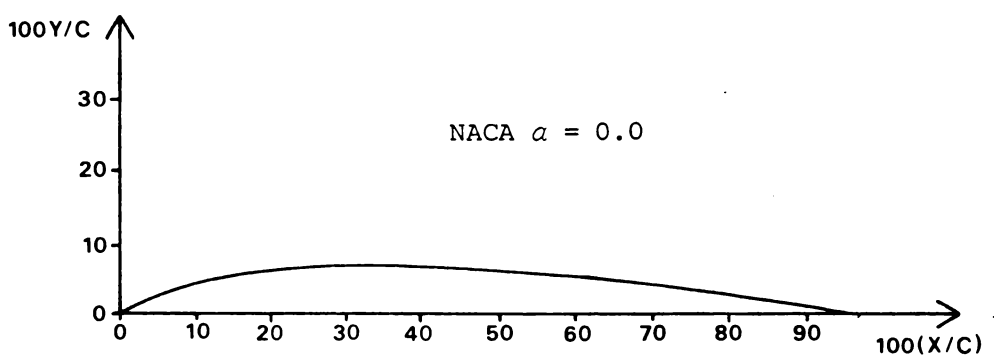

Fig. 3.3 The profile NACA a = 0.0 (Riegels (1961))

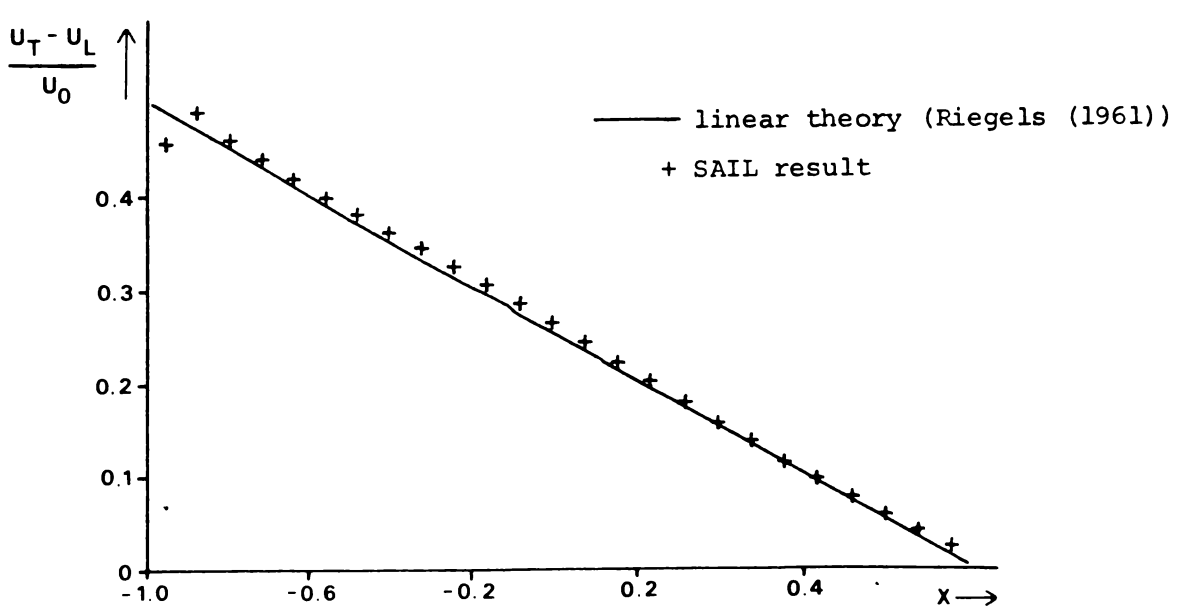

Fig. 3.4 Velocity distribution for NACA a = 0.0 at $\alpha = 5^{\circ}$.

3.3 *LIFT COEFFICIENT AND CENTRE OF PRESSURE*

The results for the flat plate are well known with

$$C_L = 2\pi\alpha, \qquad (3) \quad (\alpha \text{ in radians})$$

and centre of pressure (x_P) at 25% of the chord. These are in good agreement with experimental results up to about $\alpha = 6^\circ$ (Riegels (1961)) and in Figs. 5 and 6 the good agreement with thin airfoil theory is again shown.

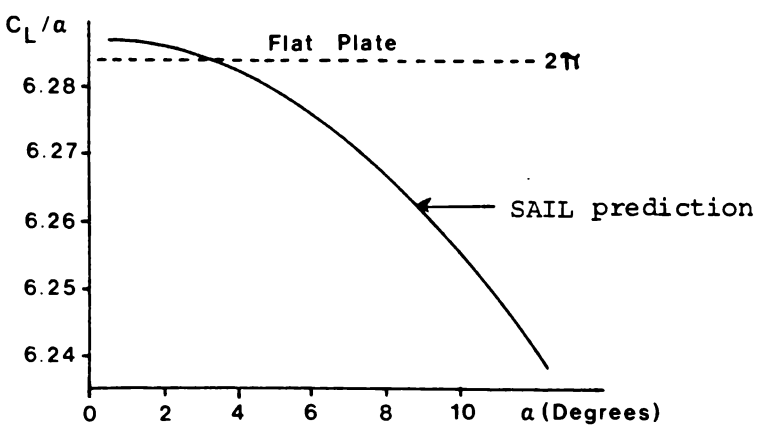

Fig. 3.5 C_L/α results for flat plate, showing close agreement between SAIL and thin airfoil theory.

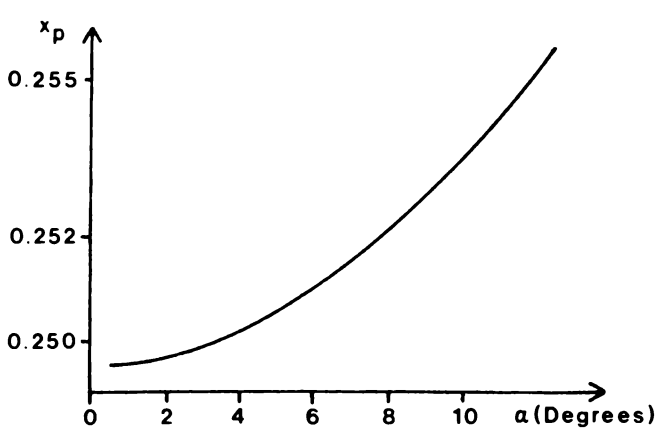

Fig. 3.6 Centre of pressure x_P for flat plate predicted by SAIL. Note close agreement with thin airfoil theory prediction of 0.25.

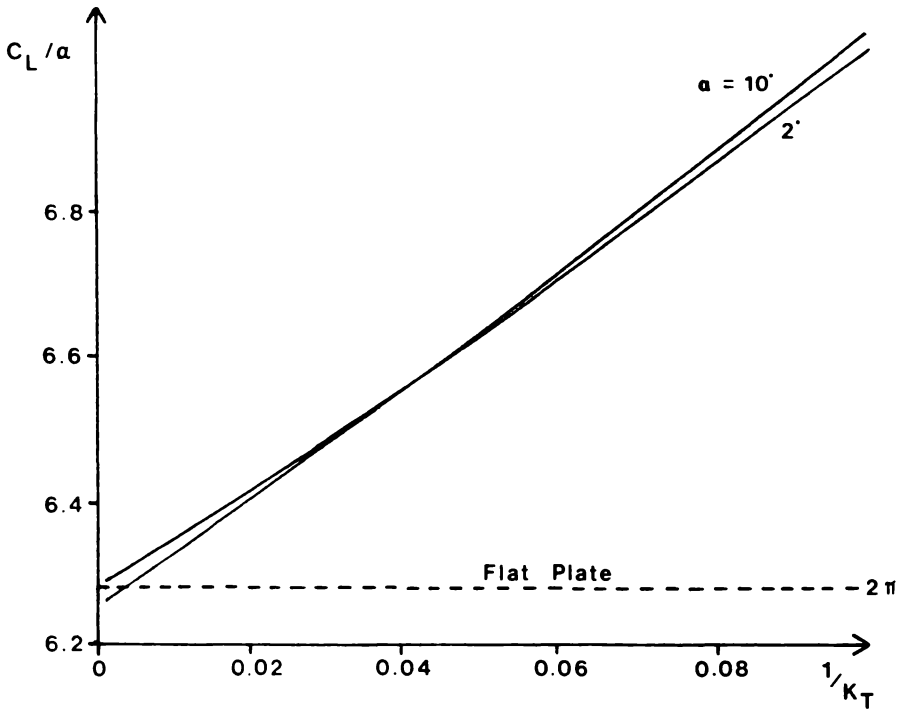

Fig. 3.7 C_L/α versus $1/K_T$ for sails. Note good agreement of SAIL with thin airfoil theory predictions as $1/K_T \to 0$.

Consider a sail with $K_T = T/\frac{1}{2}\rho c u_0^2 >> 1$; the sail profile tends to that of a flat plate as $K_T \to \infty$. As shown in Figs. 7 and 8, both x_P and C_L approach the flat plate values.

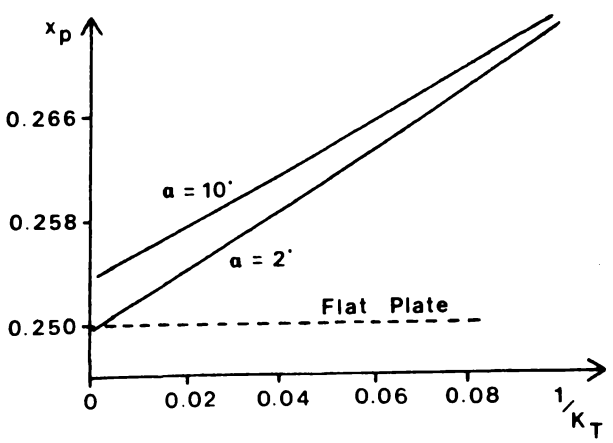

Fig. 3.8 Centre of pressure x_P versus $1/K_T$ for sails.

For the parabolic aerofoil ($y = \alpha(1 - x^2)$) (Sneyd(1978))

$$\lim_{\alpha \to 0} \frac{C_L}{\alpha} = 4\pi \ , \tag{4}$$

$$\lim_{\alpha \to 0} x_P = 0.375 \tag{5}$$

and again excellent agreement is obtained (c.f. Figs. 9 & 10).

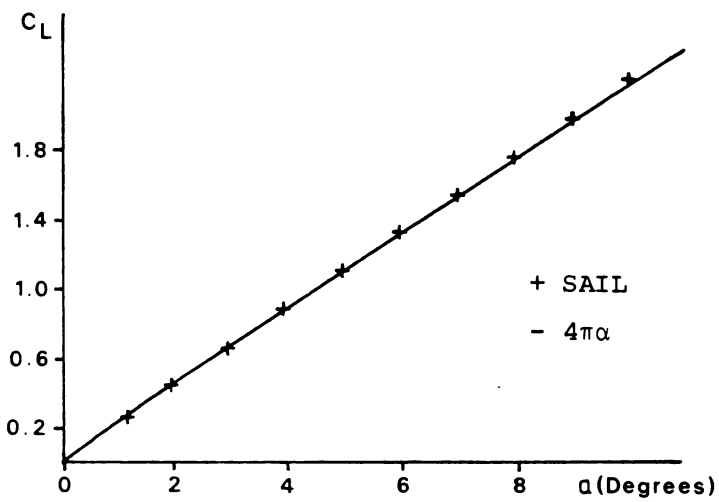

Fig. 3.9 Lift coefficient C_L versus angle of attack for the parabolic aerofoil.

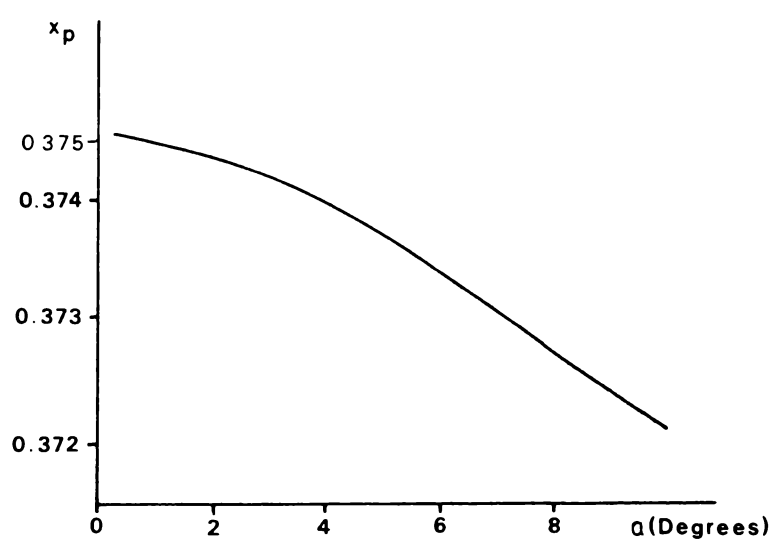

Fig. 3.10 Centre of pressure x_P for the parabolic aerofoil, predicted by SAIL.

As a further test for SAIL we compare results predicted for the Göttingen 417 a profile with experimentally observed results (Riegels 1961)). The profile is a curved plate with maximum thickness of 2.9% of the chord, so that a mean camber representation closely resembles the profile (Fig. 3.11). The results shown in Fig. 3.12 for the lift coefficient, and Fig. 3.13 for the centre of pressure indicate that the SAIL prediction corresponds very closely to the experimentally observed results (Riegels (1961)), until severe separation occurs at $\alpha \approx 8^{o}$.

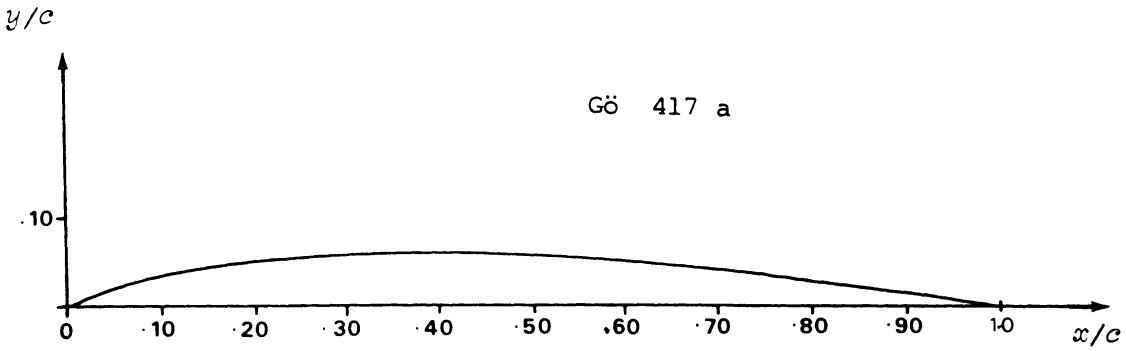

Fig. 3.11 Göttingen 417 a profile.

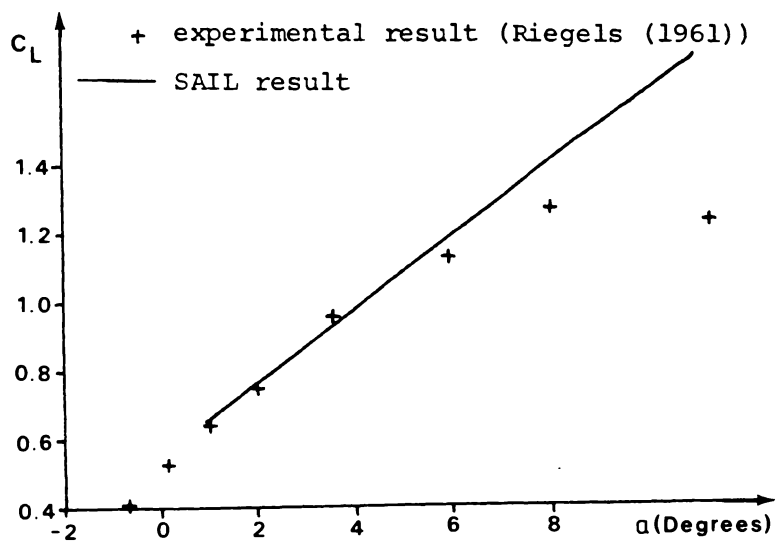

Fig. 3.12 Lift coefficient for Gö 417 a.

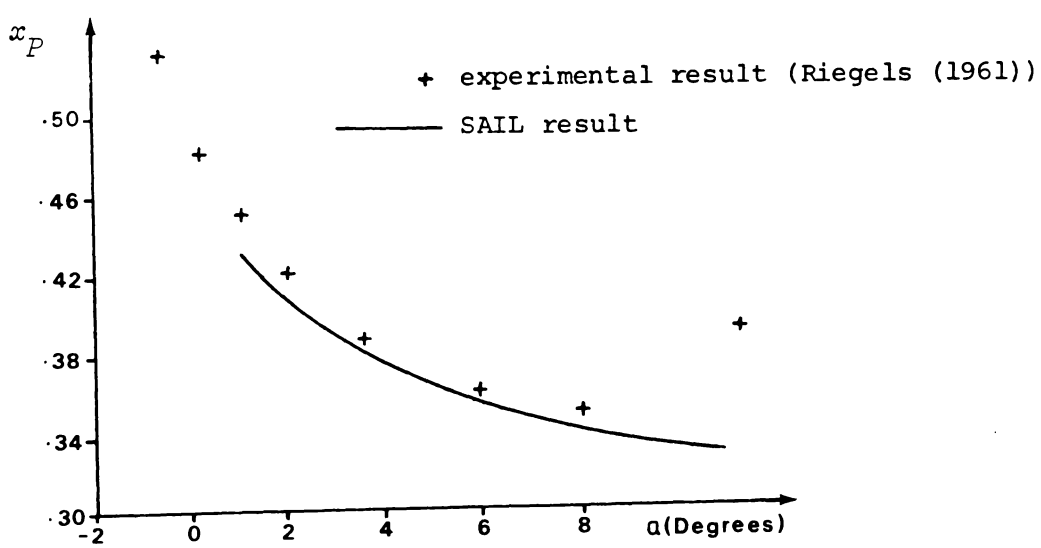

Fig. 3.13 Centre of pressure for Gö 417 a.

CHAPTER 4. EXPERIMENTAL PROCEDURE

4.1 INTRODUCTION

In this chapter a mechanical apparatus is described which was used to test a single surface, constant tension, non-porous sail in a two-dimensional flow. Suitable wind-tunnel facilities were made available at the B.G. deBray Aeronautics Laboratory, University of Auckland School of Engineering. Results for lift, drag and pitching moment were obtained for a range of airspeed, angle of attack and sail tension. The results are given in M.K.S. units, and corrected for wind tunnel effects. A photographic record of sail profiles was made for comparison with theory.

4.2 APPARATUS

The apparatus supporting the sail and its tensioning system (Fig. 1 and Plate 1) had to be solid unit, so that when attached to the mounting struts no extraneous forces were transmitted to the balance. This meant that each attachment point required a low friction bush so that it could be free to pivot in the vertical plane on the mounting struts.

Plastic film ("mylar") 0.05 mm thick was chosen for the membrane for several reasons including

(i) strength,

(ii) flexibility,

(iii) thinness,

(iv) non-porosity,

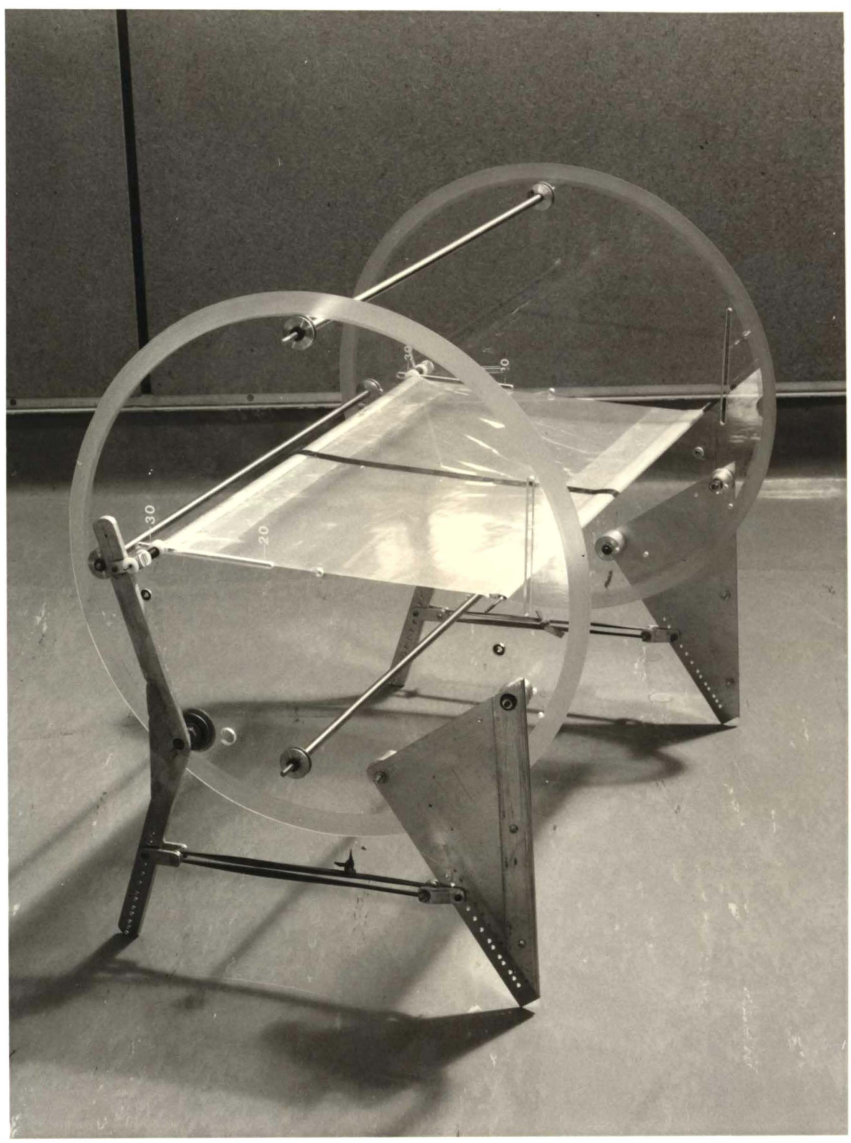

Plate 1. Assembled test rig showing sail membrane, endplates and tensioning system.

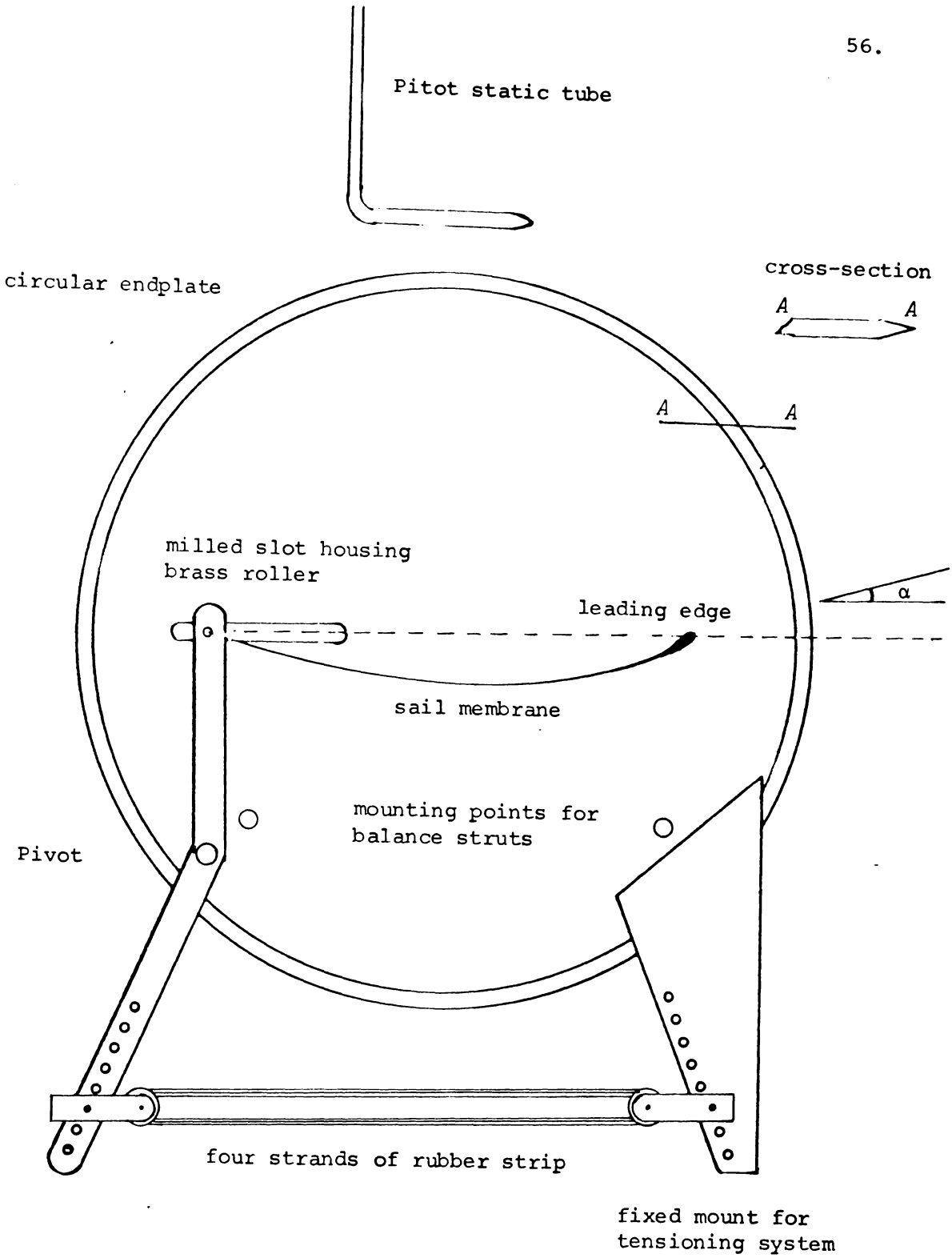

Fig. 4.1 Configuration of endplates and tensioning system.

(v) transparency,

and (vi) inextensibility.

The model dimensions were 54 cm span and 30 cm chord, and to minimise spanwise bow solid leading and trailing edges were milled from aluminium strip. They were milled to a symmetric streamlined profile so as not to contribute to the camber or the lift, and their cross-sections (c.f. Fig. 2) were designed to keep the maximum bow to within 1% of the span (i.e. maximum bow < 0.54 cm).

Fig. 4.2 Leading and trailing edge cross sections.

In practice no bow was noticed except at very high air velocity, when the lift force and the pitching moment were too large to be measured by the balance.

End plates were used to maintain two-dimensional flow across the membrane (c.f. Plate 1). Very little literature could be found on end plate design, but circular endplates of a size suitable for the dimensions of the working section were employed. The resulting diameter was 45 cm, just 1.5 times as large as the maximum chord. This was thought to be sufficient to render vortex shed and induced drag negligible, as the endplates are of similar relative dimensions to those shown in Riegels (1961). The endplates were cut from ¼" clear perspex

so that a photographic record could be made of the sail profile.

The tensioning system was required to provide a constant tension even when the sail billowed and the chord varied. Consider the tensioning system depicted in Fig. 3.

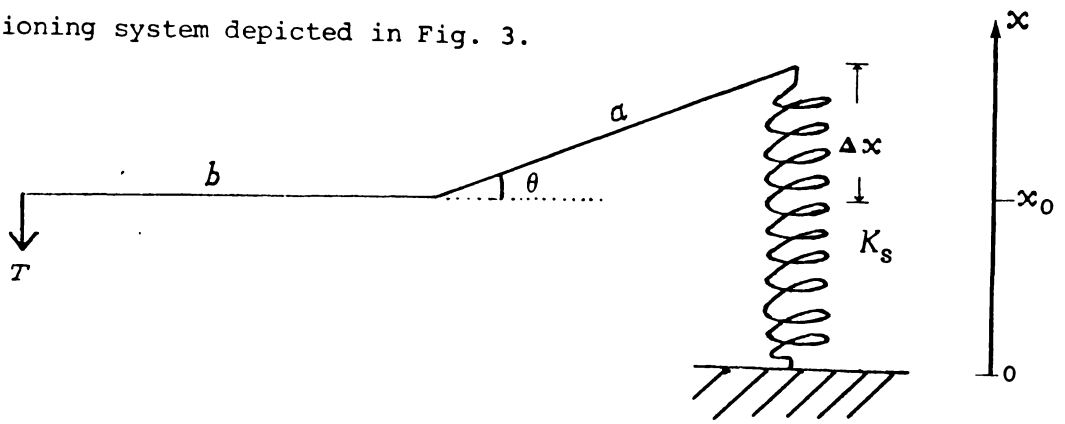

Fig. 4.3 Tensioning system to give constant T.

We denote the tension in the sail by T, and the spring constant by K_s. The tension is given by

$$T = \frac{a}{b}\cos\theta K_s(x_0 + \Delta x),$$

or

$$T = \frac{a}{b}K_s(x_0\cos\theta + a\cos\theta\sin\theta) \qquad (2)$$

since $\Delta x = a\sin\theta$. For constant tension we require $\frac{dT}{d\theta} = 0$, so differentiating equation (2) with respect to θ yields

$$\frac{dT}{d\theta} = \frac{a}{b}K_s(a\cos 2\theta - x_0\sin\theta)$$

$$= 0,$$

or

$$\frac{x_0}{a} = \frac{\cos 2\theta}{\sin\theta}$$

Considering size limitations of the working section, the endplates, and spring extensions, we chose

$$\left.\begin{aligned}\theta &= 35^\circ \\ x_0 &= 0.596a\end{aligned}\right\}, \qquad (3)$$

so that from (2) tension

$$T = 0.958 \frac{a^2}{b} K_s . \qquad (4)$$

The lengths a and b were chosen so that a maximum tension of 20 N could be applied with spring constant $K_s = 100\ Nm^{-1}$. (This corresponds to tension number $K_T = 2.0$ when $u_0 \sim 15\ ms^{-1}$.) Again considering size limitations, we chose $b = 15$ cm so that from (4) $a_{max} \approx 20$ cm. To give a range of forces, several lengths a were chosen between 9 cm and 20 cm. Rubber strip was chosen to give the tensioning force, as suitable springs were unavailable. The force-distance relationship of the rubber strips was only approximately linear (c.f. Fig. 4).

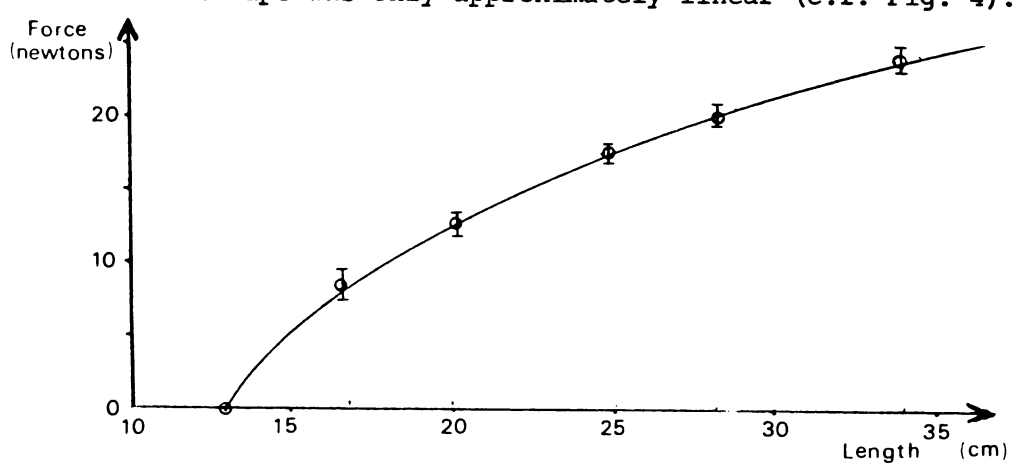

Fig. 4.4 Force versus extension for four strands of rubber strip.

A 52 cm rubber strip made into four strands of 13 cm length was found to give a suitable spring constant. Ball races were used at the pivot point of the tensioning arms to reduce frictional forces. This system was found to give a near constant force over the required range of movement. Two such tensioning systems were made, and one was mounted on the outside of each endplate. The resultant calibration of the total tensioning system is shown in Fig. 5.

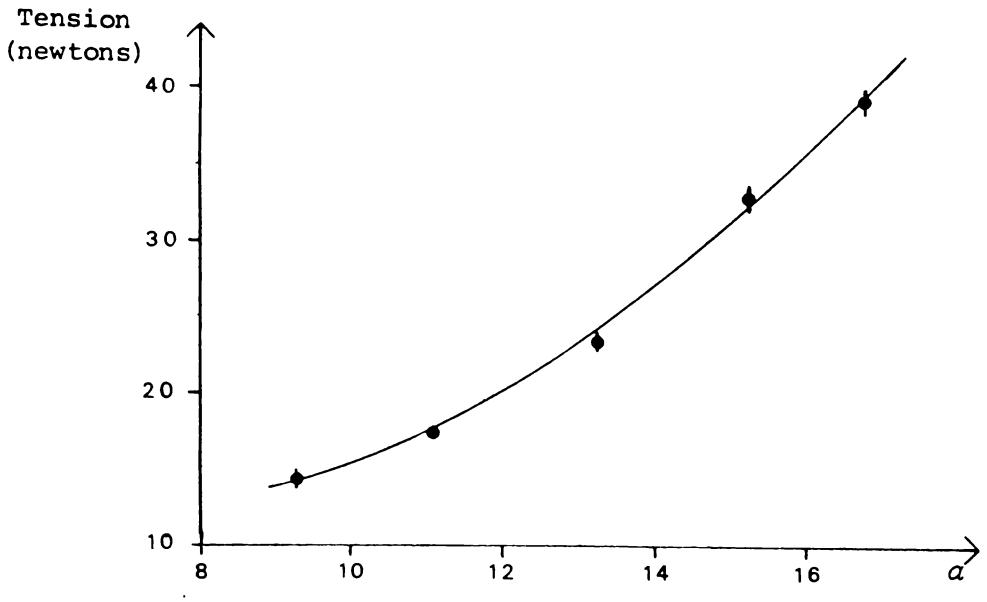

Fig. 4.5 Tension versus arm-length a. Error bars indicate variation of T as arm is rotated through typical angle.

Pins were fitted to the tips of the leading edge, so that when mounted in holes in the endplates they allowed the leading edge to pivot freely. The trailing edge was required to move along the chord line to permit the sail to billow, so a slot was milled in each endplate allowing a brass roller carrying the trailing edge mounting pin to run freely along the slot (c.f. Plate 1).

4.3 WIND TUNNEL FACILITIES

The wind tunnel used is a return flow tunnel with low and high speed testing sections (c.f. Plate 2). The high speed section was chosen, since it incorporates a three component balance for measurement of lift, drag and pitching moment. It has a working section of 61 cm by 76 cm, and is designed so that there is zero static pressure gradient along the working section. This is accomplished by corner insets in all four corners of the section. The airspeed is continuously variable over the range 0 - 75 ms^{-1}, although for our tests an airspeed of 30 ms^{-1} was never exceeded.

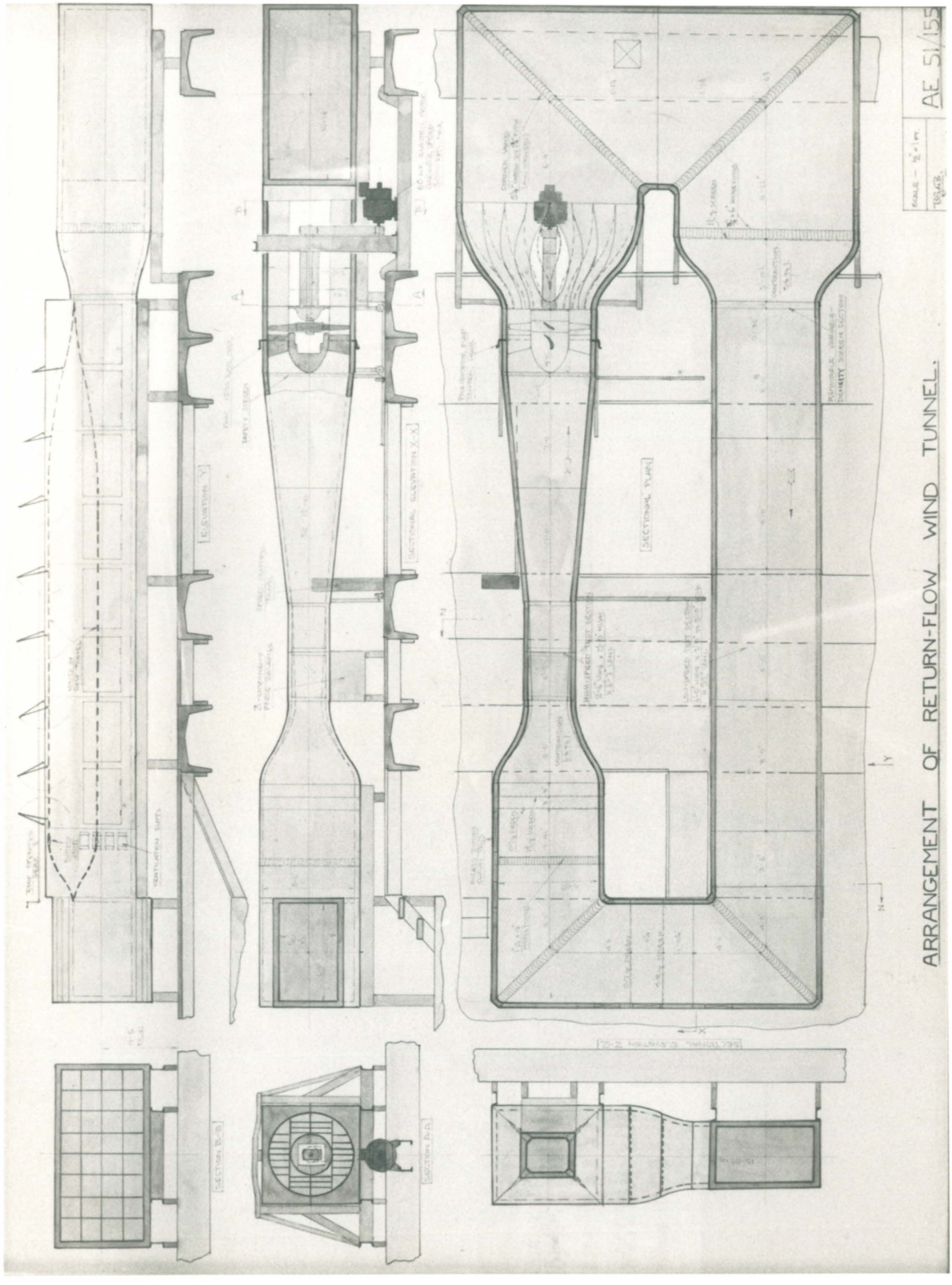

Plate 2. Arrangement of return-flow wind tunnel in B.G. deBray Aeronautics Laboratory.

Typical Reynolds numbers (based on chord) for the experimental results were in the range 1×10^5 - 3.2×10^5 - i.e. just in the sub-critical Re range. It is somewhat questionable whether Re_{crit} in our case defines the point at which transition of the laminar boundary layer into turbulent flow occurs, for small diameter leading edges have a *turbulating* effect on the boundary layer and hence delay separation. It is also possible, that the join in the mylar film, where it attaches to the leading edge, acts as a *turbulator* (c.f. Fig. 6).

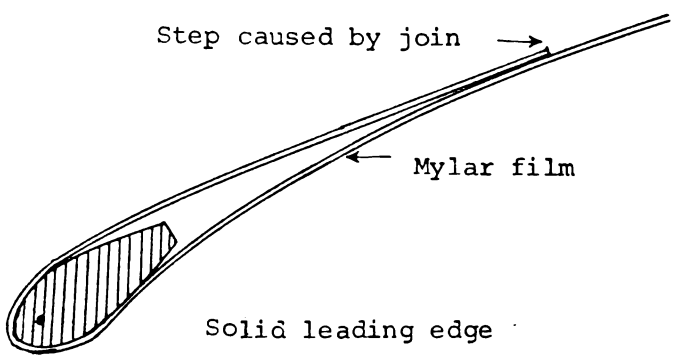

Fig. 4.6 Attachment of mylar film to leading edge showing discontinuity at film edge.

No apparatus for flow visualisation of the boundary layer was available but observation of the membrane indicated that severe separation only occurred at high angles of attack. The membrane was completely stable until separation occurred at which point surface vibration became apparent.

A pitot-static tube mounted from the roof of the tunnel was used to determine the airspeed, and the manometer output was in mm H_20. The air pressure (inches Hg) was recorded at 4-hourly intervals, and the air temperature (^{o}C) in the tunnel was recorded at 30-minute intervals. Letting ρ_{air} denote the air pressure, T the tunnel temperature in the working section and h the manometer reading, one finds airspeed

$$u = \sqrt{\frac{2 \times g \times h}{\rho_{air}}} \; ms^{-1} \qquad (5)$$

where air density

$$\rho_{air} = \frac{P_{air}}{R(T+273.15)} \; . \qquad (6)$$

and R is the gas constant.

Evaluation of equation (6) (with conversion to MKS units) yields

$$\rho_{air} = \frac{11.961 \, P_{air}}{(T+273.15)}$$

The rear mounting strut could be racked up or down to alter the angle of attack, and was fitted with a counter. The tunnel has been designed so that the air flows horizontally throughout the test section, so the sail was aligned (using a level) to set zero angle of attack. The counter was set to zero at this point, and an inclinometer used to calibrate the the counter up to angles of 11^{o}.

The "turbulence level" for the test section of the tunnel is 0.3%, and has corresponding critical Reynolds number (Hansen, 1978)

$$Re_{crit} \approx 3.1 \times 10^{5},$$

where $$Re = \frac{u_0 L}{\nu} \; ,$$

L is a typical length scale (m)

and $\nu = 1.496 \times 10^{-5} \; m^2 \; s^{-1}$.

4.4 *WIND TUNNEL CORRECTIONS*

Results obtained from wind tunnel tests cannot be applied directly to full size aircraft, since the test conditions are unavoidably different to those in full scale flight. To compensate for these differences various corrections are applied to account for three aspects:

(a) model supports;

(b) finite cross-sectional area of the airstream in the tunnel;

and (c) differences in size, surface finish, airspeed and turbulence.

(a) *Model Supports*

(i) Mounting Apparatus.

A correction is required for the drag due to the mounting struts, endplates and tensioning apparatus. Consequently, the forces acting on the entire apparatus minus the sail were determined. Only the drag varied with variations in airspeed, so that from our drag readings we must subtract the drag due to the mounting apparatus (c.f. Fig. 7).

(ii) Leakage.

The leakage across the end gaps at the tips of a two-dimensional wing affects lift and drag. The usual way to determine the correction required is to extrapolate from tests with different air gaps, but it was thought that with the low airspeeds and the very small air gaps used (~2 mm) this correction would be negligible. If flow through the air gaps was significant, then the camber at the tips would be noticeably different from that at the mid span. Tests were carried out to observe the tip profile; it was found that no observable difference could be seen except at very high airspeed (well outside our test range), so no

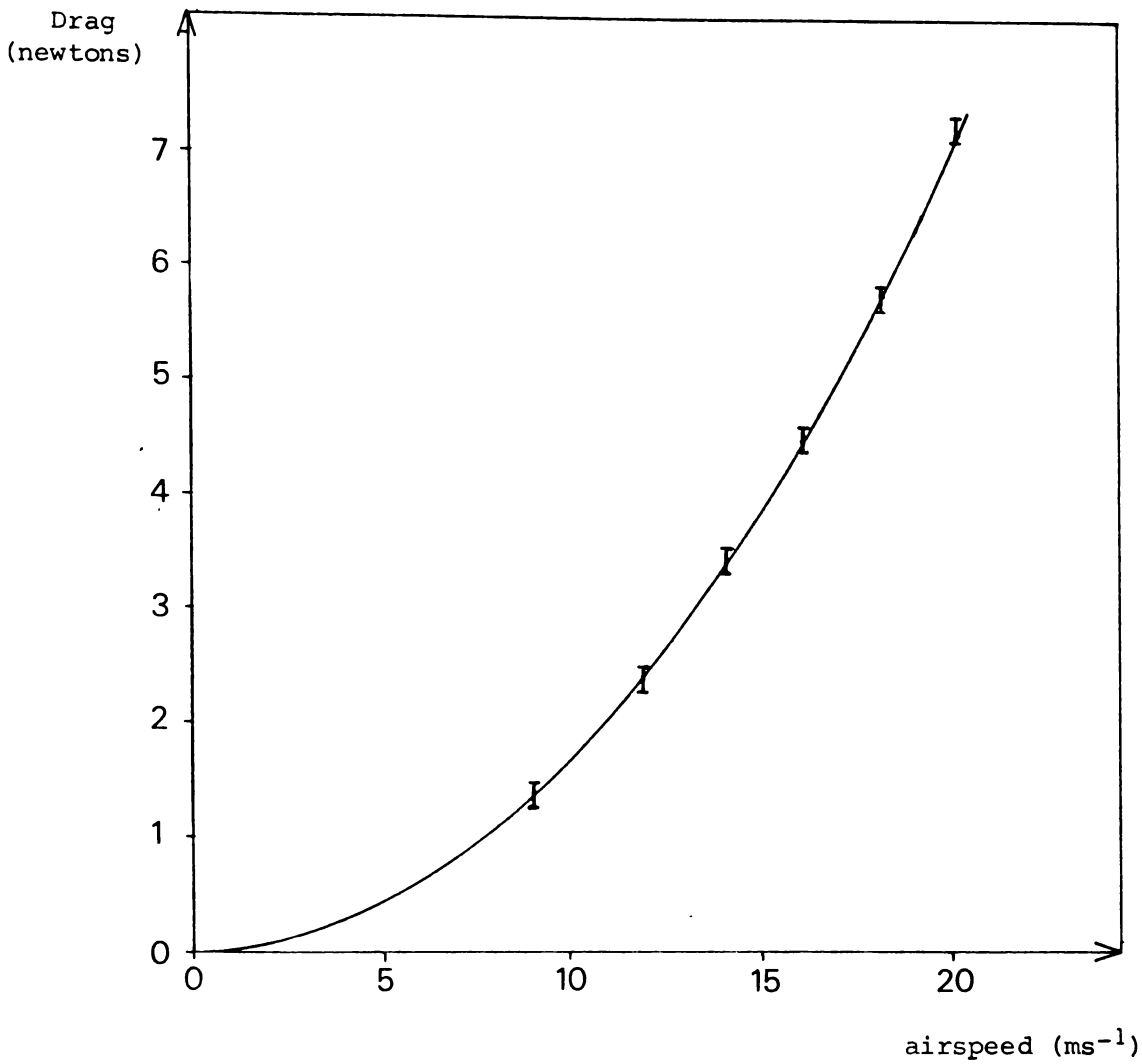

Fig. 4.7 Drag of mounting apparatus and endplates versus airspeed.

correction was applied. Corrections for balance alignment and interference drag were not required either.

(b) *Finite Cross Section*

(i) Horizontal Buoyancy.

No correction for horizontal buoyancy due to static pressure gradient was required, since the high speed test section includes pressure correction fillets to give

$$\frac{dP}{dL} = 0.$$

(ii) Blockage

The reduction in flow cross-section due to the presence of the sail and mounting apparatus increases the flow velocity round the model, and its wake. The correction for solid blockage depends on the ratio of model cross-sectional area to that of the tunnel. For a two-dimensional body of thickness t in a tunnel of height h, the correction for solid blockage is given by (Pope (1954), Pankhurst (1952))

$$\frac{u_1}{u} = \tau_1 \lambda_1 \left(\frac{t}{h}\right)^2 ,$$

where u_1 is the increase in effective velocity due to solid blockage,

u is the empty tunnel velocity,

τ_1 is jet coefficient (=0.822 for closed tunnel),

and λ_1 is body coefficient (~5 for airfoil).

Since $\frac{t}{h} \sim 10^{-4}$ the correction is negligible.

Wake blockage arises from the higher velocity outside the wake affecting the pressure in the wake bubble, and hence the drag. For a

two-dimensional wing of chord c in a rectangular tunnel of height h, the wake blockage correction is (Pope (1954), Pankhurst (1952))

$$\frac{u_2}{u} = \tfrac{1}{4} \frac{c}{h} C_{D_T},$$

where u_2 is increase in effective velocity due to wake blockage, and C_{D_T} is the measured drag coefficient in the tunnel. A typical drag coefficient is $C_{D_T} \sim 0.2$, so that the correction becomes

$$\frac{u_2}{u} \approx 0.025, \quad \text{which we consider}$$

is just significant. Thus the corrected velocity is

$$u_F = u(1 + \frac{u_2}{u})$$

and recalling chord and tunnel dimensions becomes

$$u_F = u(1 + \frac{C_{D_T}}{8}), \tag{7}$$

where u_F is the corresponding free air velocity.

(iii) Boundary Constraint.

Models developing lift modify the flow streamlines of the empty tunnel (c.f. Fig. 8). The constraint at the tunnel walls effectively increases the camber and the angle of attack.

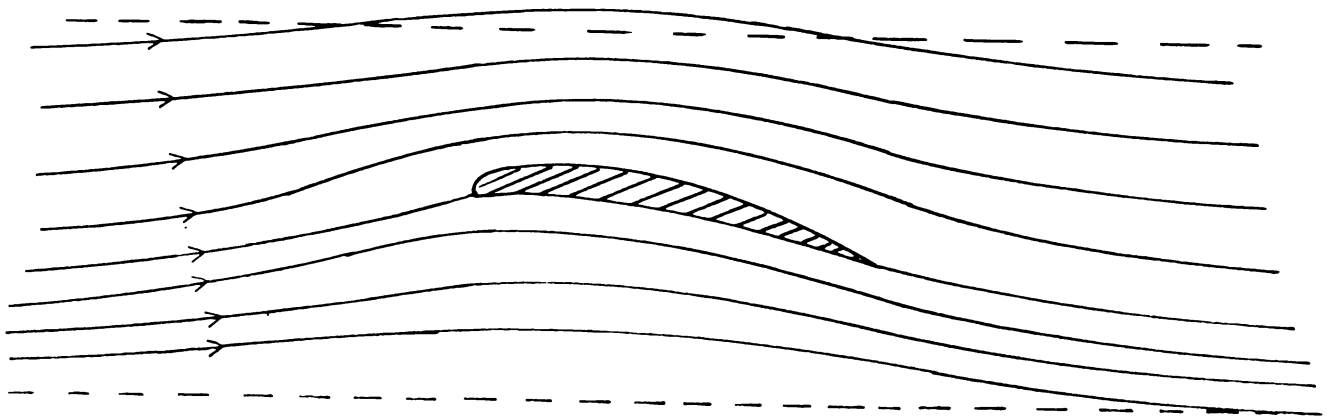

Fig. 4.8 Aerofoil modifying fluid flow.

———— Streamlines in free air.

— — — — Tunnel walls.

The camber increase (Pope (1954), Pankhurst (1952))

$$(\gamma_F - \gamma_T) = \frac{\pi}{192}\left(\frac{c}{h}\right)^2 C_{L_T}$$

$$\approx 0.004\, C_{L_T},$$

where γ is the ratio of maximum camber to chord, F refers to free air and T to tunnel conditions. Typically $C_{L_T} \sim 1.5$, so that $(\gamma_F - \gamma_T) \sim 0.01$, which we consider negligible.

The increase in angle of attack is

$$(\alpha_F - \alpha_T) = \frac{\pi}{96}\left(\frac{c}{h}\right)^2 (C_{L_T} + 4\, C_{M_T})$$

$$\approx 0.008(C_{L_T} + 4C_{M_T}), \qquad (8)$$

where C_{M_T} is the pitching moment coefficient about the ¼ chord. It is found that α_F differs from α_T by much less than 1%, so no correction was made.

(c) *Scale*

There is no requirement to extrapolate the wind tunnel results to simulate full scale flight, since comparison is to be made with theories which involve no absolute length scale. Consequently corrections for surface finish, turbulence levels and Reynolds numbers were not made.

To summarize, the only corrections made were to the velocity, given by equation (7), and the drag to account for the mounting apparatus.

4.5 DETERMINATION OF CENTRE OF PRESSURE FROM PITCHING MOMENT

From experimentally determined values of lift, drag and pitching moment we can determine the position of the centre of pressure for the sail. As is common in wind tunnel tests, the model is inverted (c.f. Plate 3), so that the lift acts in the same direction as gravity. The measured pitching moment is then the moment applied to the rear strut about the leading edge mounting strut. Note that usually the front strut is mounted at the ¼ chord position, so that the measured moment is then the pitching moment about the ¼ chord. However, in this case the chord was variable, so it was thought best to mount the apparatus as shown in Fig. 9.

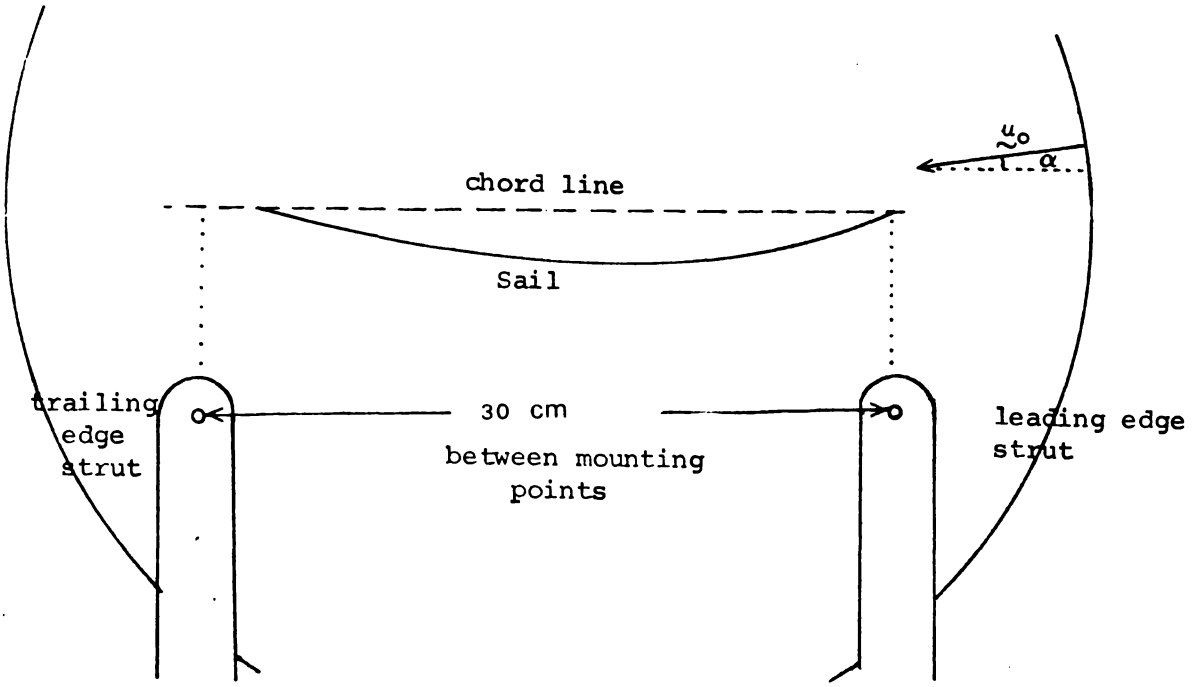

Fig. 4.9 Mounting strut attachments on endplates.

Consider the force diagram (Fig. 4.10):

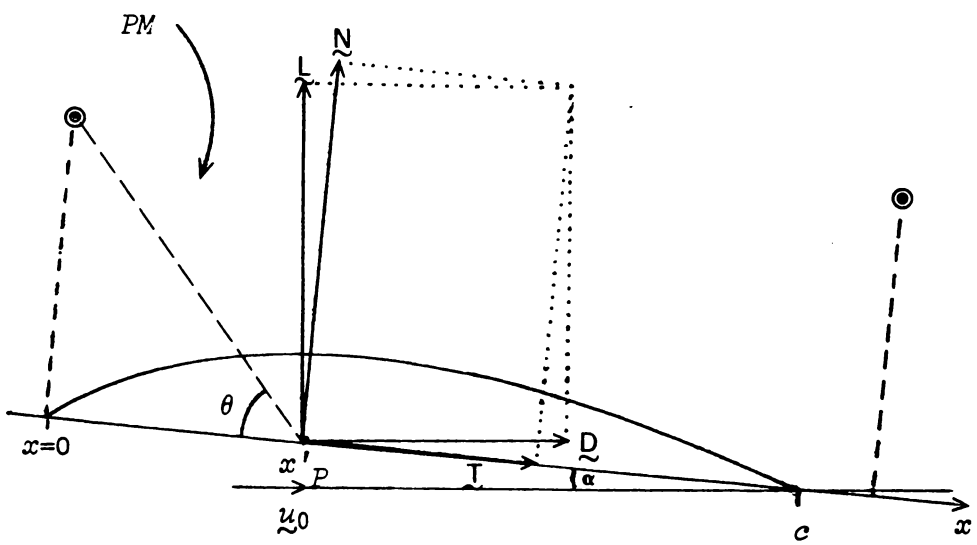

Fig. 4.10 Force diagram.

N - force normal to the chord
T - force tangential to the chord
PM - measured pitching moment
x'_P - distance between the leading edge and centre of pressure
a' - distance from leading edge to strut attachment point.

If $x_p = \frac{x'_p}{c}$ denotes the (dimensionless) position of the centre of pressure, $a = \frac{a'}{c}$ denotes the (dimensionless) distance between the leading edge and the mounting strut,

$$C_L = \frac{L}{\frac{1}{2}\rho c S u_0^2} ,$$

and $$C_D = \frac{L}{\frac{1}{2}\rho c S u_0^2} ,$$

where S is the span, we have

$$C_N = C_L \cos\alpha + C_D \sin\alpha$$

and $$C_T = -C_L \sin\alpha + C_D \cos\alpha.$$

Letting $$\theta = \tan^{-1}\left(\frac{a}{x_p}\right) \qquad (11)$$

we obtain

$$C_M = -(C_N \cos\theta + C_T \sin\theta)(a^2 + x_p^2)^{\frac{1}{2}} ,$$

or $$C_M = -(C_L \cos(\alpha+\theta) + C_D \sin(\alpha+\theta))(a^2 + x_p^2)^{\frac{1}{2}}.$$

Rearranging we have

$$x_p = [-a^2 + C_M^2/(C_L \cos(\alpha+\theta) + C_D \sin(\alpha+\theta))^2]^{\frac{1}{2}}, \qquad (12)$$

so that by simultaneously solving equations (11) and (12) we can determine the centre of pressure. This may be achieved by an iterative method: we initially guess $x_{p_0} = 0.25$, and iterate using the scheme

$$x_{p_n} = [-a^2 + C_M^2/(C_L \cos(\alpha+\theta) + C_D \sin(\alpha+\theta))^2]^{\frac{1}{2}}$$

where $\theta = \tan^{-1}\left(\frac{a}{x_{p_{n-1}}}\right)$. A small FORTRAN routine was written to accomplish this, and it was found that convergence was rapid to an accuracy of 10^{-6}, far less than experimental error.

The pitching moment coefficient about the ¼ chord is given by

$$C_{M_{\frac{1}{4}}} = (C_L \cos\alpha + C_D \sin\alpha)(x_p - \tfrac{1}{4}).$$

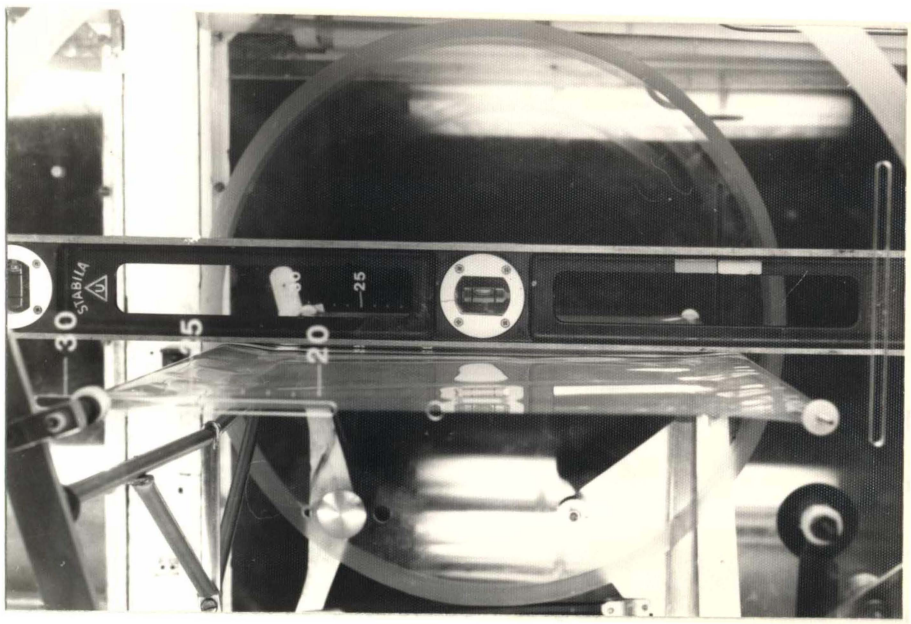

Plate 3. Leveling the sail for zero angle of attack.

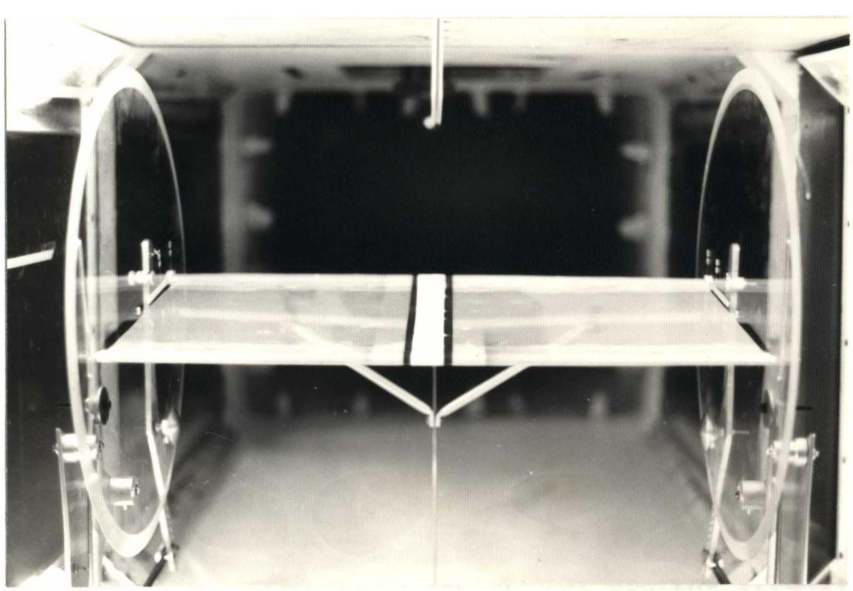

Plate 4. View looking down the test section.

CHAPTER 5 RESULTS

5.1 *INTRODUCTION*

Utilizing the routine SAIL developed in chapters 2 and 3, various properties of two-dimensional sail wings can be determined. Results are shown for typical profiles, profile parameters, lift coefficient and centre of pressure. Comparisons are made with experimental and linear theory results where possible. Experimental results for drag coefficient and lift to drag ratio are also discussed.

Previously we have described the profile camber by the function $y(x)$, where $0 \leq x \leq c$. We define the dimensionless *camber function*

$$C(x') = y(x)/c$$

where $$x' = x/c.$$

However for the sake of convenience we choose to neglect the dash, so that $C(x)$ defines the camber at x as a fraction of the chord, and $0 \leq x \leq 1$.

It is observed that sail wings (e.g. hang gliders) operate with significant profile cambers $(C(x)_{max} \gtrsim 0.02)$. Observation of Fig. 5.6(a) indicates that such wings would operate with $K_T \lesssim 6$, while 10^o is probably the upper limit on α for soaring flight, so it is to this area $(K_T \lesssim 6, \alpha \lesssim 10^o)$ that we have confined our study.

Throughout this chapter *all* calculations involving angle of attack have used radians as the unit of angle. However for clarity units of degrees are shown in all figures where angle of attack is the independent variable.

5.2 *CRITICAL TENSION NUMBER*

The tension number K_T, defined by

$$K_T \quad \frac{T}{\frac{1}{2}\rho c u_0^2} ,$$

is a dimensionless parameter relating the tension to the dynamic pressure force acting on the sail. For sails of constant tension there exists a *critical tension number* (K_{Tc}) such that for $K_T < K_{Tc}$ the tension force is insufficient to maintain the aerodynamic forces.

It is seen that as $K_T \to K_{Tc}$ (from above) the camber function $C(x)$ increases rapidly (c.f. Fig. 5.4). For $K_T < K_{Tc}$ the linear theories (Thwaites (1961), Nielsen (1963)) predict profiles which are not purely convex - however it is highly unlikely that such profiles are stable in reality, the sail flapping or luffing as is often seen with yacht sails. SAIL is unable to predict a convergent solution for the camber when $K_T \leq K_{Tc}$.

The most accurate estimates of K_{Tc} to date have been obtained using the linear theories of Nielsen (1963) and Chambers (1966), the results being $K_{Tc} = 1.72745$ (Nielsen)

and $K_{Tc} = 1.7272$ (Chambers).

Results obtained from SAIL indicate that K_{Tc} is not a constant but a function of angle of attack, the critical value increasing with α. Recall that the equation relating tension and aerodynamic forces is

$$P(x) = \frac{-Ty''(x)}{(1 + y'(x)^2)^{3/2}} .$$

The linear theories make the assumption that the slopes are negligible everywhere, and hence approximate the restoring force by $-Ty''(x)$. This is clearly an overestimation for sails with non-negligible camber, and results in the linear theories predicting smaller camber functions than the exact theory.

As $K_T \to K_{Tc}$ the maximum camber $C(x)_{max} \to \infty$ so that $\frac{1}{C(x)_{max}} \to 0$. A linear regression analysis was carried out on data for $\frac{1}{C(x)_{max}}$ (generated by SAIL) using the least squares method. Correlation coefficients were calculated and values of K_{Tc} were obtained by extrapolation. The correlation coefficients (all > 0.999) indicated the validity of a linear approximation. Figure 5.1 shows the variation of K_{Tc} with α. Note that SAIL results approach those of the linear theories as $\alpha \to 0$.

Dr. M. Irvine (University of Auckland) suggested the possibility of estimating K_{Tc} by assuming the sail profile to be a circular arc. Clearly the maximum lift a circular arc profile can generate, occurs when the profile becomes a semicircle, and hence we would expect that in this case $K_T \approx K_{Tc}$.

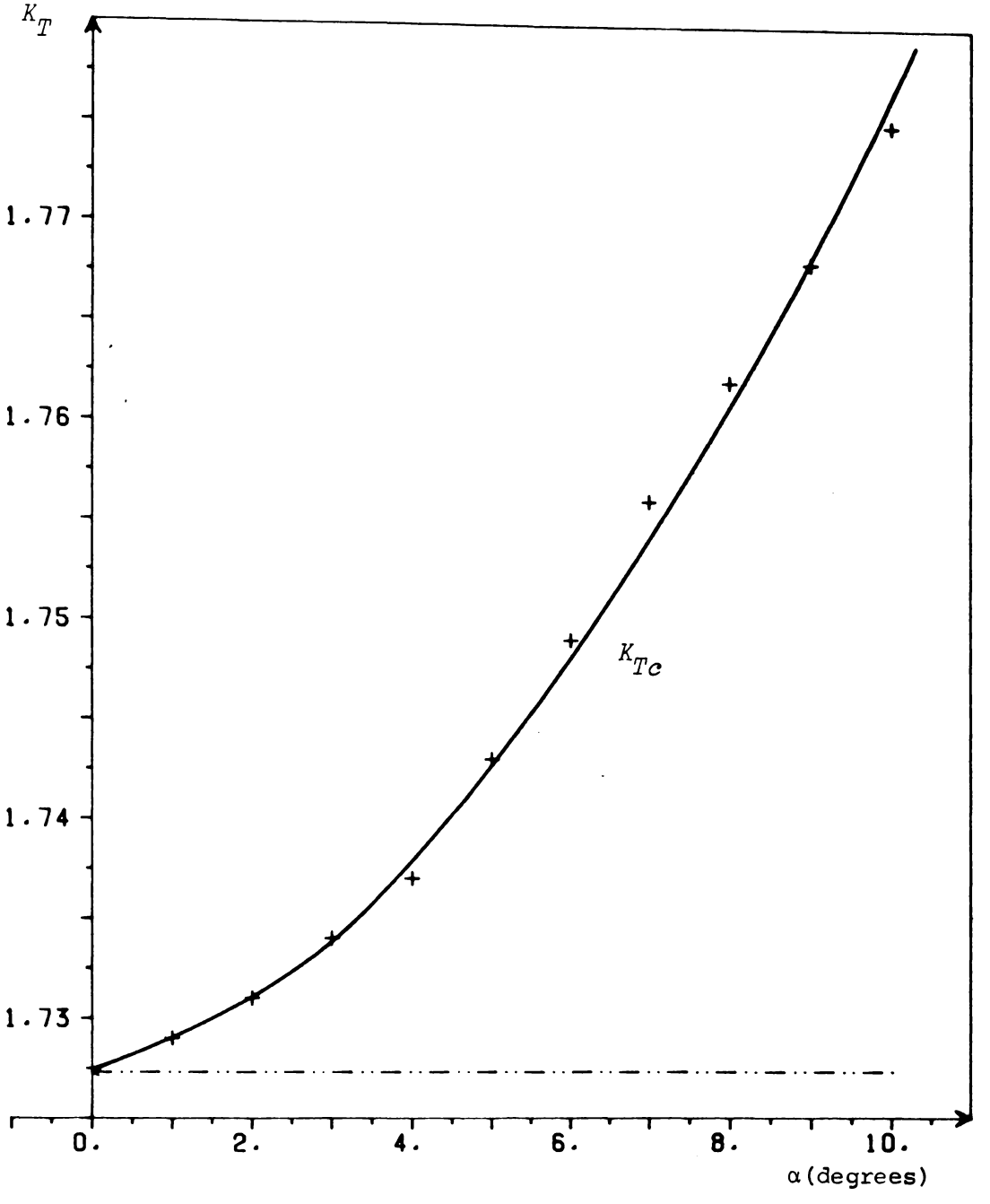

Fig. 5.1 Variation of critical tension number with angle of attack. SAIL prediction for K_{Tc} approaches linear theory result as $\alpha \to 0$.

\+ SAIL result

——— smooth curve approximation

–·–·–·– linear theory prediction (1.7273)

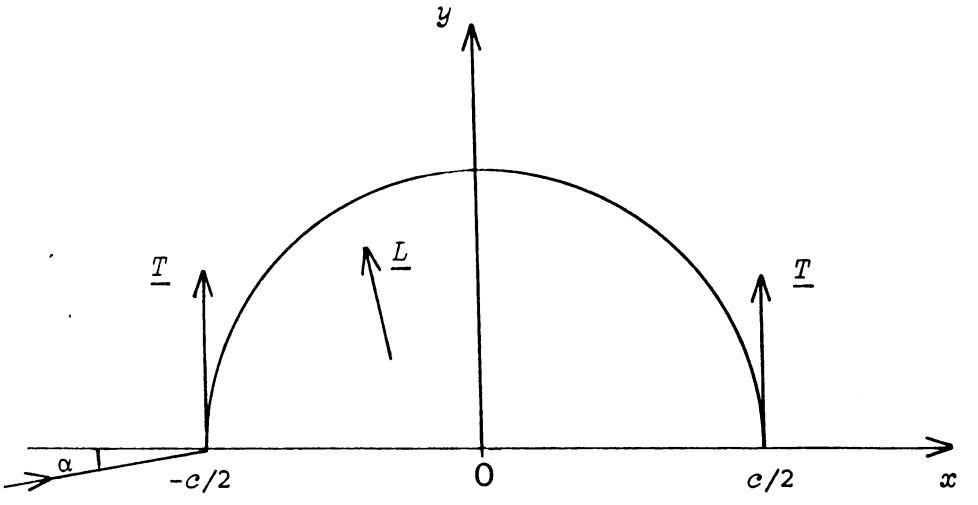

Fig. 5.2 Sail with semicircular profile.

The lift coefficient for a circular arc profile is readily obtained as

$$C_L = 2\pi \frac{\sin(\alpha + \beta)}{\cos\beta}$$

where β is defined in the ξ plane as

$$\beta = \tan^{-1}\left(\frac{2h}{c}\right)$$

and h is the maximum camber.

Immediately we have for the semicircular profile,

$$C_L = 2\sqrt{2}\,\pi \sin(\alpha + \pi/4)$$

or

$$L = \sqrt{2}\,\pi\rho c\, u_0^2 \sin(\alpha + \pi/4).$$

For equilibrium we require

$$2T\cos\alpha = \sqrt{2}\ \pi\rho c u_0^2 \sin(\alpha + \pi/4)$$

so that

$$K_{Tc} = \sqrt{2}\ \pi\ \sin(\alpha + \pi/4)/\cos\alpha$$

$$= \pi(1 + \tan\alpha). \qquad (1)$$

Clearly this approximation also indicates that K_{Tc} increases with increasing angle of attack, although its value is somewhat higher than predicted by SAIL.

Experimental results for K_{Tc} are difficult to compare with theory, since the large camber obtained just before criticality causes severe separation (stall) of the airflow from the top surface of the profile. This reduces the pressure differential across the membrane below its theoretical value and hence also reduces the lift and camber. However the onset of criticality in the wind tunnel tests did occur and in a very spectular manner. As the airspeed was increased (reducing K_T) beyond the stall, the sail took up more camber as expected, until suddenly the trailing edge started oscillating rapidly back and forth. This phenomenon is readily explained:

(i) At criticality the force normal to the chord exceeds the tension forces causing the sail to billow rapidly (i.e. camber function $C(x) = y(x)/c$ rapidly increases).

(ii) When the sail has very large camber, total separation occurs reducing the lift substantially, and allowing the membrane to relax back into a low camber profile.

(iii) With the sail in a lifting configuration again the profile billows rapidly.

Thus the sail oscillated violently with a frequency of approximately 10 Hz.

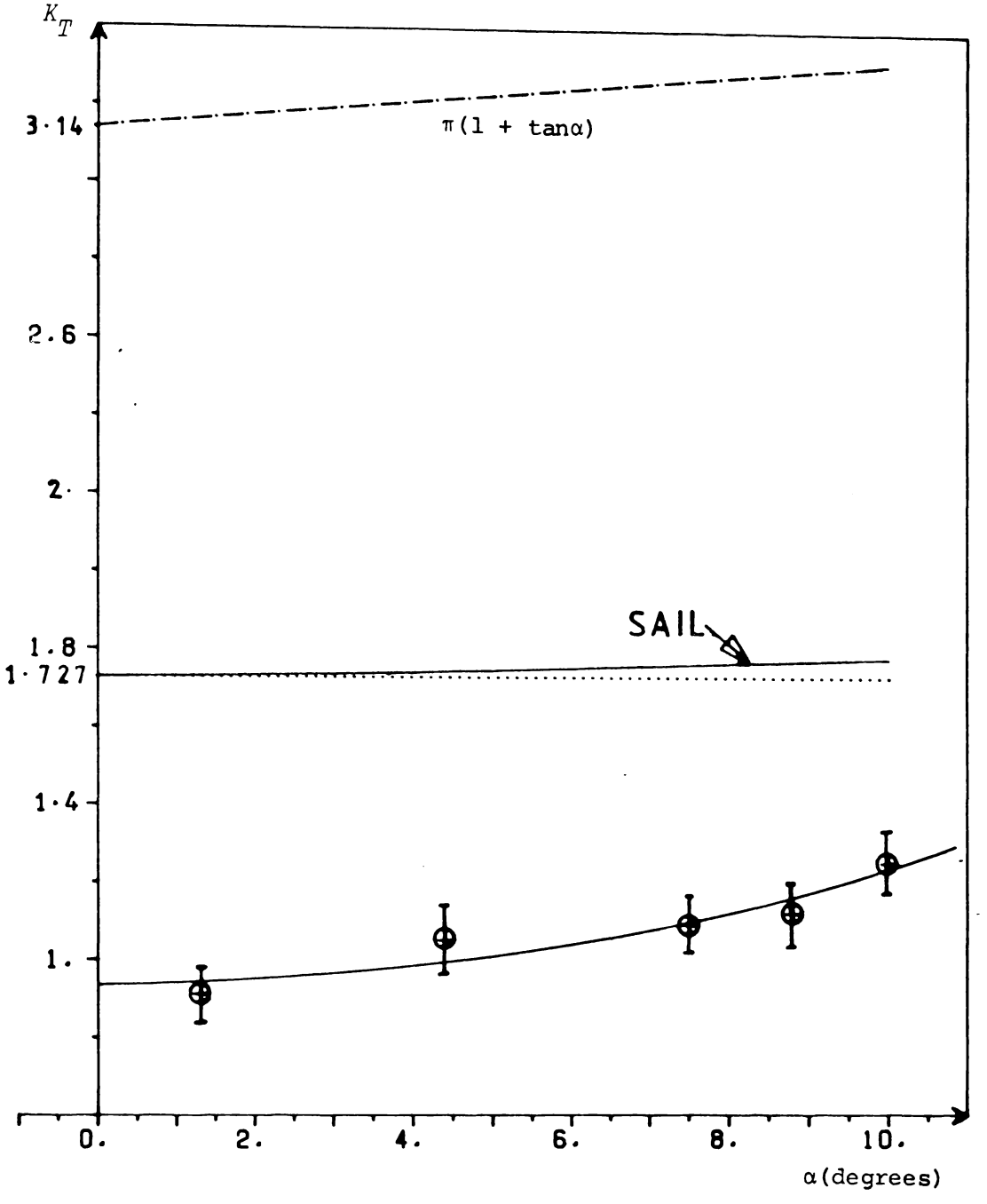

Fig. 5.3 Critical tension number versus angle of attack. Comparison of theoretical results with experimentally observed values. Experimental results were obtained by averaging several trials, error bars indicating 2σ .

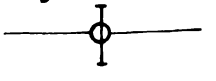

experimental

SAIL

linear theory

circular arc approximation ($\pi(1 + \tan\alpha)$)

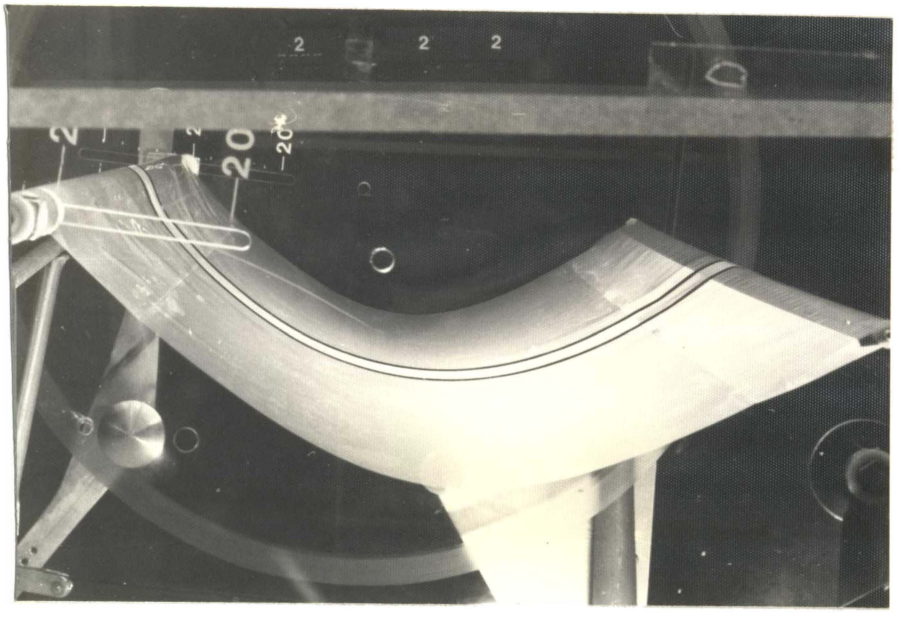

Plate 5. Profile just prior to luff.

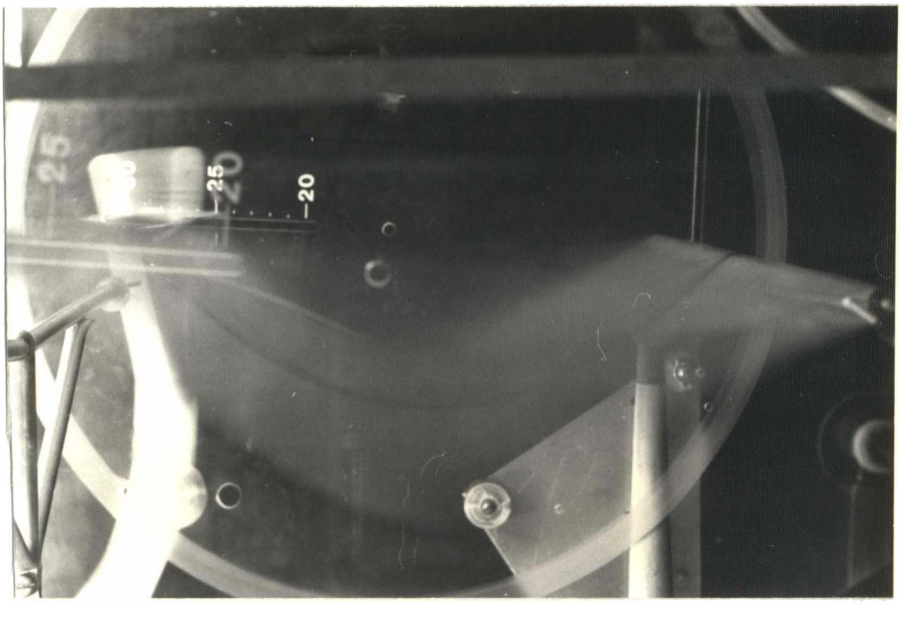

Plate 6. Time exposure during luff.

5.3 *PROFILES*

SAIL predicts convergent solutions for the profile only when $K_T > K_{Tc}$, and it is seen that all such solutions have positive camber and no points of inflexion. For $K_T \geq 6$ the sail properties are approaching those of a flat plate and hence the linear approximations are valid and almost indistinguisable from SAIL results.

Typical profiles are shown in Fig. 5.4 (not to scale) with the linear predictions for comparison. Note that for $K_T = 5$ the differences are small, especially for small angles of attack. However as $K_T \to K_{Tc}$ the cambers become noticeably different, as the non-linearities included in SAIL become significant.

Fig. 5.5 compares experimentally observed profiles with SAIL predictions. The experimental results were obtained by photographing the membrane during the wind tunnel tests. For moderately cambered sails the profile remained completely stable, but as K_T was reduced the sail surface initially vibrated (small amplitude) at a high frequency, and then at criticality luffed.

The most important parameters characterizing the profile are the *maximum camber* $(C(x)_{max})$ and *position of maximum camber*, and are both expressed as a fraction of the chord. Observations of hang gliders in flight, indicate that typical sail wings operate with

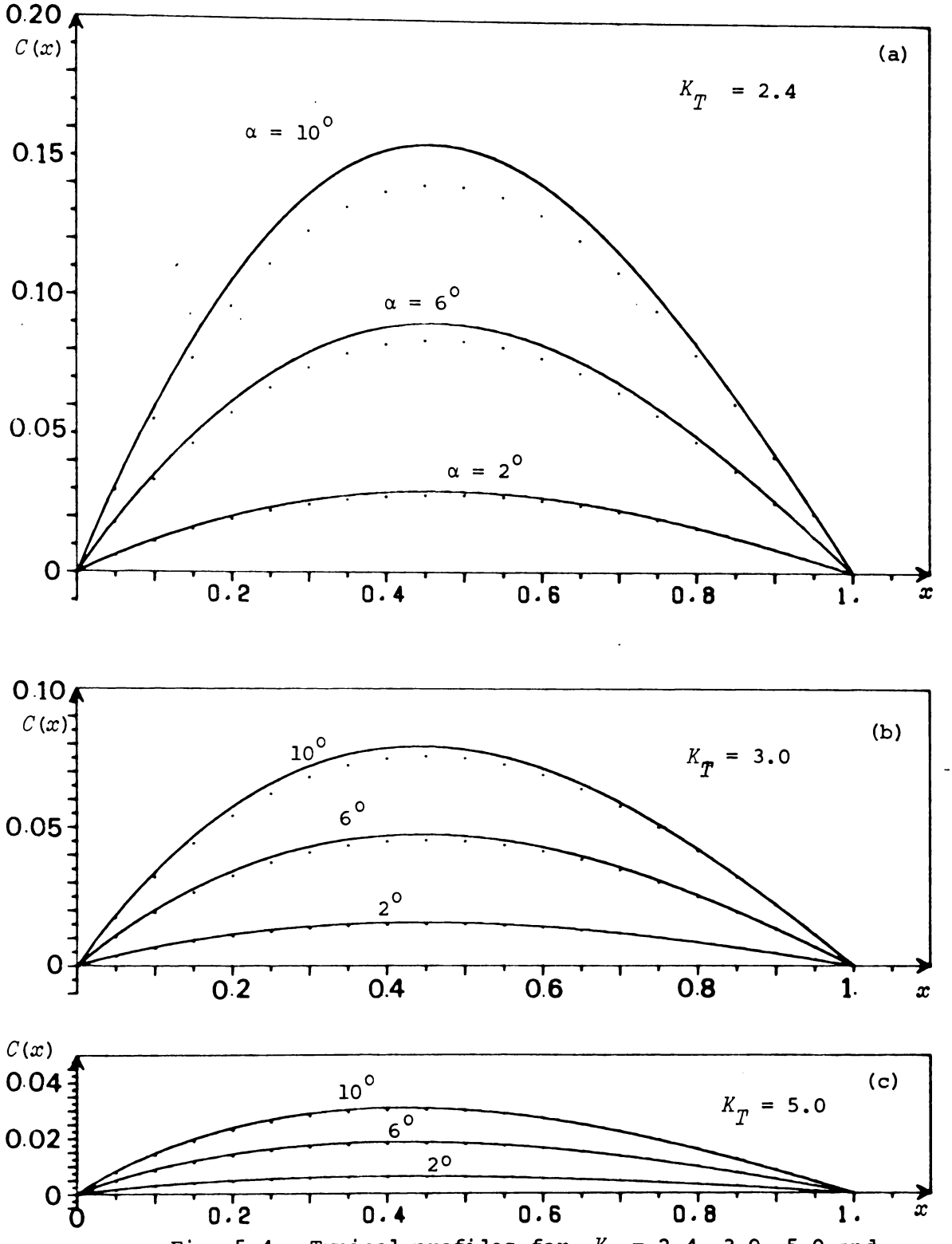

Fig. 5.4 Typical profiles for K_T = 2.4, 3.0, 5.0 and $\alpha = 2^\circ$, 6° and 10°.

——— SAIL

····· Nielsen

(Note exaggeration of vertical scale.)

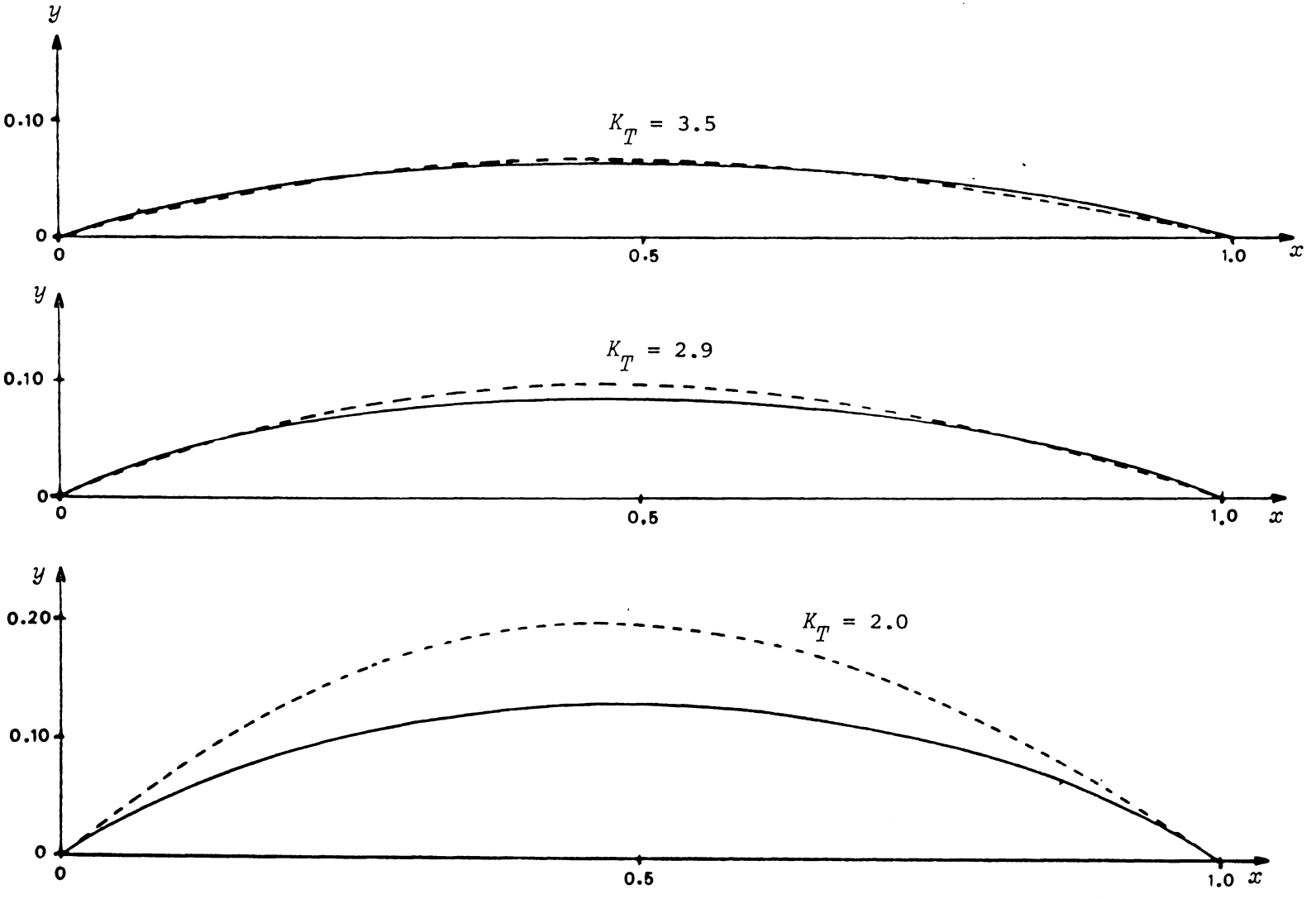

Fig. 5.5 Comparison of experimental and theoretical sail profiles ($\alpha = 10^{o}$)

——— experimental, – – – – – – SAIL

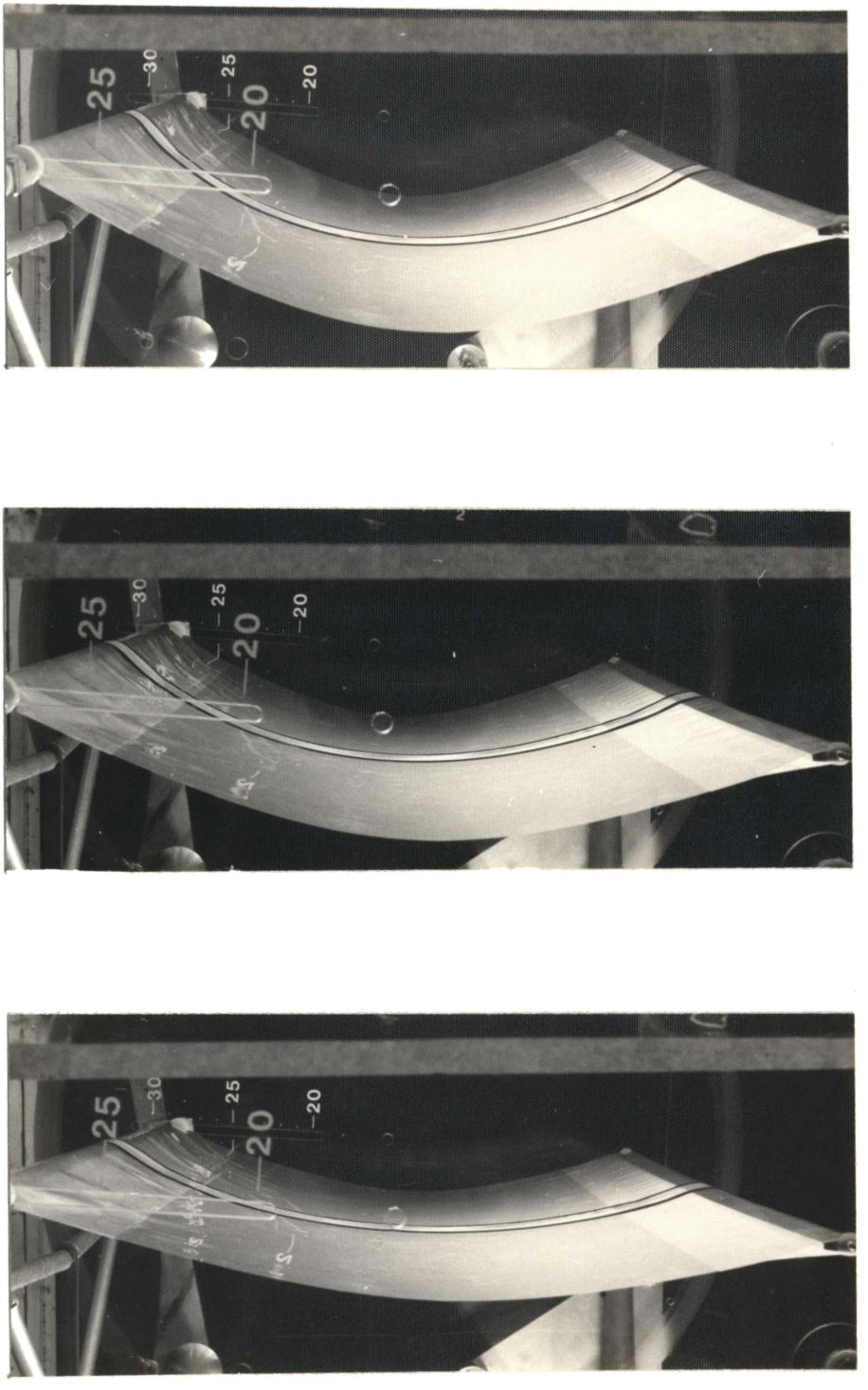

Plate 7. Typical sail profiles during tests.

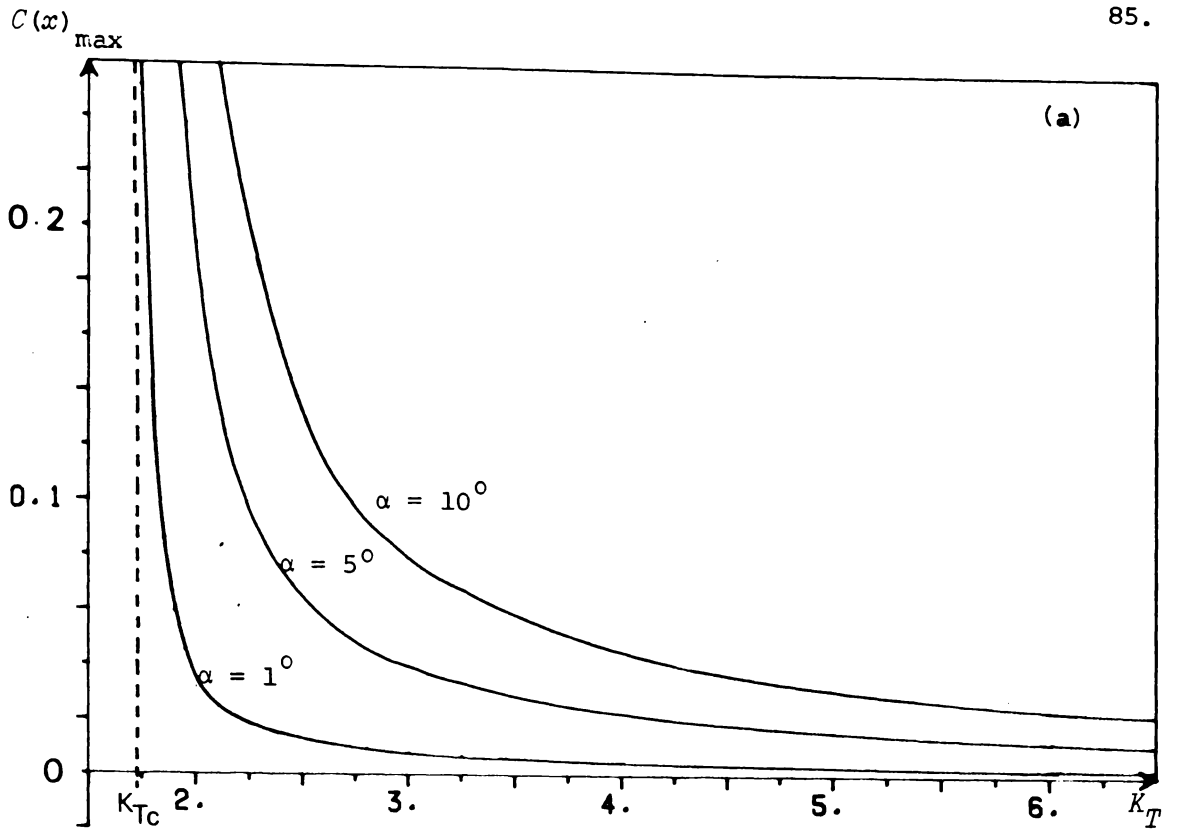

(a) Variation of maximum camber with tension number.

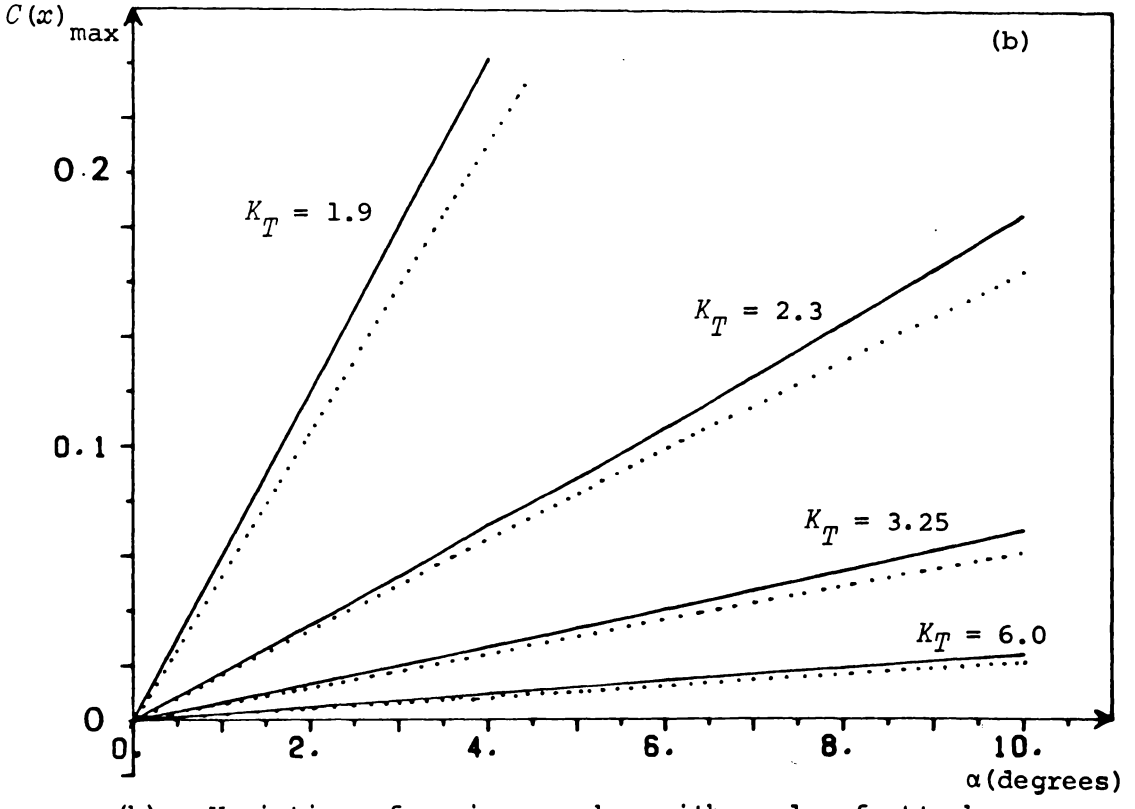

(b) Variation of maximum camber with angle of attack, and comparison with linear theory result (Nielsen ....)

Fig. 5.6 Maximum camber predicted by SAIL.

$C(x)_{max} \sim 0.1$ although somewhat higher values have been noted.[1] For small K_T , SAIL predicts large cambers, and in fact as $K_T \to K_{Tc}$, $C(x)_{max} \to \infty$. However maximum cambers greater than $c/4$ are not of great interest as they rarely (if ever!) occur under flight conditions. Fig. 5.6 shows the variation of maximum camber with K_T and α . Note that extremely high cambers are possible, even for very low angles of attack if K_T is close to its critical value.

The position of maximum camber is found to vary between $x = 0.5$ for $K_T \to K_{Tc}$ and $x = 0.4$ for very high tension numbers. This variation is due to the movement of the centre of pressure with K_T. The lift due to camber has its centre of pressure at the half chord point, while the lift due to an inclined flat plate has its centre of pressure at the quarter chord point. Fig. 5.7 shows the variation of the position of maximum camber of a function of tension number.

The camber function may be expanded as a power series in α , i.e.

$$C(\alpha, K_T, x) = C_0(K_T, x) + \alpha\, C_1(K_T, x) + \alpha^2\, C_2(K_T, x) + \ldots\ldots$$
$$= \sum_{n=0}^{\infty} C_n(K_T, x)\, \alpha^n \quad .$$

---

[1] Television coverage of the 1978 New Zealand Bird Man Rally showed one entrant's craft in stable flight with $C(x)_{max} \sim 0.2$. The wing consisted of a single surface of stretchable transparent plastic fixed to leading and trailing edge spars. The craft flew slowly and the camber was completely stable.

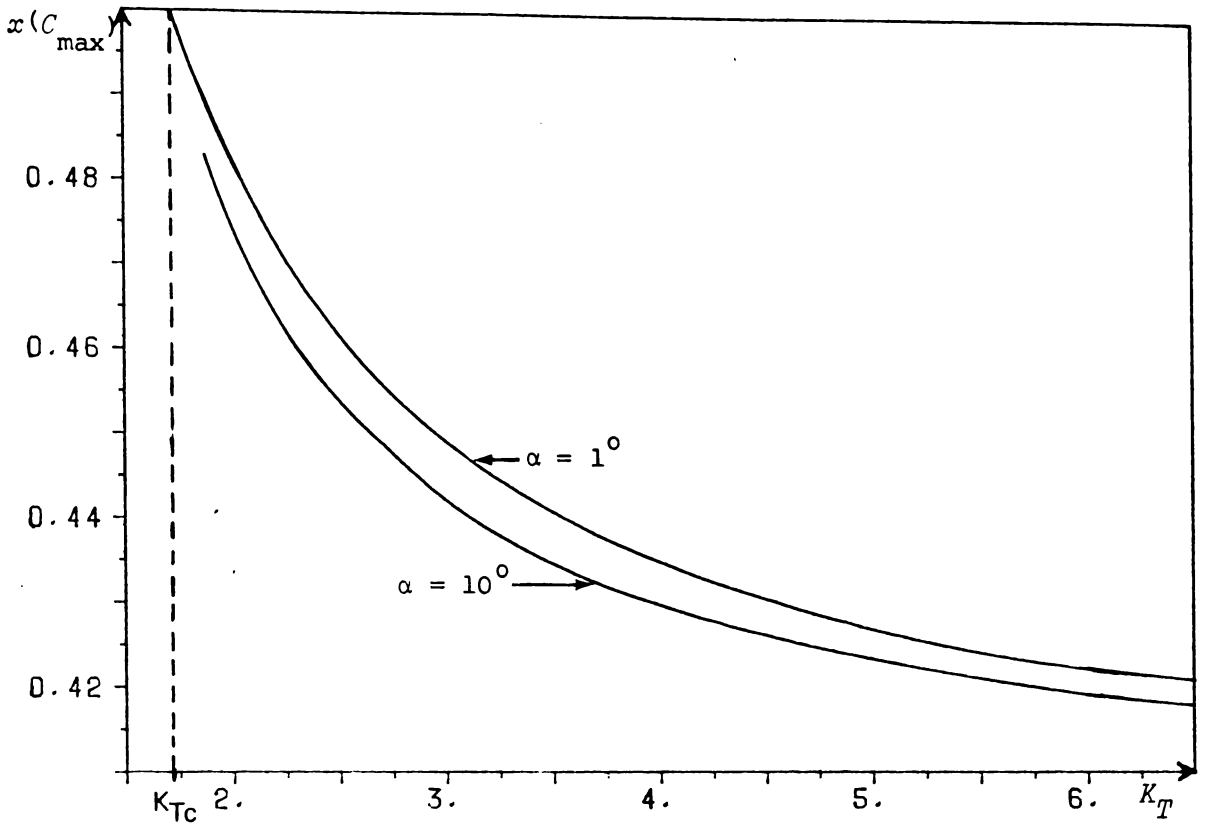

Fig. 5.7 Position of maximum camber ($x(C_{max})$) as a function of tension number.

However $C(\alpha,K_T,x)$ must be an odd function of α, since if the sign of α is reversed the sail simply billows an equal amount in the opposite direction. Thus only odd powers of α contribute (the coefficients for even powers of α being zero), so that

$$C(\alpha,K_T,x) = \sum_{n=1(n \text{ odd})}^{\infty} C_n(K_T,x)\,\alpha^n \qquad (2)$$

The linear theories predict a camber function which is directly proportional to α, and so evaluate only the first term of the series. With the exact solution obtained from SAIL we are able to analyze further coefficients in the power series.

Using a non-linear least squares regression technique the

coefficients C_1 and C_3 were obtained for several values of K_T, at the mid-chord point (Table 5.1). Calculations were performed with the angle of attack measured in units of radians.

K_T	2.1	2.5	4.0	10.0
$C_1(K_T,0.5)$	1.571	0.734	0.252	0.0704
$C_3(K_T,0.5)$	3.595	0.685	0.0586	-0.0405

Table 5.1 Typical values for coefficients C_1 and C_3 for use in equation 5.2.

5.4 *LIFT*

Recall from 2.7.1 that the lift is usually expressed in terms of a dimensionless lift coefficient C_L, defined as

$$C_L = \frac{L}{\frac{1}{2}\rho u_0^2 c} .$$

SAIL results for C_L are shown and comparisons made with both linear theory and experimental results.

Typical full size aircraft in normal flight, operate with C_L in the range 0.4 to 0.9, while high performance gliders may produce lift coefficients up to 1.8. With the use of flaps, slats and other lift producing devices C_L may be increased significantly, although at the expense of increased drag.

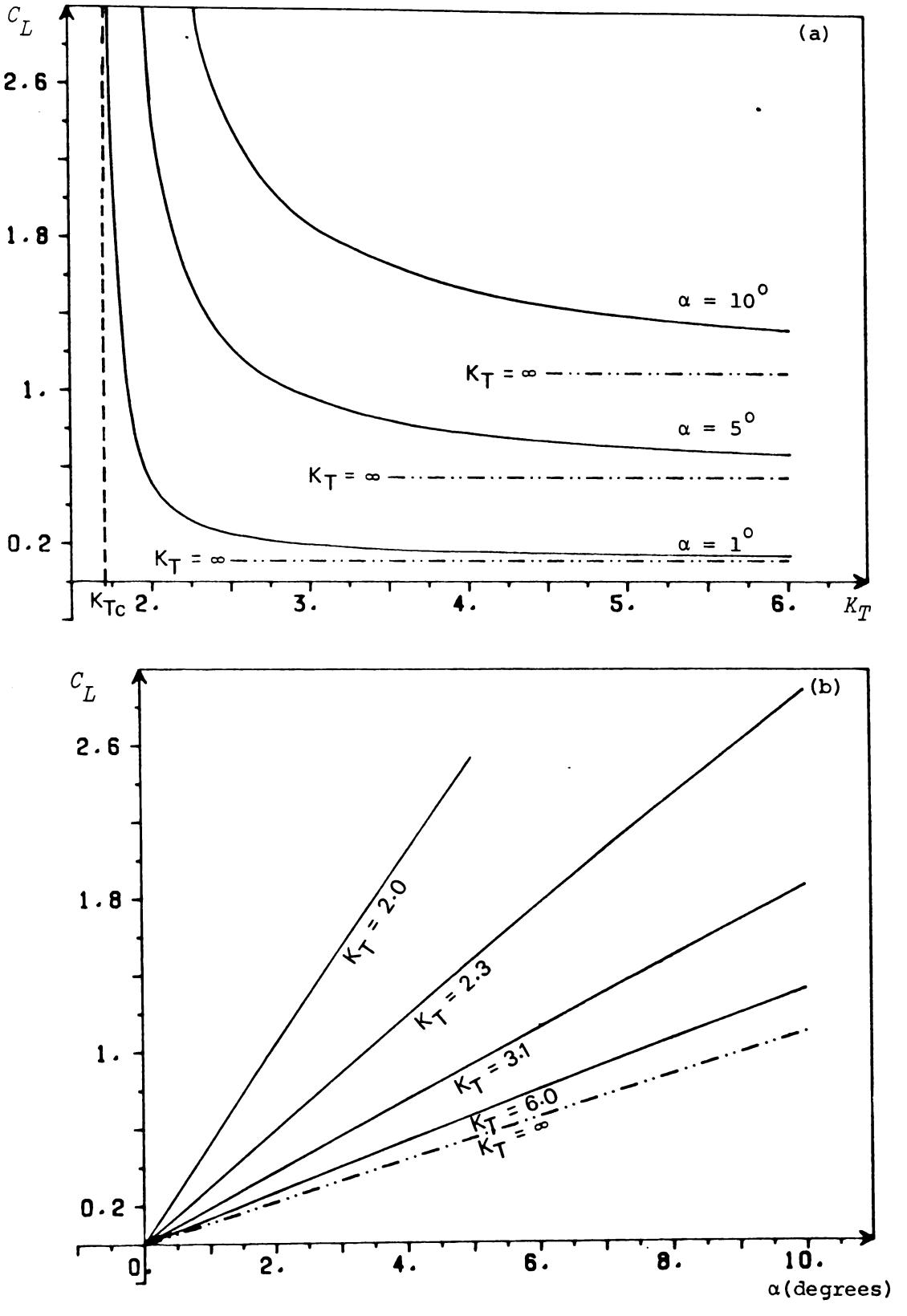

Fig. 5.8 Variation of lift coefficient C_L with
(a) tension number
and (b) angle of attack.
The limits shown for C_L when $K_T = \infty$
are the flat plate value of $2\pi\alpha$.

Observation of Figs. 5.8 show that C_L behaves as expected, increasing with increasing angle of attack and decreasing with increasing tension number. Note that high C_L values are attainable for even low angles of attack, and that as K_T approaches its critical value ($K_{Tc}(\alpha)$) C_L increases rapidly. The use of low angles of attack to generate high lift coefficients would in practice be questionable, since very small variations in K_T (e.g. a small decrease in u_0) result in large variationsin C_L.

Note that as $K_T \to \infty$, C_L approaches the flat plate value of $2\pi\alpha$ as expected. The linear theories of Thwaites (1961) and Sneyd, et al. (1979) predict C_L to be directly proportional to α, i.e.

$$C_L = \alpha \, \bar{C}_L(K_T) \ .$$

Equation (72) of Thwaites (1961) gives an empirical formula for the lift coefficient, namely,

$$C_L = 2\pi\alpha + 6.36 \left(\frac{\varepsilon}{c}\right)^{\frac{1}{2}}$$

where $\varepsilon = s - c$, (s is sail length) and $\frac{1}{\alpha}\left(\frac{\varepsilon}{c}\right)^{\frac{1}{2}}$ is a function of K_T only. The actual constant given in the equation and the abstract (Thwaites (1961)) is 0.636. However a private communication between Professor Thwaites and Nielsen (1963) confirms that the value should be 6.36. Nielsen (1963) gives a similar empirical formula (equation 31)) for the lift coefficient:

$$C_L = 2\pi\alpha + 7.28\left(\frac{\varepsilon}{c}\right)^{\frac{1}{2}} - 1.69 \left(\frac{\varepsilon}{c}\right)^{\frac{1}{4}} \ .$$

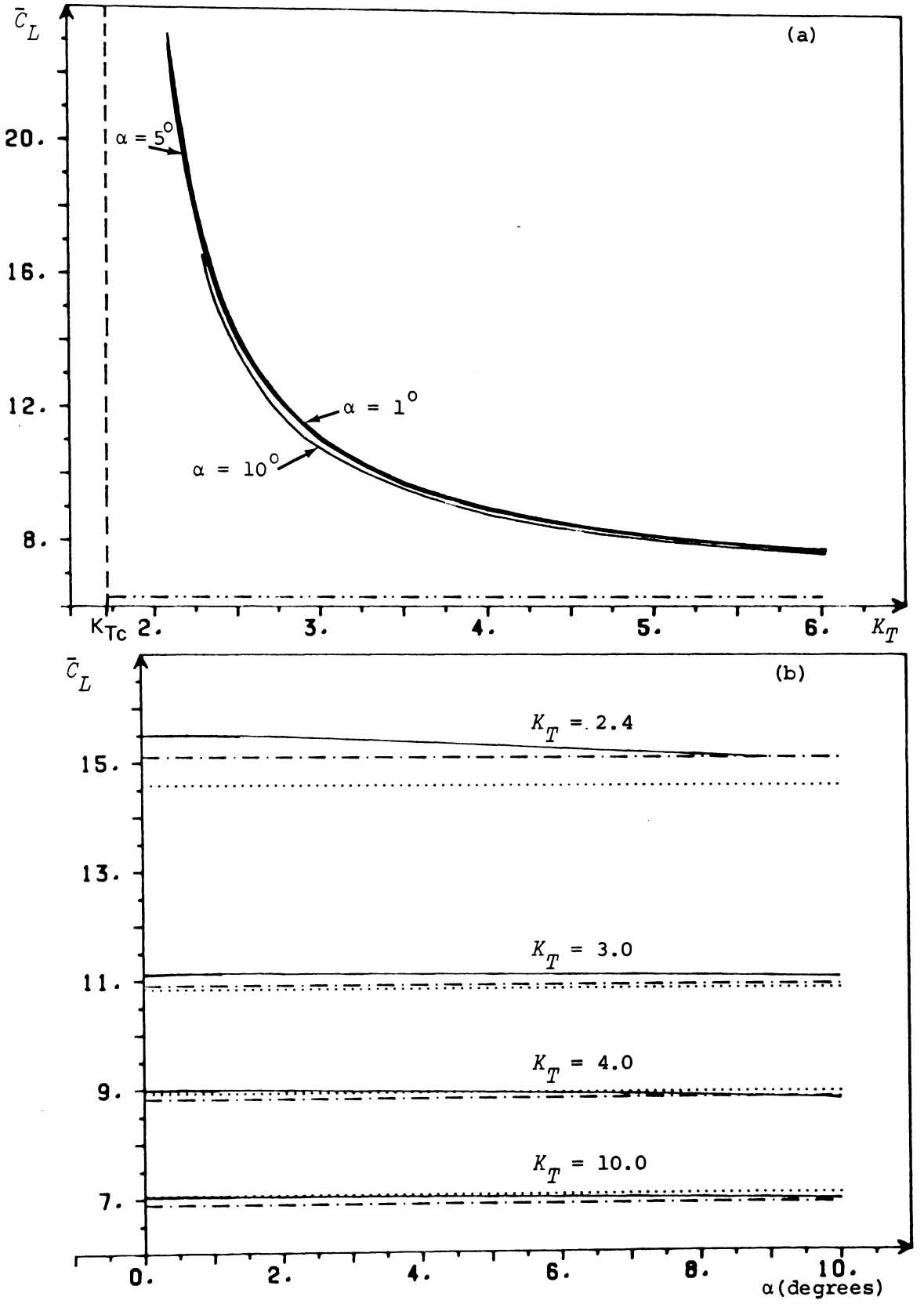

Fig. 5.9 Variation of $\bar{C}_L$ with K_T and α . Note small dependence on angle of attack, and increased lift over linear theory predictions.

——— SAIL, —·—·—·—Nielsen, ····· Thwaites.

However notice that C_L/α is still a function of angle of attack, since the last term becomes

$$-1.69\left(\frac{\varepsilon}{c}\right)^{\frac{1}{2}} = -1.69\ \alpha^{\frac{1}{2}}\left(\frac{\left(\frac{\varepsilon}{c}\right)^{\frac{1}{2}}}{\alpha}\right)^{\frac{1}{2}} .$$

The bracketed term of the R.H.S. of the identity is shown by Nielsen to be a function of K_T only, resulting in $\bar{C}_L$ being a function of $\alpha^{\frac{1}{2}}$. It is likely that there is an error in the last term of Nielsen's equation (31) since linear theory predictions of $\bar{C}_L$ are expected to be independent of angle of attack. This opinion is supported by the fact that Table (2) in Nielsen's paper lists values for $\bar{C}_L$ as a function of K_T only. It is these values that are used in the comparison with SAIL results, shown in Fig. 5.9(b).

The more accurate results obtained from SAIL indicate that $\bar{C}_L$ is indeed a function of angle of attack, decreasing with increasing angle of attack. This variation is thought to be due to the camber increasing not quite in proportion to α, and the lift increasing not quite in proportion to the maximum camber. Fig. 5.9(a) shows the variation of $\bar{C}_L$ with K_T for various α. Note that the variation with angle of attack is only small, so that the linear theory predictions for C_L are a good approximation to SAIL results for all cases except when the tension number approaches its critical value.

Experimental results for C_L appear to agree quite well with theory (Fig. 5.10). Note however the 'shift' in tension number, and the sudden reduction of slope as severe separation occurs. The shift

in K_T could be due to boundary layer effects reducing the air speed over the sail by increasing the blockage factors discussed in chapter 4. Since the sail is of negligible thickness compared to tunnel depth, no cross-sectional blockage correction was thought necessary. However the boundary layer thickness δ is given by $\delta \sim \frac{5.2\,\ell}{\sqrt{R_e}}$ (Kuithe et al. (1976)) so that for a typical test $\delta \sim 0.2$ cms. A small correction could thus have been included for profile thickness but it is thought that its effect would be negligible.

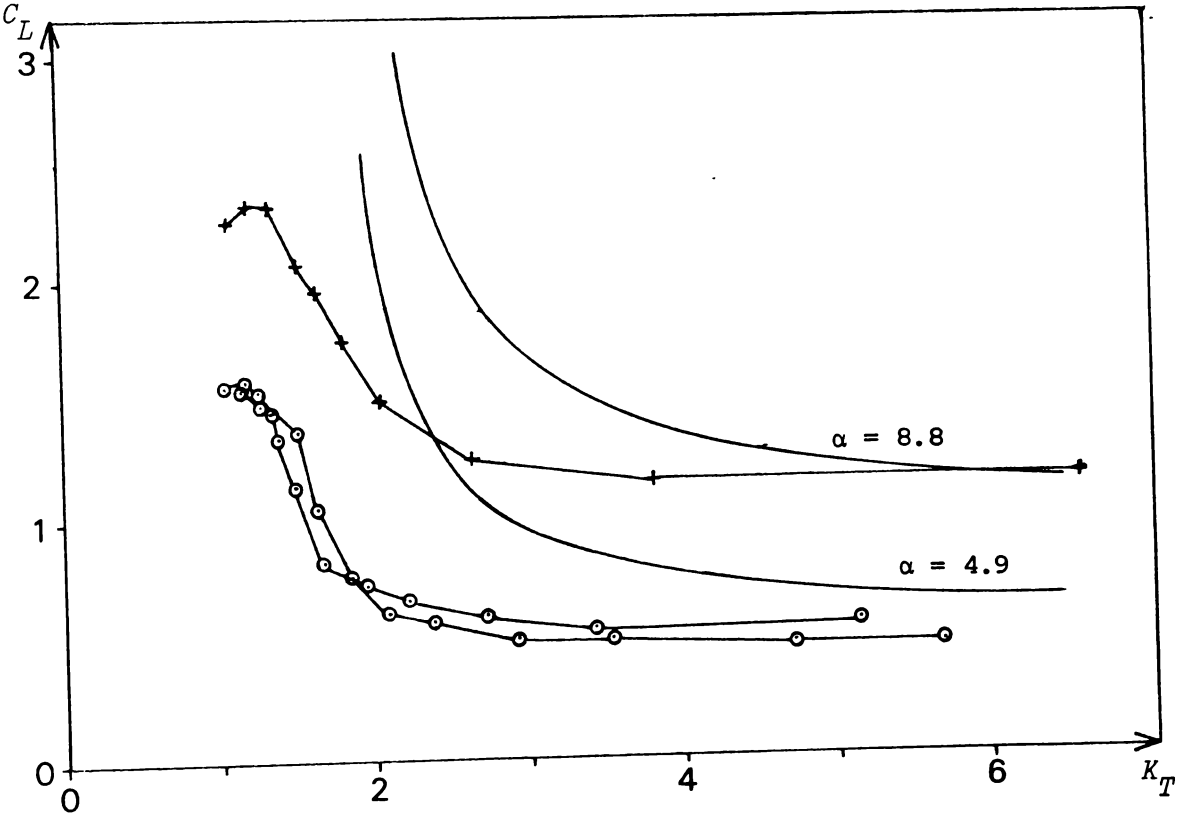

Fig. 5.10 Experimentally observed values of lift coefficient versus tension number, and comparison with theory.

—— SAIL

⊙ α = 4.9°

\+ α = 8.8° (2 runs)

5.5 *STABILITY*

Recall that the centre of pressure, x_P, is the point on the aerofoil chord through which the aerodynamic forces effectively act. Thus the longitudinal stability for a profile is determined by the sign of $dx_P/d\alpha$. When positive, an increase in α (e.g. due to an upgust) moves the centre of pressure toward the trailing edge. This produces a moment which tends to rotate the profile so as to decrease α toward its original value. Thus $\frac{dx_P}{d\alpha} > 0$ represents longitudinal stability, and conversely $\frac{dx_P}{d\alpha} < 0$ represents longitudinal instability.

Typical rigid aerofoils exhibit intrinsic longitudinal instability, with their centre of pressure being given by

$$x_P = c(\tfrac{1}{4} + c_3/(c_1 + c_2\alpha))$$

where c_1, c_2 and c_3 are positive constants, so that $\frac{dx_P}{d\alpha} < 0$. In marked contrast to this, sails can exhibit both positive and negative longitudinal stability. Linear theories predict

$$x_P = c\left(\tfrac{1}{4} + \frac{C_M}{C_L}\right)$$

where the moment coefficient $C_M = \alpha\, \bar{C}_M(K_T)$, and

the lift coefficient $C_L = \alpha\, \bar{C}_L(K_T)$,

so that $\frac{dx_P}{d\alpha} = 0$ (i.e. neutral stability). SAIL results indicate that flexible membrane wings have regimes of both longitudinal stability and instability, depending on the value of K_T. Figs. 5.11 show the variation of x_P with both tension number and angle of attack.

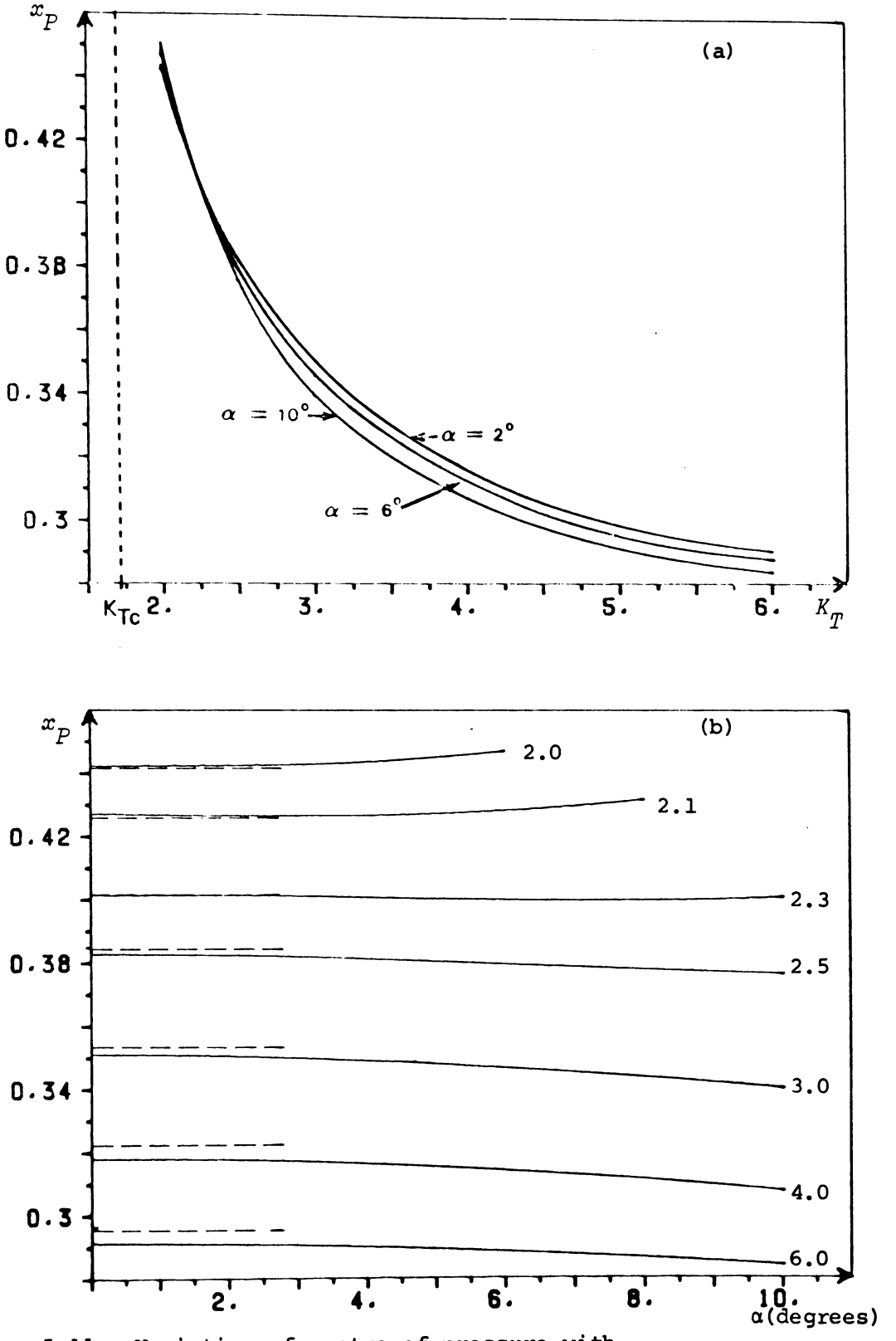

Fig. 5.11 Variation of centre of pressure with
(a) tension number
and (b) angle of attack.

——— SAIL — — — — Nielsen

Observation of Fig. 5.11 (a) indicates the very powerful effect that variation of tension number has on the centre of pressure. A very small change in K_T may have a much larger effect on x_P than, for example, a large change in α. It is possible that this powerful effect could be used as a pitch control mechanism for full size sail wings. An increase in K_T, obtained by tightening the chordwise tension, would cause a pitch up moment, while conversely a decrease in K_T would produce a pitch down moment. The variation in centre of pressure with α is small but significant. Note that for $K_T < 2.3$ the sail possesses positive longitudinal stability, while at higher tension numbers instability is predicted.

We may express the centre of pressure as a power series expansion in angle of attack, i.e.

$$x_P(K_T,\alpha) = a_0(K_T) + a_2(K_T)\alpha^2 + a_4(K_T)\alpha^4 + \ldots.$$

$$= \sum_{n=0\,(n\ \text{even})}^{\infty} a_n(K_T)\alpha^n \qquad (\alpha \text{ in radians}).$$

Note that x_P must be an even function of α since if the sign of α is reversed, only the camber and lift change direction, the centre of pressure remaining at the same point on the chord line. Clearly $a_0(K_T) = x_P(K_T,0)$, and should be close to the value for the centre of pressure predicted by thin aerofoil theory. If we assume that all terms of order greater that α^4 yield negligible sums then the above equation may be simplified to

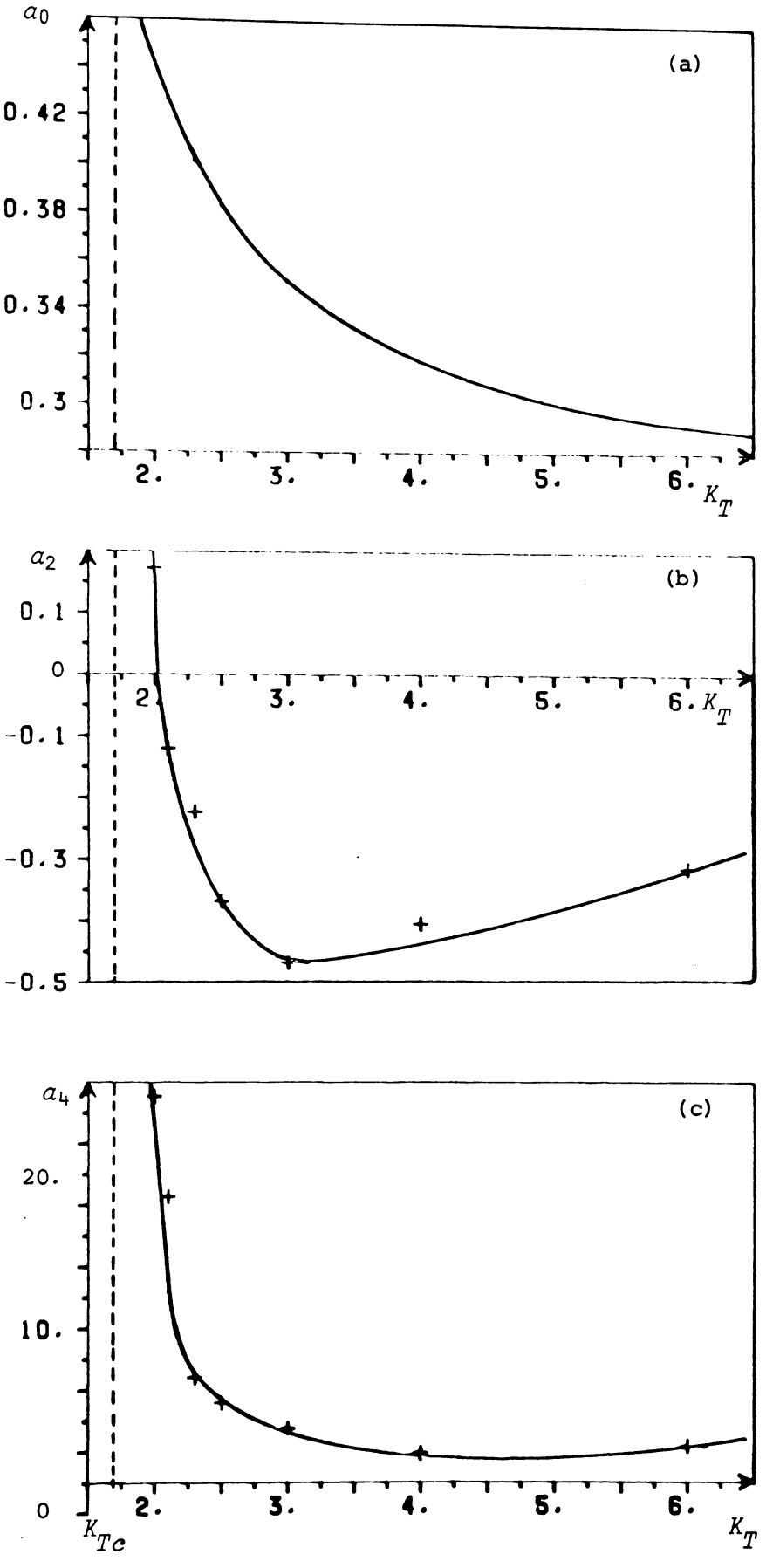

Fig. 5.12. Coefficients $a_0(K_T)$, $a_2(K_T)$ and a_4 K_T derived from SAIL results.

\+ derived values

——— smooth curve approximation

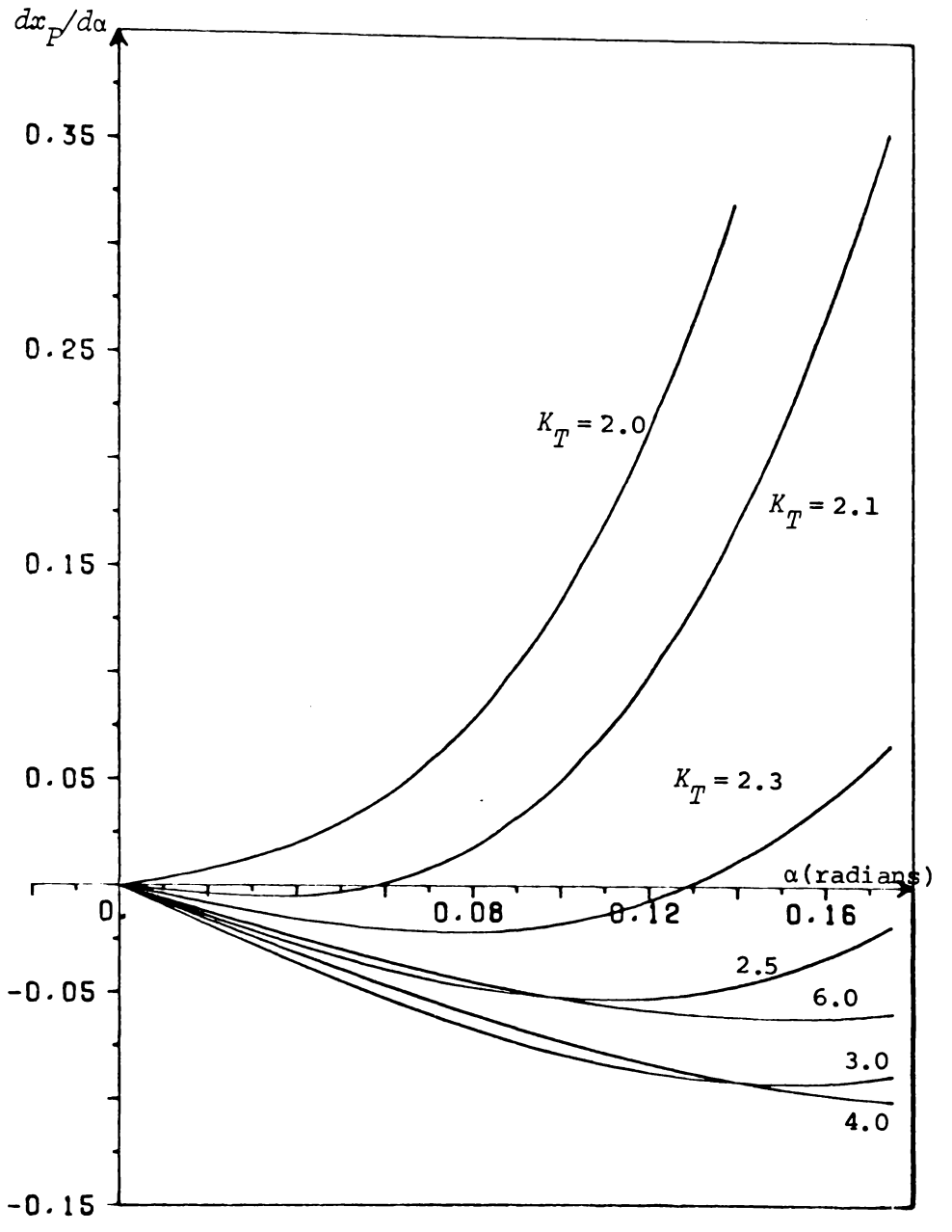

Fig. 5.13 $dx_P/d\alpha$ versus angle of attack.

The sail wing possesses longitudinal stability when $dx_P/d\alpha > 0$.

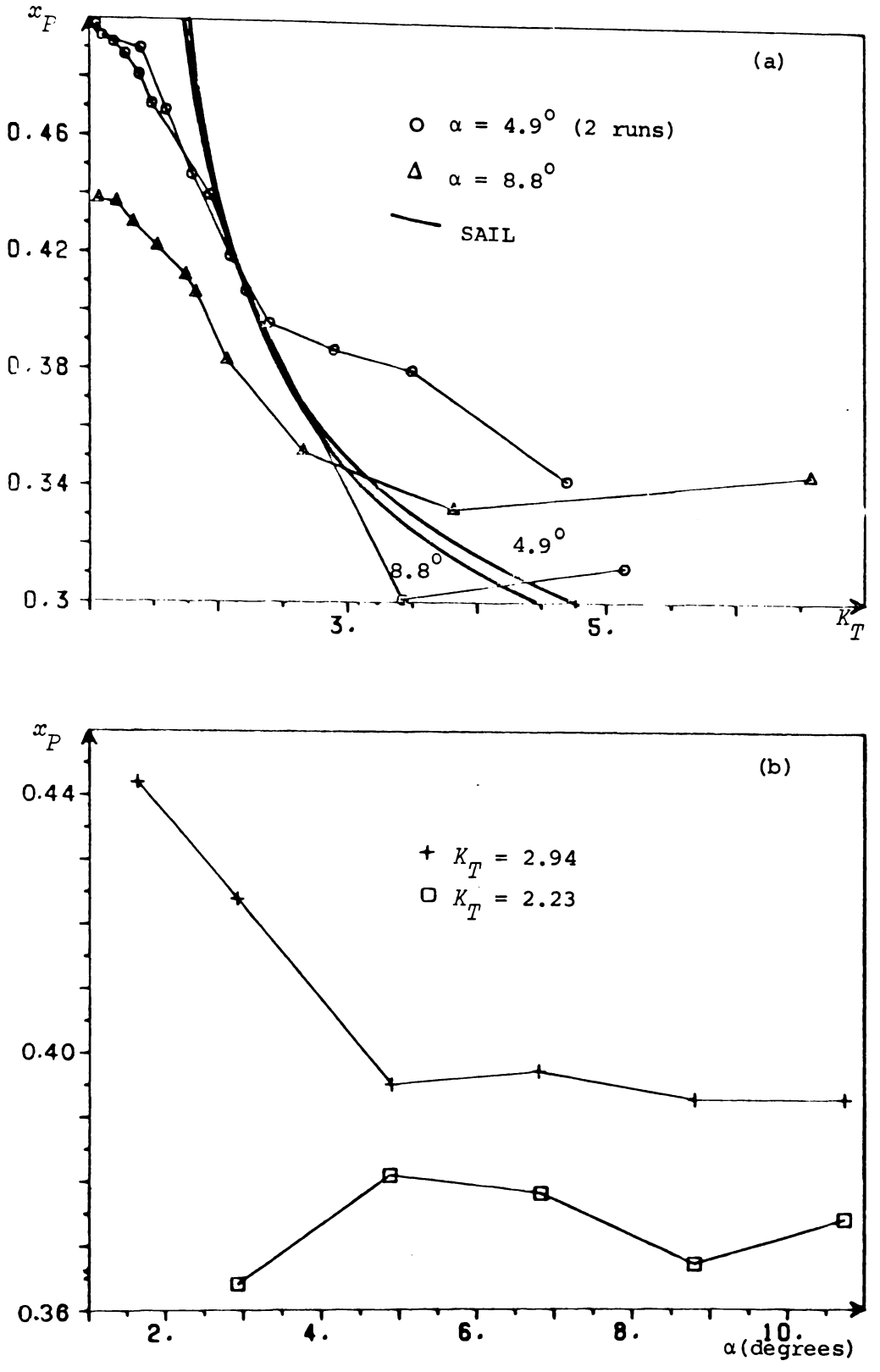

Fig. 5.14 Experimental results for centre of pressure versus (a) tension number and (b) angle of attack.

$$x_P(K_T,\alpha) \approx a_0(K_T) + a_2(K_T)\alpha^2 + a_4(K_T)\alpha^4 \quad .$$

An estimation for $_2a_2(K_T)$ and $a_4(K_T)$ may be obtained using a least squares non-linear regression technique on data for $x_P(K_T,\alpha) - a_0(K_T)$. The evaluated coefficients are displayed in Figs. 5.12 for a few selected values of K_T .

Numerical values for the longitudinal stability may be obtained using

$$\frac{d}{d\alpha} x_P(K_T,\alpha) \approx 2\ a_2(K_T)\alpha + 4\ a_4(K_T)\alpha^3 \quad .$$

Results for $\frac{dxP}{d\alpha}$ are shown in Fig. 5.13. Note that all computations were performed using radians as the unit of angle.

Experimental results for x_P are derived from measurements of pitching moment, lift and drag, as detailed in chapter 4, section 5. It was found that the results obtained were not reproduceable (see Fig. 5.14) especially for sails of low camber. However the general trends of x_P remaining roughly constant with variation of angle of attack can be seen.

The balance apparatus used, was not particularly suited to measuring the pitching moment, and this limitation was mentioned in discussions with staff and technicians in the University of Auckland School of Engineering. The major source of error appears to be caused by the mounting strut pivots (c.f. Figs. 4.1 and 4.9) where small frictional forces are thought to cause significant torques affecting the pitching moment measurement. Both brass and teflon bushes were

tried but with no obvious improvement in the results. A more sophisticated and suitable balance/sail configuration needs to be de designed specifically for the study of centre of pressure movement before more accurate and reliable results for x_p are obtained. A microprocessor monitoring strain gauge output could feasibly calculate and display the centre of pressure at a high sample rate with more precision than the mechanical balance used.

5.6 DRAG

Drag results shown were obtained from the experimental investigation detailed in chapter 4, and have been corrected for mounting apparatus drag. No theoretical comparison is made, since SAIL, being an inviscid fluid approximation, predicts zero drag.

The drag coefficient for three-dimensional wings is defined by

$$C_D = \frac{D}{\frac{1}{2}\rho u_0^2 c S}$$

where S is the span. For wings with fixed camber, C_D is typically less than 0.1, although at the stall this value increases rapidly and may attain values ~ 0.5. Fig. 5.15(a) shows samples of the variation of drag coefficient with angle of attack. Note that the C_D values are quite high, the minimum observed being ~ 0.09. Both sets of data are for sails of low tension number, so that significant camber was present especially for the higher angles of attack ($C_{max} \approx 0.02$ for

$\alpha \approx 2^{\circ}$ and $C_{max} \approx 0.2$ for $\alpha \approx 11^{\circ}$). Note that the sail of lower tension number ($K_T = 1.94$) gave a steeper slope for the C_D curve. This is expected and is caused by the sail taking up camber more rapidly than sails of higher tension number. (Indeed this situation was observed during the wind tunnel tests.)

Fig. 5.15(b) shows the variation of drag coefficient with tension number. The $C_{D_{min}}$ occurs when $K_T \sim 2.2$, where the sail is beginning to develop significant camber. For $K_T < 2$ the camber has increased to the point where form drag and severe separation are contributing a major proportion of the total drag.

The high drag coefficients may be caused by one or more of many factors including:

(i) The experiments were carried out in the sub-critical Reynolds number range ($Re \lesssim 3 \times 10^5$) so that the boundary layer would have been turbulent, giving increased drag.

(ii) The endplate dimensions may have been too small to render induced drag negligible. It was suggested that endplates may be required to extend several chords downwind of the trailing edge to reduce induced drag to an acceptable limit.

(iii) The gap between endplates and sail membrane ($\sim$ 2 mm) may have allowed significant leakage of air from the lower surface to the upper, and hence increase the induced drag.

(iv) The leading and trailing edge profiles may have caused turbulence or accelerated separation in some way.

(v) The mylar plastic sail membrane possessed a smooth glossy surface which is not conducive to delaying the point of boundary layer separation.

Other experimental investigations by Apperley (1977) and Chapleo (1968) have also reported high drag coefficients (~ 0.3) for sails. However both used fabric membranes so that extreme surface roughness, stitching and porosity could also have contributed to the drag figures observed.

The overall performance of a wing can often be estimated by determining the ratio of lift to drag. Typical values for high performance wings are ~ 15. The drag coefficients measured in the wind tunnel tests were comparitively high so that the lift to drag ratios appear quite low. Fig. 5.16(a) shows the variation of L/D as a function of angle of attack. Note the better performance achieved by the sail of lower tension number ($K_T = 1.94$), except for $\alpha \approx 10^{\circ}$ where severe separation has occurred. Fig. 5.16(b) indicates the variation of L/D with tension number. Note that the lift to drag ratio attains a maximum value of approximately 7 when $K_T \approx 1.7$. Thus it is in this region that we would expect wail wings to operate most efficiently.

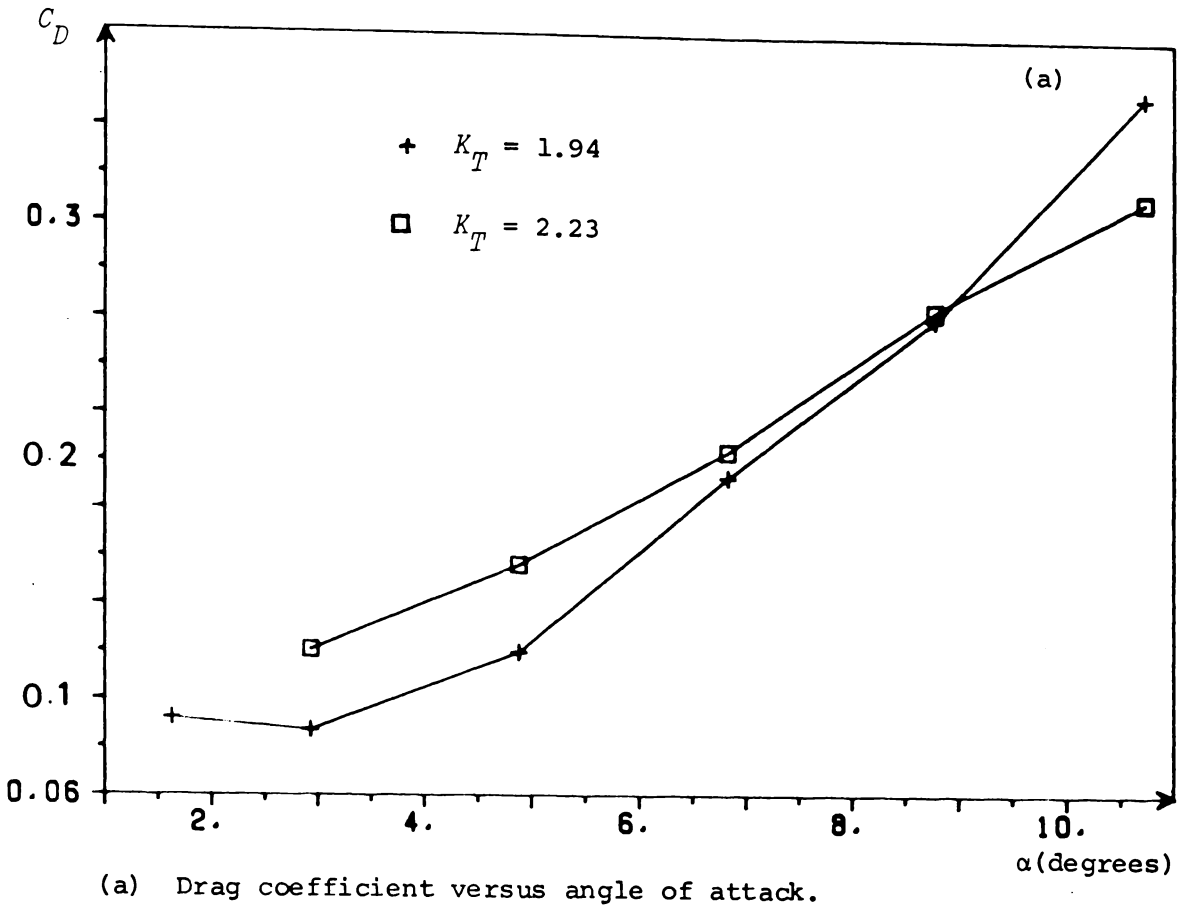

(a) Drag coefficient versus angle of attack.

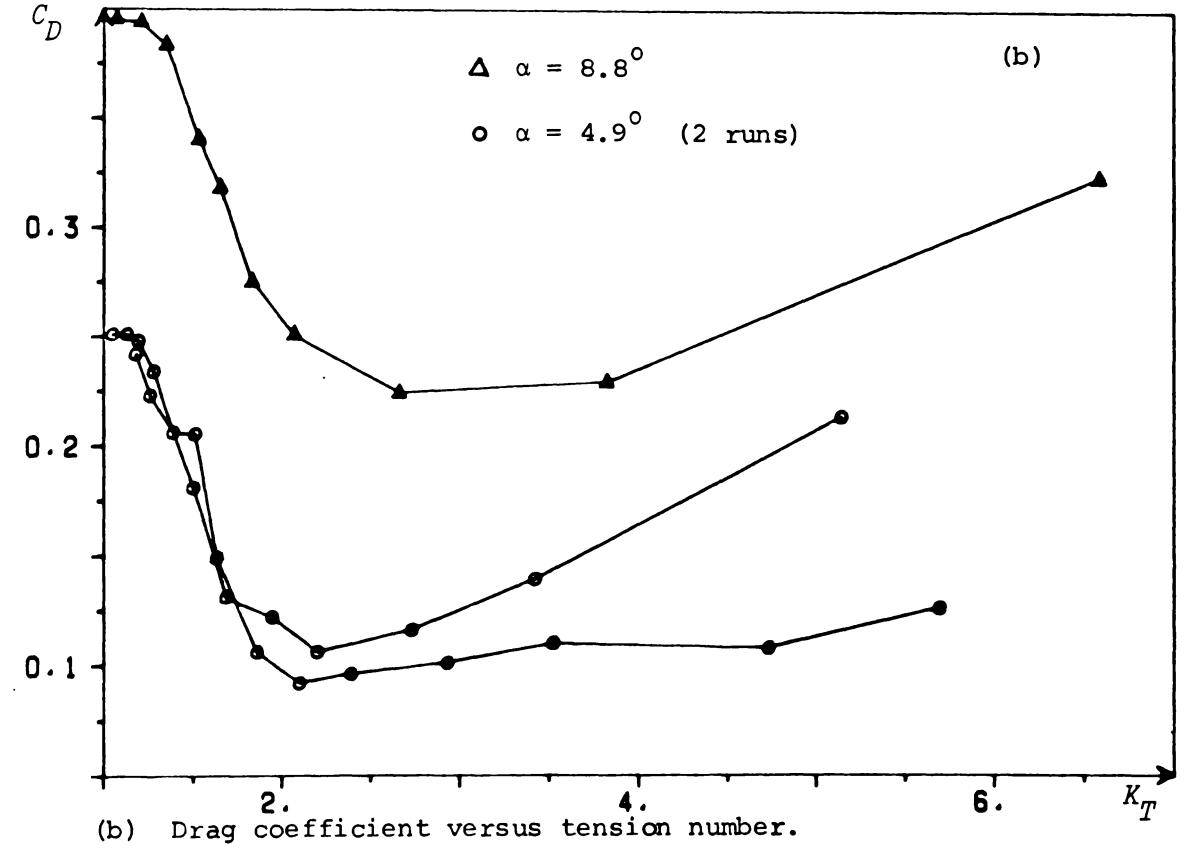

(b) Drag coefficient versus tension number.

Fig. 5.15 Experimentally observed drag coefficients.

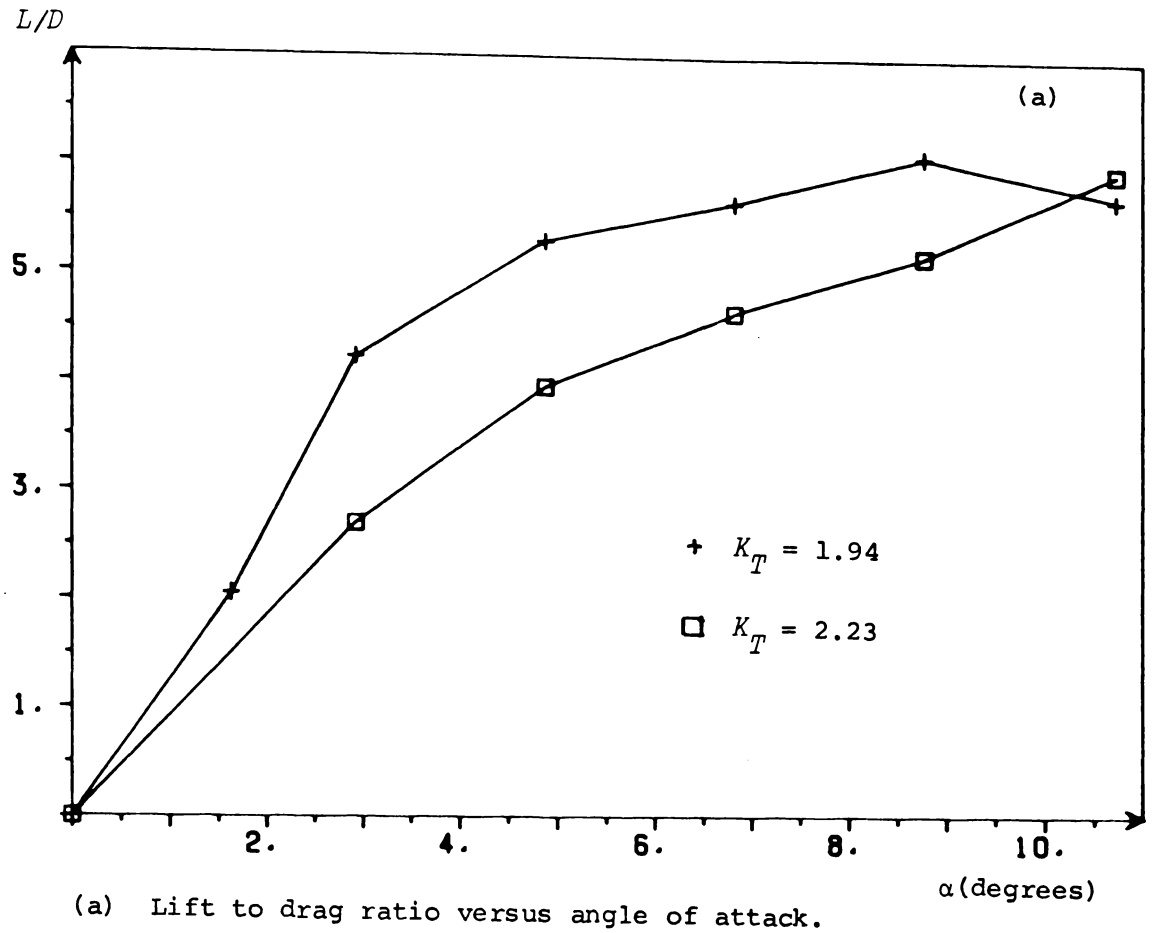

(a) Lift to drag ratio versus angle of attack.

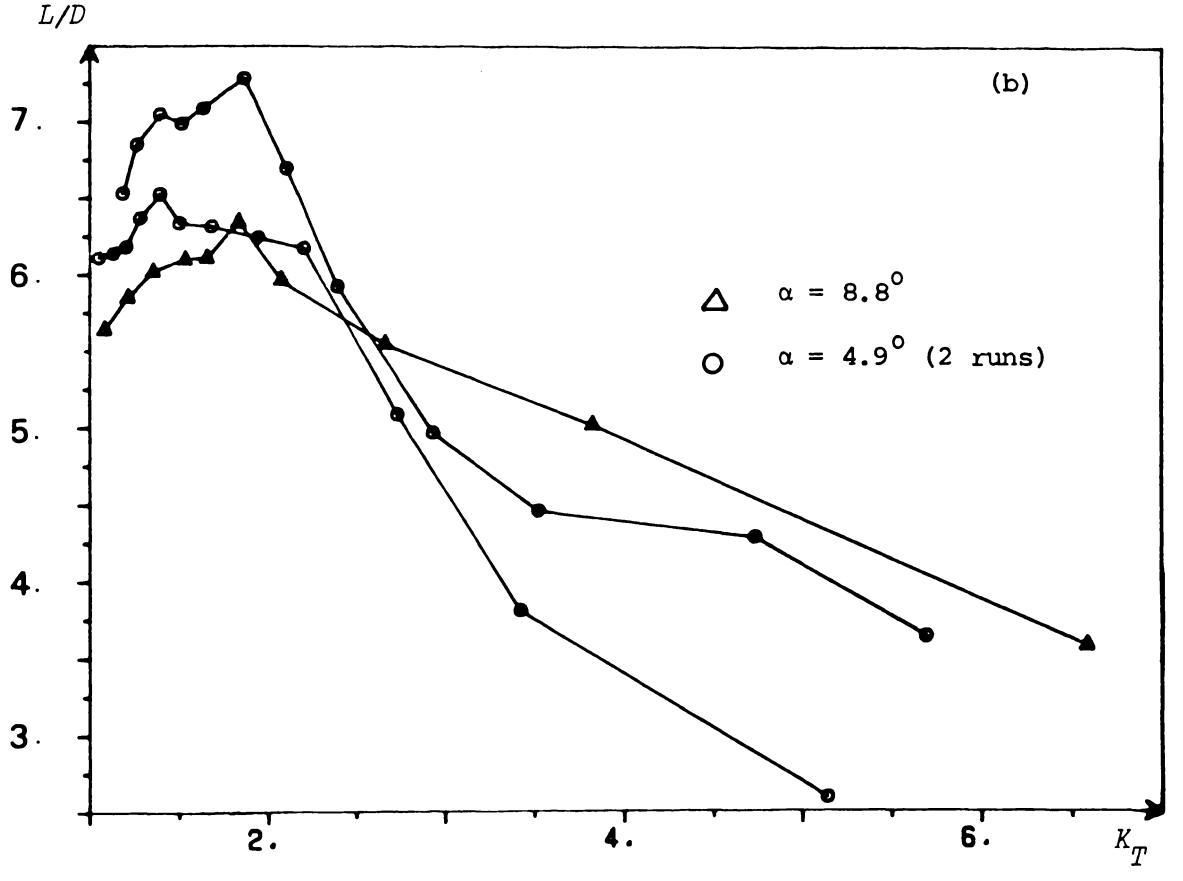

(b) Lift to drag ratio versus tension number.

Fig. 5.16 Experimentally observed lift to drag ratios.

Chapter 6 CONCLUSIONS

In order to obtain reasonable performance, sail-wing aircraft would operate with moderate to large lift coefficients and with the lift to drag ratio near its maximum value. Results shown in chapter 5 indicate that these features may be obtained when the maximum camber is significant (i.e. $C(x)_{max} \geq 0.02$). It is in this region that SAIL results are noticeably different to the linear theory predictions and thought to be a better representation of the real situation.

The non-linearities included in SAIL result in all the parameters studied (i.e. $C(x)$, C_L, x_P etc) becoming more complex functions of angle of attack and tension number than predicted by the linear theories. It was found that critical tension number K_{Tc}, increased with angle of attack, and indeed this trend was observed in the experimental investigation. The ratio C_L/α was shown to be dependent on α, decreasing with increasing angle of attack.

Perhaps the major discovery however is that two-dimensional sails in inviscid flow may be either longitudinally stable or unstable, depending primarily on the value of the tension number. For low K_T ($\lesssim 2.3$) the sail possesses longitudinal stability, and in fact becomes more stable as the angle of attack is increased. In either case the centre of pressure movement with variation of angle of attack is small when compared to the powerful influence variation of tension number has. Unfortunately, lack of reproduceability of the wind tunnel results for x_P, meant that variation of centre of pressure with α was

unable to be observed. A more precise and compatible balance/sail configuration is required before accurate experimental results for centre of pressure are obtained. In general however, the experimental results did show the same trends as theoretical predictions.

The large drag coefficients and relatively low lift to drag ratios obtained experimentally have also been observed by Apperley (1975) and Chapleo (1968). Both authors attributed these characteristics to fabric porosity. However throughout the current study non-porous membranes have been used, so that some other drag inducing mechanism must be responsible. It is well known that sharp leading edges are capable of producing large drag values when at a non-zero angle of attack to the incident airstream. Backflow and large velocity gradients are known to exist in the region of the leading edge and it is proposed that this mechanism rather than porosity is causing a significant proportion of the drag coefficients observed. In order to reduce the C_D values it is suggested that a leading edge of 'nice' shape be used. This requires that double skinned sails be employed to fair the leading edge profile into the rest of the aerofoil shape.

A preliminary experimental investigation of double skinned sails was performed using leading and trailing edges of circular cross section. The most notable characteristics observed were:

(i) small variations of internal pressure resulted in large variations of profile thickness,

(ii) lower drag coefficients obtainable,

(iii) drag control by varying profile thickness,

and (iv) ratio of L/D maximum increased.

It was found that for pressure differentials (between internal and external pressures) less than a certain value, the two membranes collapsed together. The resultant profile was essentially a single surfaced sail, the leading and trailing edges becoming faired into the profile quite rapidly. Another advantage of circular leading edges is that if allowed to rotate, different membrane lengths top and bottom are possible.

The routine SAIL would require only minor alterations to enable the calculation of double surfaced sail profiles. The extra input parameter of internal pressure (or pressure differential) is required. The sail equation is also modified so that both top and bottom membrane profiles can be determined independently. For the case where upper and lower surfaces coincide, the current single surface representation would be used.

It is hoped that this work promotes further investigations of sail-wings, both theoretical and experimental. The fields of study are many and varied, some suggestions being:

(i) more detailed analyses of double skinned sails, experimental and theoretical,

(ii) further, more accurate experimental studies of single surfaced sails,

(iii) theoretical investigations including boundary layer effects,

(iv) experiments on surface finish and porosity effects on sails,

(v) stretchable sails,

(vi) three-dimensional analyses,

and (vii) flexible plates.

APPENDIX 1: METHOD OF CALCULATING HARMONIC CONJUGATE FUNCTIONS

Consider the function $u(\theta)$ satisfying Laplace's equation on the boundary of a circle. We desire to find the harmonic conjugate function $v(\theta)$ on the boundary such that

$$f(z) = u(\theta) + i\, v(\theta)$$

is analytic (i.e. obeys Cauchy-Reimann equations).

The function $u(\theta)$, $0 \leq \theta \leq 2\pi$ may be specified numerically in two ways:

(i) by specifying its values at $2N$ equally spaced points around the circle, i.e. let

$$\theta_p = \frac{p\pi}{N} \qquad (0 \leq p \leq 2N-1)$$

and $u_p = u(\theta_p)$.

(ii) by specifying the first $2N$ Fourier coefficients of $u(\theta)$, i.e.

$$u(\theta) = \tfrac{1}{2} a_0 + \sum_{r=1}^{N-1} (a_r \cos r\theta + b_r \sin r\theta) + \tfrac{1}{2} a_N \cos N\theta.$$

Clearly

$$\begin{aligned} u_p &= u(\theta_p) \\ &= \tfrac{1}{2} a_0 + \sum_{r=1}^{N-1} (a_r \cos r\theta_p + b_r \sin r\theta_p) + \tfrac{1}{2} a_N \cos N\theta_p \end{aligned} \tag{1}$$

so that u_p is given in terms of a_p and b_p. It is also possible to express the a_p, b_p in terms of u_p using the following relationships:

$$\sum_{p=0}^{2N-1} \cos n\theta_p \cos m\theta_p = N\left(\delta^N_{m-n} + \delta^N_{m+n}\right) \tag{2}$$

$$\sum_{p=0}^{2N-1} \sin n\theta_p \sin m\theta_p = N\left(\delta^N_{m-n} - \delta^N_{m+n}\right) \tag{3}$$

and

$$\sum_{p=0}^{2N-1} \sin n\theta_p \cos m\theta_p = 0 \tag{4}$$

where $\delta^N_r = \begin{cases} 0 & \text{if } r \text{ is not a multiple of } 2N \\ 1 & \text{if } r \text{ is a multiple of } 2N. \end{cases}$

From equation (1) we have

$$\sum_{p=0}^{2N-1} u_p \cos n\theta_p = \tfrac{1}{2} a_0 \sum_{p=0}^{2N-1} \cos n\theta_p + \tfrac{1}{2} a_N \sum_{p=0}^{2N-1} \cos n\theta_p \cos N\theta_p$$

$$+ \sum_{r=1}^{N-1} \left\{ a_r \sum_{p=0}^{2N-1} \cos r\theta_p \cos n\theta_p \right.$$

$$\left. + b_r \sum_{p=0}^{2N-1} \sin r\theta_p \cos n\theta_p \right\}$$

$$= a_0 N \delta^N_n + \tfrac{1}{2} a_N N\left(\delta^N_{N+n} + \delta^N_{N-n}\right)$$

$$+ \sum_{r=1}^{N-1} a_r N\left(\delta^N_{r+n} + \delta^N_{r-n}\right)$$

$$= N a_n .$$

Thus
$$a_n = \frac{1}{N} \sum_{p=0}^{2N-1} u_p \cos n\theta_p$$

and similarly
$$b_n = \frac{1}{N} \sum_{p=0}^{2N-1} u_p \sin n\theta_p \qquad (5)$$

Now if $v(\theta)$ is the harmonic conjugate of $u(\theta)$

$$v(\theta) = \sum_{r=1}^{N-1} (a_r \sin r\theta - b_r \cos r\theta) + \tfrac{1}{2} a_N \sin N\theta$$

so that
$$v_p = v(\theta_p)$$

$$= \sum_{r=1}^{N-1} (a_r \sin r\theta_p - b_r \cos r\theta_p) \qquad (6)$$

since $\sin N\theta_p = 0$.

Substituting (5) into (6) yields

$$v_p = \frac{1}{N} \sum_{r=1}^{N-1} \left\{ \sin r\theta_p \sum_{q=0}^{2N-1} u_q \cos r\theta_q - \cos r\theta_p \sum_{q=0}^{2N-1} u_q \sin r\theta_q \right\} ,$$

where the coefficient u_q is given by

$$u_q = \frac{1}{N} \sum_{r=1}^{N-1} (\sin r\theta_p \cos r\theta_q - \cos r\theta_p \sin r\theta_q)$$

$$= \begin{cases} \dfrac{\cot (p - q)\pi}{2N} & \text{for } (p - q) \text{ odd} \\ 0 & \text{for } (p - q) \text{ even} . \end{cases}$$

Thus letting $p - q = r$ we obtain

$$v_p = \frac{1}{N} \sum_{r=1 \ (r \text{ odd})}^{2N-1} u_{p-r} \cot \frac{r\pi}{2N}$$

$$= -\frac{1}{N} \sum_{r=1 \ (r \text{ odd})}^{N} \cot \frac{r\pi}{2N} \, (u_{p+r} - u_{p-r}) .$$

APPENDIX 2: PROGRAM LISTING

```
C
C
C               MAIN PROGRAM FOR DETERMINING SAIL PROFILE AND
C               PARAMETERS
C
C
      REAL LIFT,COF,X(100),Y(100),XZ(100),YZ(100),KT,ALPHA
      REAL ALMAX,DELALF,AKMAX,DELK,AK,C,SLEN,MC,PMC,AREA
      REAL PI,CL,DELDEG,DEGMAX
      COMMON /FCAM1/XZ,YZ
      COMMON /SAILB1/COF,CL,LIFT,X,Y,P
      COMMON /SAILB3/SLEN,MC,PMC,AREA,BETALE,BETATE,C50
      CALL ASSIGN(2,'PPP.DAT')
      CALL ASSIGN(3,'PROF.DAT')
      PI = 3.1415926536
      C=2.
C
C
C               INPUT PARAMETERS 1)ANGLE OF ATTACK
C                                2)TENSION NUMBER
C
C
      WRITE(5,100)
 100  FORMAT('  ENTER ALPHA MAX,DELTA ALPHA,# STEPS')
      READ(5,110)DEGMAX,DELDEG,NALFA
      ALMAX = DEGMAX*2.*PI/360.
      DELALF = DELDEG*2.*PI/360.
 110  FORMAT(2F10.5,I2)
      WRITE(5,101)
 101  FORMAT('  ENTER K MAX,DELTA K,# STEPS (AERODYNAMIC)')
      READ(5,110)AKMAX,DELK,NK
      WRITE(2,25)
 25   FORMAT(' ALPHA',T15,'KT AERO',T27,'COF',T38,'CL',T49,'BETA L.E.',
     1T60,'BETA T.E.',T71,'S/C',T82,'MAX CAM',T93,'P.M.C.',5X,'Y(0.5)')
      ALPHA = ALMAX+DELALF
      DO 20 I=1,NALFA
      ALPHA = ALPHA-DELALF
      AK = AKMAX+DELK
      DO 21 J=1,NK
      AK = AK-DELK
C**********                                  SET INITIAL SAIL SHAPE *****
      DO 10 L = 1,50
      X(L) =1.-(2.*(L-1)/50.)
 10   X(L+50) = -X(L)
      DO 11 L=1,100
      AA = ALPHA
      Y(L) = PI*((X(L)+2.)/4.)-ASIN(X(L))*(X(L)+.5)
      Y(L) =AA/(AK-1.727)*(Y(L)-(1.+X(L)/2.)*SQRT(1.-X(L)*X(L)))
 11   CONTINUE
      CALL SAIL(ALPHA,AK,C,ICON)
      IF(ICON.EQ.1)GOTO 20
      BETALE = BETALE*180./PI
      BETATE = BETATE*180./PI
      DEG = ALPHA*360./(2.*PI)
      C50 = C50*50.
      CLALF = CL/ALPHA
      WRITE(2,24)ALPHA,AK,COF,CL,BETALE,BETATE,SLEN/C,MC,PMC,C50
      DO 1112 L=1,51
 1112 WRITE(3,1110)(X(L)/2.+0.5),Y(L)/2.
 1110 FORMAT(2F10.6)
 24   FORMAT(10(1X,F10.6))
 21   CONTINUE
 20   CONTINUE
      END
```

```
      SUBROUTINE SAIL(ALPHA,AK,C,ICON)
C
C
C      SUBROUTINE TO DETERMINE THE PROFILE OF A SAIL
C     WITH INPUT PARAMETERS:
C             1)TENSION NUMBER (AK)
C             2)ANGLE OF ATTACK (ALPHA)
C             3)CHORD (C)
C
C     AN INITIAL ESTIMATE OF THE PROFILE USING THIN AEROFOIL
C     THEORY IS USUALLY MADE IN THE MAIN PROGRAM AND IS PASSED
C     TO THIS ROUTINE THRU COMMON BLOCK  SAILB1
C
C
C             THE PARAMETER  ICON  IS USED AS AN INDICATOR
C             OF WETHER THE PROFILE CONVERGED TO THE REQUIRED
C             DEGREE OF ACCURACY AND IS TESTED ON RETURN OF
C             CONTROL TO THE MAIN PROGRAM
C
C
C             ALL OUTPUT IS VIA COMMON BLOCKS
C
C
      REAL A,AA,A0,AFI,ALPHA,AK,APPROX(100),C,C0,DAPROX(50)
      REAL DPSI(100),DEPSLN(100),DY(50),DEPS0,DPSI0,DEPSFI,DPSIFI
      REAL ERR(100),EPSBAR(100),EPSLON(100),ERRMAX,ERRMIN,ERRDIF
      REAL EPS0,EPSFI,F(100),FI,GAMMA,GAMMA0,H,IT1ERR,IT2ERR,IT3ERR
      REAL LASTY(100),LASTER,LIFT,LSTERR,P(50),PHI0,NEWPSI(100)
      REAL PHI(100),PSI(100),R(100),R0,S,T(100),THETA,U(100),U0
      REAL PI,XZT(100),YZT(100),XZ(100),YZ(100),X(100),Y(100)
      REAL SLEN,MC,PMC,AREA
      REAL SL(50),COP,CL,LAMBDA
      COMPLEX ZI,CENTRE,Z(100),ZT(100),ZETA,ZT0
      COMMON /FCAM1/X,Y
      COMMON /SAILP1/COP,CL,LIFT,XZ,YZ,P
      COMMON /SAILB3/SLEN,MC,PMC,AREA,BETALE,BETATE,C50
      COMMON /CONJB1/XCOT(50)
C
C
C
C*******                                        GENERATE DATA FOR LATER USE
C
C
      LASTER = 5.
      NITT = 0
      ITEST =0
      NPTS = 100
      PI = 3.14159265
      TWOPI = 2.*PI
      U0 = SQRT(10./(0.5*1.1*C*AK))
      ZI = CMPLX(0.,1.)
      ERRMAX = 1.0
      DO 3 I=1,50,2
 3    XCOT(I) = COS(I*PI/NPTS)/SIN(I*PI/NPTS)
      N=50
      A = C/4.
      GOTO 7
C
C
C
```

```
C*******                                          DETERMINE HEIGHT AND RADIUS
C*******                                          OF APPROX. ARC AND COORDS
C*******                                          OF TRANSFORMED CENTRE
 5       DO 6 I=1,NPTS
 6       LASTY(I) = Y(I)
 7       DO 155 I=1,NPTS
         X(I) = XZ(I)
 155     Y(I) = YZ(I)
         H = FCAM(0.0,N)
         IT1ERR = 5.                      !RESET INITIAL ERROR
         IT2ERR = 5.                      !MAXIMA FOR THIS ITERATION
         IT3ERR = 5.
         CX = 0.
         CY = 0.5*H
         CENTRE = CMPLX(CX,CY)
C
C
C*******                                          DETERMINE COORDS OF CIRCLE
C*******                                          IN ZETA PLANE WITH EQUISPACED
C*******                                          POINTS
C
         TEMP01 = (SQRT(H*H+1.))/2.
         DO 10 I=1,NPTS
         ZT(I) = (TEMP01*CEXP(2.*PI*ZI*(I-1)/NPTS))+CENTRE
         YZT(I) = AIMAG(ZT(I))
         XZT(I) = REAL(ZT(I))
  10     CONTINUE
C*******                                          DETERMINE X COORDS IN Z PLANE
C*******                                          FROM EQUISPACED POINTS IN ZETA
C*******                                          PLANE, AND THEN Y COORDS FROM
C*******                                          CALC'ED X COORDS
         DO 20 I=1,NPTS
         XZ(I) = REAL(ZT(I)+(0.25/ZT(I)))
         YZ(I) = FCAM(XZ(I),50)
 20      Z(I) = CMPLX(XZ(I),YZ(I))
C*******                                          TRANSFORM Z PLANE VALUES INTO
C*******                                          ZETA PLANE ENSURING CORRECT SIGN
         DO 30 I=1,NPTS
         IF(YZT(I).LT.0.)GOTO 31
  30     CONTINUE
  31     N1=I
         DO 40 I=N1,NPTS
         IF(YZT(I).GE.0.0)GOTO 41
  40     CONTINUE
  41     N2=I
         DO 50 I=1,NPTS
         ZT(I) = CMPLX(0.,0.)
         IF((Z(I)*Z(I)-1.).EQ.CMPLX(0.,0.))GOTO45
         ZT(I) = CSQRT(Z(I)*Z(I)-1.)
         IF(AIMAG(Z(I)*Z(I)-1.).LT.0.)ZT(I) = -ZT(I)
 45      IDEL = 1
         IF((N1.LE.I).AND.(N2.GT.I))IDEL = -1
         ZT(I) = (Z(I)+IDEL*ZT(I))/2.
  50     CONTINUE
         DO 60 J=1,NPTS
         XZT(J) = REAL(ZT(J))
 60      YZT(J) = AIMAG(ZT(J))
C*******                                            DETERMINE CENTRE
C*******                                            AND RADIUS
         CX=0.
         CY=0.
         DO 62 I=1,NPTS
         CX = CX+XZT(I)
 62      CY = CY+YZT(I)
         CX = CX/NPTS
         CY = CY/NPTS
         CENTRE=CMPLX(CX,CY)
         RO =0.0
         DO 80 I=1,NPTS
         RO = RO + CABS(ZT(I)-CENTRE)
  80     CONTINUE
         RO = RO/NPTS
```

```
C*******                                                CALCULATE PSI(M)
        DO 104 M 1,NPTS
        R(M) = CABS(ZT(M)-CENTRE)
        PSI(M) = ALOG(R(M)/RO)
 104    CONTINUE
C*******                                                CALCULATE T(M), ANGLE IN RADS
        DO 105 M=1,NPTS
        IF(ABS(YZT(M)-CY).LT.ABS(XZT(M)))GOTO 106
        T(M) = ACOS(XZT(M)/R(M))
        IF(YZT(M).LT.CY)T(M) = TWOPI-T(M)
        GOTO 105
 106    T(M) = ASIN((YZT(M)-CY)/R(M))
        IF(XZT(M).LT.0.)T(M) = PI-T(M)
        IF(T(M).LT.0.)T(M) = T(M)+TWOPI
 105    CONTINUE
C*******                                                INTERPOLATE AROUND CURVE
C*******                                                TO GIVE EQUALLY SPACED POINTS
C*******                                                GENERATE PHI(M) - EQUALLY
C*******                                                INCREMENTED ANGLES.
        DO 110 M=1,NPTS
 110    PHI(M) = TWOPI*M/NPTS
C*******
C*******                                                SEARCH THRU T(N) UNTILL FIND
C*******                                                FIRST T(N)>PHI(M)
        DO 116 I=1,NPTS
        IF(YZT(I).GE.CY)GOTO 117
 116    CONTINUE
 117    DO 120 M=1,NPTS
        DO 112 J=I,NPTS+I-1
        MODJ = MMOD(J,NPTS)
        IF(T(MODJ).GT.PHI(M))GOTO 113
 112    CONTINUE
 113    J = MODJ-1
        IF(J.EQ.0)J=NPTS
C*******
C*******                                                NOW WANT TO FIND VALUE OF PSI(
C*******                                                 AT ANGLE PHI(M) BETWEEN POINTS
C*******                                               (T(N),PSI(N))&(T(N+1),PSI(N+1)
C*******                                               CALL THIS NEW VALUE NEWPSI(M)
        CALL MPOLY(T,PSI,NPTS,J,PHI(M),NEWPSI(M))
  120   CONTINUE
C*******                                              NOW HAVE CURVE IN ZETA PLANE
C*******                                              HENCE ZETA GIVEN BY
        DO 121 M=1,NPTS
        PSIN = NEWPSI(M)
        FFFI = PHI(M)
        ZT(M) = CENTRE+(RO*CEXP(CMPLX(PSIN,FFFI)))
        XZT(M) = REAL(ZT(M))
        YZT(M) = AIMAG(ZT(M))
 121    CONTINUE
        DO 130 I=1,NPTS
        APPROX(I) = 0.
        PSI(I) = NEWPSI(I)
  130   F(I) = 0.
        TWOPI = PI*2.
 150    CONTINUE
        DO 131 I=1,NPTS
        THETA = PHI(1)-APPROX(I)
        THETA = AMOD(THETA+TWOPI,TWOPI)
        AA=THETA*NPTS/TWOPI
        IF(AA.EQ.0.)AA=100.
        F(I) = FPSI(PHI,PSI,AA,THETA,NPTS)
 131    CONTINUE
C
C
C               DETERMINE THE HARMONIC CONJUGATE FUNCTION OF F
C
C               I.E. EPSBAR = CONJUGATE(F)
C
C
        CALL CONJ(NPTS,F,EPSBAR)
C
```

```
C
C*******                                                SEARCH THRU TO FIND THE
C*******                                                LARGEST ERROR BETWEEN
C*******                                                EPSBAR AND APPROX
C
        ERRMAX = 0.
        DO 132 I=1,NPTS
        ERR(I) = ABS(EPSBAR(I) - APPROX(I))          !DETERMINE LARGEST
 132    IF(ERR(I).GT.ERRMAX)ERRMAX=ERR(I)            !ERROR
        ERRDIF = IT1ERR-ERRMAX
        IT1ERR = ERRMAX
        IF(ERRDIF.LT.0.0)GOTO 554                    !STILL CONVERGING?
        IF(ERRMAX.LE.0.000001)GOTO 504               !CONVERGED SUFFICIENTLY?
 133    DO 135 I=1,NPTS
 135    APPROX(I) = EPSBAR(I)
        GOTO 150
C
C
C               PRINT ERROR MESSAGE FOR NON CONVERGENCE
C
C
 554    WRITE(5,556)ERRMAX,AK,ALPHA
 556    FORMAT('  CONVERGENCE ONLY TO',G14.7,'AT KT,ALF=',2F10.6)
 504    CONTINUE
        DO 162 I=1,100
 162    APPROX(I) =0.0
C
C
C               DETERMINE FUNCTION EPSLON
C               ITERATIVE TECHNIQUE USED CONVERGES RAPIDLY
C
C
 165    CONTINUE
        ERRMAX = 0.
        DO 161 I=1,NPTS
        THETA = AMOD(PHI(I)-APPROX(I)+TWOPI,TWOPI)
        IF(THETA.EQ.0.)THETA=TWOPI
        AAA = THETA*NPTS/TWOPI
        IA = AAA
        EPSLON(I) = EPSBAR(IA)
        IF(FLOAT(IA).EQ.AAA)GOTO 1610
        CALL MPOLY(PHI,EPSBAR,NPTS,IA,THETA,EPSLON(I))
 1610   ERR(I) = ABS(EPSLON(I) - APPROX(I))
 161    IF(ERR(I).GT.ERRMAX)ERRMAX=ERR(I)
        ERRDIF = IT2ERR-ERRMAX
        IT2ERR = ERRMAX
        IF(ERRDIF.LT.0.)GOTO 1710                    !STILL CONVERGING?
        IF(ERRMAX.LE.0.00001)GOTO 171                !CONVERGED SUFFICIENTLY?
        DO 172 I=1,NPTS
 172    APPROX(I) = EPSLON(I)
        GOTO 165
C
C
C               PRINT ERROR MESSAGE FOR FAILURE TO CONVERGE
C
C
 1710   WRITE(5,1711)ERRMAX
 1711   FORMAT('  EPSILON ITERATION FAILED TO CONVERGE BEYOND ',F10.6)
C
C
C               DIFFERENTIATE FUNCTION PSI
C
C
 171    H=PHI(2)-PHI(1)
        CALL MIDNTN(NPTS,H,PSI,DPSI)
        CALL MIDNTN(NPTS,H,EPSLON,DEPSLN)
 170    CONTINUE
        CO = ALOG(RO/A)
C
C
C*******                                                HAVE NOW COMPLETED .
C*******                                                TRANSFORMS SO CAN
```

```
C*******                                                GENERATE DATA FOR
C*******                                                EQUATION FOR U
      ZTO   CENTRE
      PHIO  TWOPI-ATAN(CY/(A-CX))
      A0    PHIO*NPTS/TWOPI
      EPS0 = EPSI(PHI,EPSLON,A0,PHIO,NPTS)
      GAMMA0 = PHIO + EPS0
      UOFCO = UO*EXP(CO)
      SINGMA = SIN(GAMMA0-ALPHA)
C*******                                                GENERATE ZETA COORDS
C*******                                                FROM EQUISPACED POINTS
C*******                                                IN Z PLANE
      DO 174 I=1,N
      XZ(I) = (1.-(((2.*I)-1.)/N))
      XZ(NPTS+1-I) = XZ(I)
      YZ(I) = FCAM(XZ(I),N)
      YZ(NPTS+1-I) = YZ(I)
      XZZ = XZ(I)
      YZZ = YZ(I)
      Z(I) = CMPLX(XZZ,YZZ)
      ZETA = Z(I)*Z(I)-1.
      IDEL = 1
      IF(AIMAG(ZETA).LT.0.)IDEL=-1
      ZETA = IDEL*(CSQRT(ZETA))
      ZT(I) = (Z(I)+ZETA)/2.
      ZT(NPTS+1-I) = (Z(I)-ZETA)/2.
 174  CONTINUE
      DO 166 I=1,NPTS
      XZT(I) = REAL(ZT(I))
 166  YZT(I) = AIMAG(ZT(I))
C*******                                                CALCULATE PHI FOR CORR-
C*******                                                ESPONDING ZETA AND THEN
C*******                                                OTHER NECESSARY VARIABLES
C*******                                                FOR EQUATION FOR U
C
C
C              DETERMINE FLUID VELOCITY AT 100 EQUALLY SPACED
C              POINTS AROUND SAIL SURFACE
C
C
      DO 175 M=1,NPTS
      IF(ABS(YZT(M)-CY).LT.ABS(XZT(M)-CX))GOTO 176
      FI = ACOS((XZT(M)-CX)/(CABS(ZT(M)-CENTRE)))
      IF(YZT(M).LT.CY)FI=TWOPI-FI
      GOTO 177
 176  FI = ASIN((YZT(M)-CY)/(CABS(ZT(M)-CENTRE)))
      IF(XZT(M).LT.CX)FI=PI-FI
      IF(FI.LE.0.)FI = FI+TWOPI
 177  AFI = FI*NPTS/TWOPI
      EPSFI = EPSI(PHI,EPSLON,AFI,FI,NPTS)
      GAMMA = FI + EPSFI
      DEPSFI = EPSI(PHI,DEPSLN,AFI,FI,NPTS)
      DPSIFI = EPSI(PHI,DPSI,AFI,FI,NPTS)
      U(M) = SIN(GAMMA-ALPHA)-SINGMA
      ZETA = (UOFCO*ZT(M)*ZT(M)*(1.+DEPSFI))
      ZETA = ZETA/((ZT(M)-ZTO)*(ZT(M)*ZT(M)-0.25)*(DPSIFI+ZI))
      U(M) = ABS(U(M))*CABS(ZETA)
 175  CONTINUE
      A0 = (PHIO*NPTS)/TWOPI
      DEPS0 = EPSI(PHI,DEPSLN,A0,PHIO,NPTS)
      DPSI0 = EPSI(PHI,DPSI,A0,PHIO,NPTS)
C
C
C              DETERMINE PRESSURE DIFFERENCE THRU SAIL MEMBRANE
C              USING BERNOULLI'S THEOREM
C
C
      DO 137 I=1,50
      P(I)=0.55*((U(I)*U(I))-(U(NPTS+1-I)*U(NPTS+1-I)))
      APPROX(I) = Y(I)
 137  DAPROX(I) = 1.
C
```

```
C
C               NOW TO DETERMINE SAIL PROFILE FROM PRESSURE DIST
C
C
        DO 146 I=1,N
        XZ(I) = 1. - (I-1)/25.
        XZ(I+50) = -XZ(I)
        YZ(I) = FCAM(XZ(I),50)
 146    CONTINUE
        YZ(1) = 0.
        YZ(51) = 0.
        DO 157 I=1,50
        YZ(101-I) = YZ(I+1)
        X(I) = (2.-(2.*I - 1.)/50.)
        X(101-I) = X(I)
 157    CONTINUE
 138    CONTINUE
C
C
C               ITERATIVE METHOD FOR DETERMINING PROFILE
C               USING FULL SAIL EQUATION
C               USES GREENS FUNCTION METHOD AS OUTLINED IN
C               CHAPTER 2
C
C
        DO 140 I=1,N
        DO 139 J=1,N
        S = C-((J*C)/(N+1.))
        DY(J)=GG(X(I),S,C)*F(J)*DAPROX(J)
 139    CONTINUE
        CALL TRINTR(0.0,C,N,X,DY,Y(I))
 140    CONTINUE
        ERRMAX = 0.
        DO 142 I=1,N
        ERR(I) = ABS(Y(I)-APPROX(I))
 142    IF(ERR(I).GT.ERRMAX)ERRMAX=ERR(I)
        ERRDIF = IT3ERR-ERRMAX
        IT3ERR = ERRMAX
        IF(ERRDIF.LE.0.0)GOTO 558               !STILL CONVERGING?
        IF(ERRMAX.LT.0.00001)GOTO 145           !CONVERGED SUFFICIENTLY?
        DO 144 I=1,N
        APPROX(I) = Y(I)
 144    DAPROX(I) = (1.+(DY(I)*DY(I)))**1.5
        GOTO 138
C
C
C               PRINT ERROR MESSAGE FOR NON CONVERGENCE
C
C
 558    WRITE(5,559)ERRMAX,AK,ALPHA
 559    FORMAT(' IT3 CONVERGED TO',G14.7,'AT KT,ALF=',2F10.6)
 145    CONTINUE
C
C
C*******                                        HAVE GENERATED (X,Y) OF 50
C*******                                        POINTS; NOW WANT TO TRANSFORM
C*******                                        THIS TO (XZ,YZ) OF 100 EQUAL-
C*******                                        LY SPACED POINTS.
C
C
        DO 151 I=1,N
        X(I) = X(I)-1.
        X(50+I) = X(50+I)-1.
        XZ(I) = 1.-(I-1)/25.
 151    XZ(N+I) = -XZ(I)
        YZ(1) = 0.0
        YZ(N+1) = 0.0
        DO 154 I=2,N
        K=I
        IF(K.GE.(N-1))K=K-1
        K=K-1
        CALL SPOLY(X,Y,100,K,XZ(I),YZ(I))
```

```
 154    CONTINUE
        DO 158 I=2,N
        K=102-I
 158    YZ(K) = YZ(I)
        ERRMAX = 0.
        DO 159 I=1,NPTS
        ERR(I) = ABS(LASTY(I)-Y(I))
 159    IF(ERR(I).GT.ERRMAX)ERRMAX=ERR(I)
        ERRDIF = LASTER-ERRMAX
        IF(ERRDIF.LE.-0.25)GOTO 945
        LASTER = ERRMAX
        IF(ERRMAX.GE.0.00001)GOTO 5
        GOTO 191
 945    WRITE(5,560)ERRMAX,AK,ALPHA
 560    FORMAT(' SAIL CONVERGED TO',G14.7,'AT K,ALF=',2F10.6)
        ICON = 1
        GOTO 999
 191    CONTINUE
        ICON = 0
C
C               CALCULATE DY/DX ACROSS SAIL SURFACE
C
        CALL DIFNTN(-1.,1.,50,X,Y,DY)
C
C               CALCULATE LEADING AND TRAILING EDGE ANGLES
C               BETALE AND BETATE BY EXTAPOLATION OF DY/DX
C
        CALL SPOLY(X,DY,100,48,-1.,BETALE)
        CALL SPOLY(X,DY,100,1,1.,BETATE)
C
C               CALCULATE LEADING EDGE FORCE
C
C                       MUST FIRST CALCULATE R(X) AND LAMDA(X)
C                       TO BE USED IN EQATION FOR F(L.E.)
C                       NOTE THAT R(X) IS DISTANCE ALONG SAIL SURFACE
C                       AS MEASURED FROM THE LEADING EDGE.
C
        R(3) = SQRT(0.0004+Y(50)*Y(50))
        DO 882 I=2,1,-1
 882    R(I) = R(I+1)+SQRT(0.0016+((Y(48+I)-Y(47+I))**2.))
        J=47
        DO 883 I=1,3
        J = J+1
 883    F(J) = U(J)*SQRT(R(I)/C)/(U0*SIN(ALPHA))
        CALL SPOLY(X,F,100,48,-1.,LAMBDA)
C
C                       HAVE NOW CALCULATED LAMBDA
C
        FLE = -PI*1.1*U0*U0*C*(SIN(ALPHA)**2.)*LAMBDA*LAMBDA
        FLE = FLE*SIN(BETALE)*COS(ALPHA)
C
C                       FLE IS NOW THE VERTICAL COMPONENT OF THE
C                       LEADING EDGE FORCE.
C
C               DETERMINE LIFT AND CENTRE OF PRESSURE
C
C
C
        CALL LCOP(X,Y,F,LIFT,COP,ALPHA,FLE)
        CL = LIFT/(1.1*0.5*C*U0*U0)
C
C
C               DETERMINE POSITION OF MAX CAMBER AND MAX CAMBER
C
C
        CALL DIFNTN(-1.,1.,50,X,Y,DY)
        DO 178 I=1,50
        PMC = X(I)
        IF(DY(I) .EQ.0.)GOTO 879
        IF(DY(I).GT.0.0)GOTO 179
 178    CONTINUE
 179    PMC = X(I) - (DY(I)*((X(I)-X(I-1))/(DY(I)-DY(I-1))))
 879    MC = FCAM(PMC,50)
        PMC = (PMC+1.)./C                !CHORD OF 2 ASSUMED
        MC = MC./C
C
C               DETERMINE AREA UNDER SAIL MEMBRANE
C               AND SAIL LENGTH
C
        CALL TRINTR(-2.*A,2.*A,50,X,Y,AREA)
        DO 180 I=1,50
 180    SL(I) = SQRT(1.+DY(I)*DY(I))
        CALL INT(-1.,1.,50,X,SL,SLEN)
        CSO = YZ(26)
 999    CONTINUE
        RETURN
        END
```

```
      SUBROUTINE LCOP(X,Y,P,LIFT,COP,ALPHA,FLE)
C
C
C               ROUTINE TO CALCULATE LIFT AND CENTRE OF PRESSURE
C
C
      REAL Y(100),DY(50),PYDY(50),X(100)
      REAL A,B,PSQR48,PSQR50,FLE
      REAL P(50),XPX(50),LIFT,COP
      N = 50
C*******                                              DETERMINE COEFFICIENTS
C*******                                              A AND B
      B=((P(N-2)*SQRT(1.+X(N-2)))-(P(N)*SQRT(1.+X(N))))
      B = B/(X(N-2)-X(N))
      PSQR50 = P(50)*SQRT(1.+X(50))
      PSQR48 = P(48)*SQRT(1.+X(48))
      A = PSQR50-((PSQR48-PSQR50)/(X(48)-X(50)))*X(50)
C
C               CALCULATE LIFT
C               N.B. LIFT IS FORCE IN Y DIRECTION SO MUST ALLOW
C               FOR ANGLE OF ATTACK ALPHA.
C               ALSO NOTE THAT FLE IS Y COMPONENT OF THE LEADING
C               EDGE FORCE
C
      LIFT = P(1)*(1.-X(1))/2.
      DO 10 I=1,47
 10   LIFT=LIFT+(P(I)+P(I+1))*(X(I)-X(I+1))/2.
      LIFT=LIFT+2.*(SQRT(X(N-2)+1)*((A-B)+B*(X(N-2)+1)/3))
      LIFT = (LIFT/COS(ALPHA))+FLE
C
C               CALCULATE C.O.P.
C
      CALL DIFNTN(-1.,1.,50,X,Y,DY)
      DO 11 I=1,50
      PYDY(I) = P(I)*Y(I)*DY(I)
      XPX(I) = X(I)*P(I)
 11   CONTINUE
      CALL TRINTR(-1.,1.,50,X,PYDY,COP)
      COP = COP+XPX(1)*(1.-X(1))/2.
      DO 12 I=1,47
 12   COP=COP+((XPX(I)+XPX(I+1))/2.)*(X(I)-X(I+1))
      COP=COP+(2.*SQRT(1.+X(N-2))*(5.*A-4.*B)*(X(N-2)-2.))/15.
      COP=(COP+(2./15.)*SQRT(1.+X(N-2))*(3.*B*X(N-2)*X(N-2)))/LIFT
      COP = (COP+1.)*50.
      RETURN
      END




      SUBROUTINE MINMAX(ERRMIN,ERRMAX,N,ERR)
C
C
C               ROUTINE TO DETERMINE MINIMUM AND MAXIMUM VALUES
C               OF ERROR FUNCTION ERR
C
C
      REAL ERRMIN,ERRMAX,ERR(N)
      INTEGER N,I
      ERRMAX = ERR(1)
      ERRMIN = ERR(1)
      DO 1 I=1,N
      IF((ERRMAX-ERR(I)).LT.0.0)ERRMAX=ERR(I)
 1    IF((ERRMIN-ERR(I)).GT.0.0)ERRMIN ERR(I)
      RETURN
      END
```

```
      SUBROUTINE SPOLY(X,Y,N,M,XX,YY)
C
C
C               LAGRANGE THREE POINT POLYNOMIAL ROUTINE
C               RETURNS VALUE OF Y (IN YY) AT X=XX
C
C
      REAL X(N),Y(N),XX,YY
      M1 = M+1
      M2 = M+2
      YY=((XX-X(M1))*(XX-X(M2))*Y(M))/((X(M)-X(M1))*(X(M)-X(M2)))
      YY=YY+((XX-X(M))*(XX-X(M2))*Y(M1))/((X(M1)-X(M))*(X(M1)-X(M2)))
      YY=YY+((XX-X(M))*(XX-X(M1))*Y(M2))/((X(M2)-X(M))*(X(M2)-X(M1)))
      RETURN
      END
```

```
      SUBROUTINE DIFNTN(XL,XU,N,X,Y,DY)
C
C               NUMERICAL DIFFERENTIATION ROUTINE
C
C
      REAL H,XL,XU,X(N),Y(N),DY(N)
      H = X(1)-X(2)
      DY(1) = (((Y(1)-Y(2))/H)+(Y(1)/(X(1)-XU)))/2.
      DY(N) = (((Y(N-1)-Y(N))/H)+(Y(N)/(X(N)-XL)))/2.
      DY(2) = (Y(1)-Y(3))/(2.*H)
      DY(N-1) = (Y(N-2)-Y(N))/(2.*H)
 10   DO 11 I=3,N-2
 11   DY(I)=(Y(I+2)-(8.*(Y(I+1)-Y(I-1)))-Y(I-2))/(12.*H)
      RETURN
      END
      SUBROUTINE TRINTR(XL,XU,N,X,DY,Y)
C
C
C               TRAPEZOIDAL INTEGRATION ROUTINE
C
C
      REAL XL,XU,X(N),DY(N),Y
      Y = (DY(N)/2.)*(X(N)-XL)+(DY(1)/2.)*(XU-X(1))
      DO 10 I=1,N-1
      Y = Y+(X(I)-X(I+1))*((DY(I)+DY(I+1))/2.)
 10   CONTINUE
      RETURN
      END
```

```
      SUBROUTINE MDERIV(NPTS,H,F,DF)
C
C
C               MOD DIFFERENTIATION ROUTINE
C               USED FOR DIFFERENTIATING CYCLIC FUNCTIONS
C
C
      REAL F(NPTS),DF(NPTS),H
      DO 10 I=1,NPTS
      M1=MMOD(NPTS+I-2,NPTS)
      M2=MMOD(NPTS+I-1,NPTS)
      M4=MMOD(I+1,NPTS)
      M5=MMOD(I+2,NPTS)
      DF(I) = (F(M1)-8.*(F(M2)-F(M4))-F(M5))/(12.*H)
   10 CONTINUE
      RETURN
      END




      SUBROUTINE CONJ(NPTS,F,G)
C
C
C               CALCULATES HARMONIC CONJUGATE FUNCTION OF F
C               SEE APPENDIX 1 FOR DERIVATION
C
      REAL F(NPTS),G(NPTS)
      INTEGER P
      COMMON /CONJB1/XCOT(50)
      DO 10 K=1,NPTS
      G(K) = 0.
      DO 11 P=1,NPTS/2,2
      K1 = MOD(K+P,NPTS)
      K2 = MOD(NPTS+K-P,NPTS)
      IF(K1.EQ.0)K1=NPTS
      IF(K2.EQ.0)K2=NPTS
      G(K) = G(K) + XCOT(P)*(F(K1)-F(K2))
   11 CONTINUE
   10 G(K) = -G(K)/50.
      RETURN
      END




      SUBROUTINE MPOLY(X,Y,N,M,TX,TY)
C
C               MOD POLYNOMIAL INTERPOLATION ROUTINE
C               USED FOR INTERPOLATING ON CYCLIC FUNCTIONS
C
C
      REAL TX,TY,X(N),Y(N),PI
      PI = 3.1415926536
      TWOPI = 2. * PI
      M1 = MOD(M+1,N)
      IF(M1.EQ.0)M1 = N
      M2 = MOD(M+2,N)
      IF(M2.EQ.0)M2 = N
      IF(M.EQ.0)M=N
     IF(TX.LT.X(M))TX=TX+TWOPI
     IF(X(M1).LT.X(M))X(M1)=X(M1)+TWOPI
     IF(X(M2).LT.X(M1))X(M2)=X(M2)+TWOPI
     TY=((TX-X(M1))*(TX-X(M2))*Y(M))/((X(M)-X(M1))*(X(M)-X(M2)))
     TY=TY+((TX-X(M))*(TX-X(M2))*Y(M1))/((X(M1)-X(M))*(X(M1)-X(M2)))
     TY=TY+((TX-X(M))*(TX-X(M1))*Y(M2))/((X(M2)-X(M))*(X(M2)-X(M1)))
      IF(TX.GT.TWOPI)TX=TX-TWOPI
      IF(X(M1).GT.TWOPI)X(M1)=X(M1)-TWOPI
      IF(X(M2).GT.TWOPI)X(M2)=X(M2)-TWOPI
      RETURN
      END
>
```

```
      FUNCTION FPSI(PHI,PSI,A,THETA,NPTS)
C
C
C               INTERPOLATION FUNCTION RETURNS A VALUE
C               FOR PSI  AT PHI=THETA
C
C               USES INTERPOLATION SUBROUTINE MPOLY
C
C
      REAL PHI(NPTS),PSI(NPTS),PSINEW,A,THETA
      IA = A
      CALL MPOLY(PHI,PSI,NPTS,IA,THETA,PSINEW)
      FPSI = PSINEW
      RETURN
      END




      FUNCTION MMOD(M,N)
C
C               RETURNS MOD FUNCTION (MOD(N))
C               ALWAYS RETURNS A VALUE BETWEEN 1 AND N
C
C
      MM=MOD(M,N)
      IF(MM.EQ.0)MM=N
      MMOD=MM
      RETURN
      END




      FUNCTION FCAM(XX,N)
C
C
C               INTERPOLATION ROUTINE FOR DETERMINING NEW
C               POINT ON PROFILE CAMBER AT XX
C
C
      REAL X(100),Y(100),XX,YY
      COMMON /FCAM1/X,Y
      IF(ABS(XX).EQ.X(1))GOTO 14
      DO 10 I=1,N+1
      IF(X(I).LE.XX)GOTO 11
 10   CONTINUE
 11   IF(I.GE.N-1)I=I-1
      I=I-1
      CALL SPOLY(X,Y,100,I,XX,YY)
      FCAM = YY
      RETURN
 14   FCAM = 0.0
      RETURN
      END




      FUNCTION GG(X,S,C)
C
C
C               GREENS FUNCTION
C               USED IN DETERMINATION OF SAIL PROFILE)
C
C
      REAL X,S,C
      IF(X.GT.S)GOTO 1
      GG = X*(C-S)/20.
      RETURN
 1    GG = S*(C-X)/20.
      RETURN
      END
```

```
      FUNCTION ASIN(X)
C
C
C               FUNCTION RETURNING ARCSIN
C
C
      REAL X
      IF(ABS(X).EQ.1.)GOTO 10
      A = ATAN(X/SQRT(1.-X*X))
      ASIN = A
      RETURN
10    A = 1.570796327
      IF(X.LT.0.)A=-A
      ASIN = A
      RETURN
      END
      FUNCTION ACOS(X)
C
C
C               FUNCTION RETURNING ARC    (X)
C
C
      REAL X
      A = 1.57079633-ASIN(X)
      ACOS = A
      RETURN
      END
```

```
      SUBROUTINE INT(XL,XU,N,X,DY,Y)
C
C
C               TRAPEZOIDAL INTEGRATION OF FUNCTION DY
C               FOR  XL<X<XU
C               VALUE RETURNED IN Y
C
C
      REAL X(N),DY(N),DYL,DYU,Y
      DYL= DY(N)+(DY(N-1)-DY(N))*(XL-X(N))/(X(N-1)-X(N))
      DYU= DY(1)+(DY(1)-DY(2))*(XU-X(1))/(X(1)-X(2))
      Y =((XU-X(1))*(DYU+DY(1))/2.)+((X(N)-XL)*(DYL+DY(N))/2.)
      DO 10 I=1,N-1
      Y = Y+(X(I)-X(I+1))*((DY(I)+DY(I+1))/2.)
10    CONTINUE
      RETURN
      END
```

REFERENCES

Apperley, L.W., 1977. On the Improved Aerodynamic Efficiency of a Sailing Vessel. Fifth and Sixth Australasian Hydraulics and Fluid Mechanics Conference. p. 285-293.

Batchelor, G.K., 1967. An Introduction to Fluid Dynamics. Cambridge University Press.

Chapleo, A.W., 1968. A Review of Two-Dimensional Sails. S.U.Y.R. Report No. 23, University of Southampton.

Chambers, U.G. , 1966. A variational Formulation of the Thwaites Sail Equation. Quarterly Journal of Mechanics and Applied Mathematics v. XIX (2), p. 221-229.

Dettman, J.W., 1965. Applied Complex Variables. The Macmillan Company.

Dugan, J.P., 1970. A Free-Streamline Model of the Two-Dimensional Sail. Journal of Fluid Mechanics v. 42 (3), p. 433-446.

Ellen, C.H., 1977. The Stability of an Isolated Rectangular Surface Embedded in Uniform Subsonic Flow. Journal of Applied Mechanics v. 44 (2) Trans. ASME, Series E, p. 201-206.

Garrick, I.E., 1952. Conformal Mapping in Aerodynamics, with Emphasis on the Method of Successive Conjugates. U.S. National Bureau of Standards No. 18 AMS - 1, p. 137-147.

Hansen, W.H., 1978. The Drag of a Sphere. Experimental Report, Department of Mechanical Engineering, University of Auckland.

Kellogg, O.D., 1929. Foundations of Potential Theory. Verlag von Julius Springer.

Kyrala, A., 1972. Applied Functions of a Complex Variable. Wiley-Interscience.

Marsden, J.E., 1973. Basic Complex Analysis. W.H. Freeman and Company.

McLeod, L. & Lewis, C., 1977. Stability Studies of the Hang Glider. Project Report in Mechanical Engineering, Department of Mechanical Engineering, University of Auckland.

Milne-Thomson, L.M., 1968. Theoretical Hydrodynamics. Fifth Edition, Macmillan & Co. Ltd.

Monna, A.F., 1975. Dirichlet's Principle, A Mathematical Comedy of Errors and its Influence on the Development of Analysis. Oosthoek, Scheltema and Holkema.

Morse, P.M. & Feshback, H., 1953. Methods of Theoretical Physics, Part 1. McGraw-Hill Book Company.

Nielsen, J.N., 1963. Theory of Flexible Aerodynamic Surfaces. Journal of Applied Mechanics v. 30, p. 435-442.

Ostrowski, A.M., 1952. On the Convergence of Theodorsen's and Garrick's Method of Conformal Mapping. U.S. National Bureau of Standards No. 18, AMS - 1, p. 149-163.

Pankhurst, R.C. & Holder, D.W., 1952. Wind Tunnel Technique.

Pope, A., 1951. Basic Wing and Airfoil Theory. McGraw Hill.

Pope, A., 1954. Wind Tunnel Testing. Second Edition, Wiley and Sons Inc., New York.

Riegels, F.W., 1961. Aerofoil Sections. Butterworths.

Shenstone, B.S., 1968. Unconventional Flight. The Aeronautical Journal v. 72 (692), p. 655-666.

Stern, J., 1973. Generalisation of Watson's Formulae and Applications to Aerofoil Theory. Aeronautical Quarterly (November), p. 261-272.

Theodorsen, T., 1931. Theory of Wing Sections of Arbitrary Shape. NACA Report No. 411, Washington.

Theodorsen, T. & Garrick, I.E., 1933. General Potential Theory of Arbitrary Wing Sections. NACA Report No. 452, Washington.

Thwaites, B., 1960. (Editor) Incompressible Aerodynamics. Oxford University Press.

Thwaites, B., 1961. The Aerodynamic Theory of Sails. Part I - Two-Dimensional Sails. Proceedings of the Royal Society, Series A, v. 261, p. 402-442. London.

Watson, E.J., 1945. Formulae for the Computation of Functions Employed for Calculating the Velocity Distribution about a Given Airfoil. Aeronautical Research Council, R. and M. No. 2176.

Woods, L.C., 1961. Cambridge Aeronautical Series, III, The Theory of Subsonic Plane Flow. Cambridge University Press.